ISSN 1000-9620

Marine Science Bulletin

Volume 6 • Number 2 2004

ISSN 1000-9620
02>

NATIONAL MARINE DATA AND
INFORMATION SERVICE OF CHINA

MARINE SCIENCE BULLETIN

Vol.6 No.2 Oct., 2004

CONTENTS

Summer Monsoon and Annual Variability of Sea Surface Slope and Their Effects on Alongshore Current near Qingdao ……*Pu Shuzhen* (蒲书箴) *et al.* (1)

Specifying and Configuring Routing Policies of Relative AS in RPSL ……*Xia Dengwen* (夏登文) *et al.* (9)

Quality Control of ARGO Data Based on Climatological T-S Models ……*Ji Fengying* (纪风颖) *et al.* (19)

Atmospheric Equilibrium Tide Theory ……*Zhang Deyu* (张德宇) (28)

Evolution of Modern Yellow River Delta Coast ……*Yin Yanhong* (尹延鸿) *et al.* (34)

Reducing Environmental Impact of Aggregate Excavation in Small Tropic Pacific Islands……*Xue Chunting* (薛春汀) (45)

Distributional Feature of Detrital Minerals in the Superficial Sediment of South Yellow Sea ……*Wang Hongxia* (王红霞) *et al.* (51)

Optimized Composition of Functional Bacteria for Bioremediation of Sediment Environment of Shrimp Culture ……*Li Qiufen* (李秋芬) *et al.* (60)

Investigation of Macrobenthos in the Intertidal Zone of Tianjin and Discussion on Bioremediation……*Hu Guikun* (胡桂坤) *et al.* (66)

Study on the Characteristic Organic Compounds in Red Tide by Factor Analysis Method ……*Zhao Mingqiao* (赵明桥) *et al.* (74)

Annotation on Mangrove Plants ……*Wang Bosun* (王伯荪) *et al.* (83)

Fractal Characteristics of the Distribution Pattern of Mangrove *Bruguiera Gymnorrhiza* Populations in Southern China ……*Liang Shichu* (梁士楚) *et al.* (90)

Summer Monsoon and Annual Variability of Sea Surface Slope and Their Effects on Alongshore Current near Qingdao

LIBRARY
MAR 0 1 2005
National Oceanic & Atmospheric Administration
U.S. Dept. of Commerce

Pu Shuzhen (蒲书箴)[1], Cheng Jun (程 军)[1], Zhang Yijun (张义钧)[2], Shi Qiang (石 强)[3], Luo Jingxin (骆敬新)[2], Fan Wenjing (范文静)[2]

1 *First Institute of Oceanography, SOA, Qingdao 266061, Shandong, China*
2 *National Marine Data and Information Service, Tianjin 300171, China*
3 *North Branch of SOA, Qingdao 266003, Shandong, China*

Abstract Based on the monthly mean sea level data obtained from 3 years' (1999—2001) tide-gauge measurements, the annual variability of the sea level near Qingdao and Jiaozhou Bay is studied and discussed in this paper. Results show that the sea surface height at all the tide gauges becomes higher in summer than that in winter, with an obvious seasonal variability. Furthermore the sea surface height measured at a short distance outside the bay is lower than that in the bay, showing a sea surface slope downward from north to south. The reasons for the formation of the slope are explained as well. The dynamic action of the summer monsoon and the sea surface slope, and their effects on the monthly mean current are studied by means of dynamics principles. The importance of the summer monsoon and the pressure gradient generated by the sea surface slope, with their effects on the alongshore current, is pointed out and emphasized in this paper.

Keywords Jiaozhou Bay, sea surface slope, monsoon, alongshore current

LIBRARY
Pacific Islands Fisheries Science Center
NOAA Fisheries
Honolulu, Hawaii

1 Introduction to the data analysis method

Qingdao is locaded on shore of Jiaozhou Bay adjacent to the central Yellow Sea. The southern side of its downtown area (from Tuandao to Shilaoren) goes along the sea shore extending eastward from the mouth of Jiaozhou Bay. The western side of its downtown area (Xiaogang Harbour, Dagang Habour, the No.5 Pier, and the other sea ports) lies to the east of Jiaozhou Bay and opposite to the Huangdao Developing Area west of Jiaozhou Bay. Hills high or low are distributed between Tuandao and Laoshan Mountain, standing as a stretching shield and protecting Dagang Harbour and the other sea ports from the disturbance by gales and billows (See Fig. 1). It is tried in this paper to analyse and discuss the annual variation of the sea surface level (*SSL*) near Qingdao with emphasis on features of spatial variability of *SSL*. Therefore the short-period fluctuations of sea surface such as the diurnal tide or semi-diurnal tide will be filtered out of the collected tidal data (1999—2001), which include the higher frequency fluctuations, by means of the summing algorithm for obtaining the monthly mean SSL, in order to learn the seasonal variation of SSL at each tidal gauge station concerned and to explain their spatial distribution features.

First of all, the formula $(SSL)_{jk} = \frac{1}{n_{jk}} \sum_{i=1}^{n_{jk}} (SSL)_{ijk}$ is used to obtain the monthly mean $(SSL)_{jk}$ for

Received on April 28, 2004
The paper is supported by the program: ARGO Observation and Research in the Pacific-India Warm Pool (2002CB714001) and the National Key Programme for Developing Basic Sciences of China under the contract No.G1998040900 (Part 1).

the j-th month and the k-th tidal gauge station. In the formula, k = 1, 2 stand respectively for the Xiaomaidao tidal station (representing the sea area outside the Jiaozhou Bay) and the Dagang tidal gauge station (representing the sea area inside the Jiaozhou Bay) because they are the only two stations with long-term observational data. j =1, 2, 3,…, 12 respectively mean the 12 months in a year. Since $(SSL)_{jk}$ are the data relative to the zero point of the k-th gauge, the spatial variability between the tidal gauge stations cannot be learnt directly form the data. Therefore the formula $\overline{SSL}_{jk} = (SSL)_{jk} - \overline{SSL}_{k}$, where $\overline{SSL}_{k}$ means multi-year annual mean SSL, is used to obtain $\overline{SSL}_{jk}$ (See Fig. 2), which is the monthly mean SSL (j = 1, 2,…, 12) relative to the multi-year mean SSL at the k-th tidal station and independent upon the zero points of the k-th tidal gauge station.

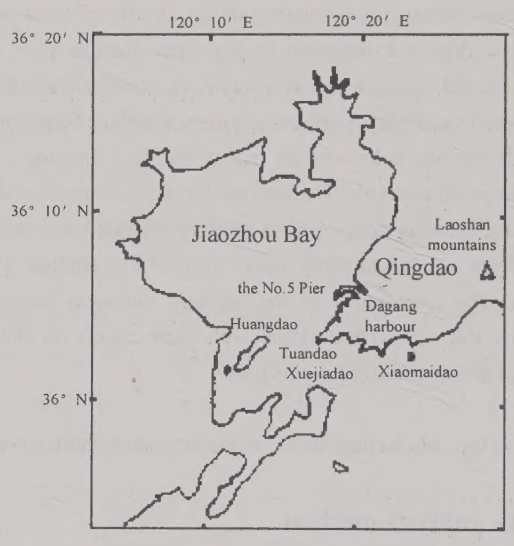

Fig. 1 Sketch map of Jiaozhou Bay

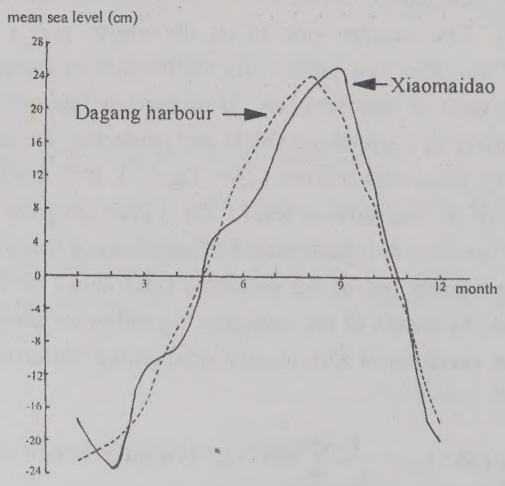

Fig. 2 Annual variations of monthly mean sea level from malti-year data (1999—2001) of Xiaomaidao (solid curve) and Dagang (dashed curve)

2 Seasonal and spatial variabilities of SSL near Qingdao

It is learnt form Fig. 2 that the seasonal variation of the multi-year monthly mean sea level $\overline{SSL}_{jk}$ for either Xiaomaidao (36° 3.0′ N, 120° 25.0′ E) or Dagang (36° 5.2′ N, 120° 18.6′ E) is obvious, The feature of the variation is that *SSL* is higher in summer and lower in winter with a difference between the two greater than 40 cm. Furthermore, the seasonal variation for the No.5 Pier (36° 5.0′ N, 120° 18.0′ E) is similar to the two (It is not illustrated here for saving space). The monthly mean sea level becomes the minimum in February, 23 cm lower than the multi-year mean sea level and the maximum in September, 26 cm higher than the multi-year mean sea level. The difference between the two reaches 46cm. Based on the seasonal variation for Damaidao and Dagang, it is easy to work out the monthly difference $\overline{SSL}_{j1} - \overline{SSL}_{j2} = \Delta(\overline{SSL})_j$. Its meaning in physics is the monthly mean sea surface slope between Xiaomaidao and Dagang, indicating the sea level difference between the inside of Jiaozhou Bay and the outside (It is shown by the vertical distance between the dashed curve and the solid curve in Fig. 2). It is noticed that the sea surface level inside the Jiaozhou Bay is higher than outside of the bay in summer (June, July, and August). For example, $\Delta(\overline{SSL})_6 = 5$ cm, $\Delta(\overline{SSL})_7 = 4$ cm, $\Delta(\overline{SSL})_8 = 1$ cm, indicating an obvious *SSL* difference Δh between the south and the north of the sea area (The temporal variation of the sea surface slope Δh is also shown by the vertical distance between the two curves in Fig.2). In the following section, Δh is divided by the longitudinal distance Δy , to estimate the sea surface slope h_y from the north to the south of the sea area. For the same reason, the *SSL* difference Δh between the No.5 Pier and Dagang (Δh is 4 cm, 3 cm, 0 cm respectively in June, July, and August) can be divided by the latitudinal distance Δx between the two places to estimate the sea surface slope h_x from the east to the west of the sea area. The sea surface slope or the *SSL* difference is irregular in the other months of a year especially in Spring or Autumn, *i.e.*, the two transitional seasons. It is better in winter but not as regular as in summer.

3 Monsoon characteristics in the sea adjacent to Qingdao

In order to discuss the mechanism for generating the sea surface slope illustrated in the above section, two aspects can be considered. One is the southeast wind dominant in the sea adjacent to Qingdao in summer. Forced by the summer monsoon, sea water will be piled up toward the northwest because of the topographic effect of Jiaozhou Bay so that SSL is higher inside the bay than outside the bay. The other is the effect of the runoffs from the coastal area into the bay. Qindao is located in the temperate climatic zone affected by monsoon, where the monsoon rainfall feature is that it rains the most frequently in July, August, and September in a year. The total rainfall in the 3 months is about 396.4 mm (based on the statistics from the data for the period of 1960—1989), more than 54 % of the annual mean rainfall. In contrast with the 3 months, the total rainfall in winter (December, January, and February) is as less as about 34.8 mm, equivalent to 4.7 % of the annual mean rainfall. Most of the monsoon rainfall will converge into the runoffs that run in their river basins and flow into the bay except that a small part of rainfall is absorbed by the land vegetation and soil. Therefore the annual variation of the monsoon rainfall makes the runoffs into Jiaozhou Bay possess their seasonal character. The flowing

capacity and rate of the runoffs reach the annual maximum in summer. For example, according to incomplete statistics, the total water volume flowing into Jiaozhou Bay from Dagu River, Nanjiaolai River, Yang River, Meshui River and Baisha River in July and August reaches more than 50 % of their annual total. The total water volume from those 5 rivers in 4 months (June—September) is more than 3 hundred millions m^3, and it is so much that the water volume could have resulted in a sea level rise as high as 1.3 cm in a sea area of the same size as Jiaozhou Bay. In contrast with the conditions of the inside of Jiaozhou Bay, there is much less runoff from the Qingdao coast into the outside of the bay, without any significant flowing volume. Therefore the summer rainfall and runoff converging into Jiaozhou Bay is another causative factor for the higher *SSL* inside of the bay rather than outside of the bay. It is easy to understand the fact that there is an obvious sea surface slope in the sea around Qingdao in summer and the slope is closely related to the monsoon and the monsoon rainfall.

The wind conditions of the Northern Yellow Sea have been discussed and their brief descriptions given in literature[1-3]. However, in order to explain in details the regularity of the annual variation of monsoon, it is necessary to conduct more calculation from the wind data.

First of all, the sea surface wind observational data (1959—1985) collected by the literature quoted above in the area (35° - 37° N, west of 124° E) are used to calculate the east and west components of sea surface resultant wind vector by means of the formulas $u_j = \frac{1}{n_j}\sum_{i=1}^{n_j} u_{ij}$ and $v_j = \frac{1}{n_j}\sum_{i=1}^{n_j} v_{ij}$ where j =1, 2, ···, 12 represent the 12 months in a year respectively. It is shown from the results that the east component u_j is positive in late autumn and winter (November, December, and January) and $u_1 = 1.9$ m/s in January, the strongest among the 3 months. u_j is negative in the other months and $u_7 = -1.8$ m/s in July, the strongest among the 9 months. It is learnt from the calculation that v_j is negative in early spring, autumn and winter (January, February, March, September, October, November, and December) and $v_{12} = -3.7$ in December, the strongest. v_j is positive in late spring and summer (April, May—August) and $v_7 = 3.5$ m/s. The orientation (the direction in which the wind blows) of the wind vector is shown in Table1.

Tab. 1 Orientation of monthly resultant wind vector (in azimuth and in 16 directions respectively) with its resultant speed

	Jan.	Feb.	Mar.	Apr.	May	Jun.	Jul.	Aug.	Sept.	Oct.	Nov.	Dec.
Orientation of w ind vector (°)	119.46	184.54	217.75	275.24	329.29	327.72	322.27	271.86	221.16	198.68	131.78	113.61
Wind direction	WNW	N	NE	E	SSE	SE	SE	E	NE	NNE	NW	NNW
Resultant wind speed	3.8	3.0	0.7	0.9	1.9	2.8	4.0	2.5	2.9	2.1	1.8	4.0

It is learnt form Tab. 1 that the wind direction of the multi-year mean wind vector turns in a clockwise way from December to May with the vector orientation about 119.46° in January and about 229.29° in May (The azimuth for the north is 0°) and then turns in an anti-clockwise way with its orientation back to about 113.61 ° in December. In general it is toward the northwest in winter (December, January, and February) and toward about the southeast in summer. The difference between the wind direction in January and the one in July is almost 200° , showing a reverse of wind direction from the summer monsoon to the winter monsoon.

4 Dynamic relation among sea surface slope, wind forcing by monsoon, and the mean current near Qingdao

In order to quantitatively estimate the effect of the wind forcing by monsoon (See Section 3) and the pressure gradient by the sea surface slope (See Section 2) on the oceanic flow both inside and outside Jiaozhou Bay, a group of dynamic equations[4] can be set up for a unit of water mass in stable state ($\frac{d\bar{u}}{dt} = 0$) as follows (See Section 9.16 and Section 11.14 in Literature 4):

$$\begin{cases} -fv + ru = \dfrac{\tau^x}{\rho D} - P_x & (1.1) \\ fu + rv = \dfrac{\tau^y}{\rho D} - P_y & (1.2) \\ u_x + v_y = 0 & (1.3) \end{cases}$$

The equations mean the dynamic balance among coriolis force, Rayleigh friction, wind stress, and pressure gradient, and the water mass continuity of incompressible fluid. Equation 1.1 and Equation 1.2 are different from the geostrophic current equation only because they include the wind stress τ_x, τ_y and the inner friction expressed by Rayleigh friction (It is very important in the nearshore area). x is toward the east and y toward the west in the equations. ρ is water density taken as a constant. τ^x, τ^y are the wind stress components exerted on a unit area of the sea surface.

ρD is the water mass in a water column with the unit area and the depth D. Therefore $\frac{\tau^x}{\rho D}$ and $\frac{\tau^y}{\rho D}$ are the wind stress borne by a unit water mass. Following the static pressure equation, we have:

$$P_x = \frac{1}{\rho}\frac{\partial p}{\partial x} = \frac{1}{\rho}\frac{\partial}{\partial x}\int_z^0 \rho g dz = gh_x \qquad (2)$$

and for the same reason

$$P_y = gh_y \qquad (3)$$

where h_x and h_y are the partial differential quotients of the sea surface height, representing the sea surface slope. u_x and v_y are the partial differential quotients of the current components. The transport across the 36° 5.2′ N section in Jiaozhou Bay (See Fig. 1. Dagang is located at the east end of the section) is considered as follows. Because it is impossible to generate the lateral transport across either the east coastline or the west coastline in Jiaozhou Bay, the transport equations, *i.e.*, the simplified barotropic (2 dimensional) equations for full depth water are:

$$\begin{cases} \int_0^D \int_{x_1}^{x_2} \rho v \, dx \, dz = \rho \overline{v_1} D \cdot b_1 \\ \int_0^D \int_{x_1}^{x_2} \rho u \, dx \, dz = \rho \overline{u_1} D \cdot b_1 = 0 \end{cases} \qquad (4)$$

where $b_1 = x_2 - x_1$ represents the width of the 36° 5.2′ N section, D is the average depth (taken from

sea chart), and $\overline{v_1}$ is the average current speed across the section.

Integrating Equation 1.1 for z and x and substituting Equation 4 for the relevant variable we have:

$$-f\overline{v_1}\rho b_1 D = b_1\overline{\tau^x} - \rho b_1 Dg\,\overline{h}_x$$

$$\overline{v_1} = \frac{-\overline{\tau^x}}{\rho Df} + \frac{g\overline{h}_x}{f}$$

If $\rho = 1\times10^3$ kg/m^3, the average depth is taken as 15 m, $f = 8.5723\times10^{-5}$s^{-1}, $\overline{h}_x$ can be estimated from the observational value mentioned in Section 2, and the formula $\vec{\tau} = C_D\rho|\vec{w}|\vec{w}$ is used together with the average wind vector mentioned in Section 3, it is easy to obtain the estimated value of the average current speed $\overline{v_1}$ respectively for June, July, or August. It will help understand the magnitude of the water motion both inside and outside of Jiaozhou Bay, and its relationship with wind stress and sea surface slope.

$$\overline{v_1} = \begin{cases} \dfrac{7.114\times10^{-3}}{1\times10^{-3}\times15\times8.5723\times10^{-5}} + \dfrac{9.8\times0.75\times10^{-6}}{8.5723\times10^{-5}} = 0.0055 + 0.086 = 0.09\ \text{m/s} & \text{(June)} \\ \dfrac{12.476\times10^{-3}}{1\times10^{3}\times15\times8.5723\times10^{-5}} + \dfrac{9.8\times0.56\times10^{-6}}{8.5723\times10^{-5}} = 0.0096 + 0.0642 = 0.07\ \text{m/s} & \text{(July)} \\ \dfrac{9.348\times10^{-3}}{1\times10^{3}\times15\times8.5723\times10^{-5}} + 0 = 0.007\ \text{m/s} & \text{(August)} \end{cases}$$

Based on the above expressions, one can see that the action of both the pressure gradient force by the sea surface slope and the wind stress will generate the average current northward. It is shown that both the summer monsoon and the sea surface slope in summer make their contribution to the northward transport in the same direction as the other.

It is deduced from the fluid continuity equation for the stable conditions that the northward transport across one latitudinal section should be equal to that across any other latitudinal section, which can be proved by the integration of Equation 1.3 (The proof is not shown here). Therefore the average current speed $\overline{v_2}$ across the latitudinal section from the south end of Tuandao (36° 02′ 36″ N, 120° 16′ 49″ E) to Huangdao can be estimated by using the following equation $\overline{v_2} = \dfrac{b_1 D_1 \overline{v_1}}{b_2 D_2}$, where D_2 = 20 m, $b_1 = 3b_2$:

$$\overline{v_2} = 2.25\,\overline{v_1} = \begin{cases} 0.2\ \text{m/s} & \text{(June)} \\ 0.16\ \text{m/s} & \text{(July)} \\ 0.016\ \text{m/s} & \text{(August)} \end{cases}$$

Obviously the northward average current is much faster in the narrow waterway from Tuandao to Huangdao than in the wide water area inside the bay.

Furthermore by use of the continuity equation as shown in (1.3), it can be easily proved that the westward transport across the longitudinal section from Tuandao to Xuejiadao is equal to the northward transport across the section from Tuandao to Huangdao. Therefore the westward average current can be estimated by use of the following equation $\overline{u_3} = -\dfrac{b_2 D_2 v_2}{b_3 D_3}$ where $b_3 = \dfrac{2}{3}b_2$, D=25 m. Then we

have:

$$\overline{u_3} = \begin{cases} -0.24 \text{ m/s} & (\text{June}) \\ -0.19 \text{ m/s} & (\text{July}) \\ -0.02 \text{ m/s} & (\text{August}) \end{cases}$$

It is learnt from the above expression that the average current flows westward across the longitudinal section between Tuandao and Xuejiadao because of the topographic effects of Jiaozhou Bay. Based on the analysis described above, the average current direction is consistent with the τ^y direction (*i.e.* northward) although τ^y of the equation (1.2) is not used. In fact it can be seen from Equation (1.1) and Equation (1.2) that, forced by coriolis force, $\overline{v}$ has a sign opposite to the sign of τ^x and consistent to the sign of τ^y (It means that the southeast wind ($\tau^x < 0$) will generate a northward current and its transport). Therefore the monsoon forcing effect is an important caution factor for generating the northward average current.

In addition, following Equation (1.3), we have $\frac{\Delta \overline{u}}{\Delta x} = -\frac{\Delta \overline{v}}{\Delta y}$. By means of the above expression, the spatial variability of both the longitudinal current $\overline{v}$ and the latitudinal $\overline{u}$ can be further discussed. In the previous calculations, $\overline{v_2}$ across the section between Tuandao and Huangdao and $\overline{v_1}$ across the 36° 5.2′ N section have been evaluated. It is also learnt that, Δy = 36° 5.2′ N − 36° 02′ 36″ N ≐ 2.6′ = 2.6 × 1.85 km = 4.81 km represents the longitudinal distance. Then in the sea area near the bay mouth between Tuandao and Xuejiadao:

$$\frac{\Delta \overline{u}}{\Delta x} = -\frac{\Delta \overline{v}}{\Delta y} \doteq -\frac{v_1 - v_2}{\Delta y} = \begin{cases} 0.023 \text{ m/s} \cdot \text{km} & (\text{June}) \\ 0.019 \text{ m/s} \cdot \text{km} & (\text{July}) \\ 0.002 \text{ m/s} \cdot \text{km} & (\text{August}) \end{cases}$$

In the sea area between Tuandao and Xuejiadao, $\Delta x = x_{Xiaomaidao} - x_{Tuandao}$ = 120° 25.0′ E − 120° 16.82′ E = 8.18′ ≐ 12.27 km. Therefore in the sea around Xiaomaidao,

$$\overline{u_4} = \begin{cases} -0.11 \text{ m/s} & (\text{June}) \\ -0.10 \text{ m/s} & (\text{July}) \\ -0.01 \text{ m/s} & (\text{August}) \end{cases}$$

By use of the method similar to the above, alongshore current can be roughly estimated for the coastal places of Qingdao east of Tuandao.

It is shown from the above calculation that there is a westward current in summer along the southern coastline east of Tuandao with its magnitude about 0.1-0.2 m/s. The westward alongshore current becomes decreased as the distance from Tuandao increases. The maximum current speed appears in the sea near Tuandao. It becomes the strongest in June and the weakest in August, tending to decrease with the lapse of time.

Finally it should be indicated that the above calculating result means the contribution made to the alongshore current only by both the sea surface slope and the monsoon action. However, the causative elements affecting the alongshore are various. For example, they might be shelf waves with long period, seiches in harbours, and tidal residual current, *etc.* Therefore the actually measured alongshore current is very complicated and even it is further entangled by the non-linear interaction of various periodic tidal

forces to become a resultant motion from which the effects of monsoon and sea surface slope could not be easily separated. Here a simple estimation method is presented for the effects.

5 Conclusion

It may be concluded from the above description as follows:

a) Based on the sea level data of the tidal gauge stations both inside and outside of Jiaozhou Bay near Qingdao (Dagang and the No. 5 Pier represent the inside of the bay and Xiaomaidao the outside), it is learnt that the monthly mean *SSL* from the multi-year data obviously has seasonal variation. Its main features show that SSL is higher in summer and lower SSL in winter.

b) Relative to the annual mean sea surface, the monthly mean *SSL* obviously has the spatial variability features either inside or outside of Jiaozhou Bay, showing *SSL* higher inside of the bay than outside and *SSL* higher in the east of the bay than in the west. The features mean that there is a sea surface slope in the sea area.

c) The direction of the sea surface wind obviously has seasonal variation in the sea near Qingdao. The monthly mean wind from the resultant wind vector changes its direction in a clockwise way in the time period from January to May, and in an anti-clockwise way from May to December. Winter monsoon blows from about the northwest with its maximum strength about 4.0 m/s in December. Summer monsoon blows from about the southeast with its maximum strength about 4.0 m/s. The seasonal reverse of the wind direction is a typical feature of the East Asia Monsoon.

d) The annual variation of the monsoon can have a certain effect on the sea surface slope in the sea area near Qindao. The effect forces the sea water outside of the bay to flow into the bay. At the same time, the plentiful rainfall which the summer monsoon brings greatly enhances the runoffs from the coastal land and to the inner part of the bay, and provides favorable conditions for the SSL increase in the bay.

e) By means of the simple dynamic equations, the monthly mean current can be estimated for the sea area around Jiaozhou Bay. The current is a result commonly forced by the wind stress, Coriolis force, the pressure gradient force generated by the sea surface slope, and the friction. The monthly mean current flows toward the same direction as the direction toward which either the wind stress or the pressure gradient force directs.

f) The dynamic equations can be also used for estimating roughly the alongshore current flowing along the southern coastline of Qingdao in summer. The alongshore current flows westward with a monthly mean current of about 0.2 m/s. Its speed becomes decreased with the increase of the distance from Tuandao. The maximum speed should appear around Tuandao. It is the strongest in June, and the weakest in August, decreasing with the lapse of time.

References

[1] Chen Guozhen (editor). Marine Atlas. Beijing: China Ocean Press. 1992, 87.

[2] Chen Zeshi (editor). Outlines of bays and estuaries of China (Vol.3). Beijing: China Ocean Press. 1991, 486.

[3] Li Fanhua (editor). Atlas of Marine Hydrography in the Sea Around Shandong. Jinan: Shandong Cartographic Publishing House. 1989, 94.

[4] Gill A E. Atmosphere-Ocean Dynamic. London: Academic Press. 1982, 489.

Specifying and Configuring Routing Policies of Relative AS in RPSL

Xia Dengwen (夏登文)[1,2], Shi Suixiang (石绥祥)[1,2], Yu Ge (于 戈)[1]

1 *School of Information Science and Engineering, Northeastern University, Shenyang 110004, Liaoning, China*

2 *National Marine Data & Information Service, Tianjin 300171, China*

Abstract Routing policies specification language (RPSL) allows a network operator to specify routing policies at various levels in the Internet hierarchy, for example at the autonomous system (AS) level. At the same time, policies can be specified with sufficient detail in RPSL so that the low level router configurations can be generated from them. This paper is a discussion on using the RPSL to describe routing policies of relative AS in the Internet routing registry (IRR). We first analyze the relationships between a pair of ASes, and then explain how to specify various relative AS routing policies in RPSL. At last, we show an example of configuring routing policies using RtConfig that is a tool developed by the Routing Arbiter Project (RAP).

Keywords routing policy, AS, RPSL, BGP, IRR

Introduction

The Internet has experienced a tremendous growth in its size and complexity since its commercialization. The Internet connects thousands of ASes operated by many different administrative domains such as Internet Service Providers (ISPs), companies and universities. Since two ISPs might merge into one and each administrative domain can possess several ASes, an administrative domain can operate one or several ASes. Routing within an AS is controlled by inter-domain routing protocols such as static routing, OSPF, IS-IS, and RIP. All pairs of ASes interconnect via dedicated links and/or public network access points, and routing between ASes is determined by the inter-domain routing protocol-Border Gateway Protocol (BGP). One distinct feature of the inter-domain routing protocol is that it allows each AS to choose its own policy in selecting the best route, and announcing and accepting routes. One of the most important factors in determining routing policies is the commercial contractual relationship between the administrative domains.

The commercial agreements between pairs of administrative domains can be classified into customer-provider, peer to peer, and mutual-transit agreement[1, 2]. A customer pays its provider for connectivity to the rest of the Internet. Therefore, a provider does transit traffic for its customers. However, a customer does not employ transit traffic between two of its providers. A pair of peers agree to exchange traffic between their respective customers free of charge. A mutual-transit agreement allows a pair of administrative domains to provide connectivity to the rest of the Internet for each other. This mutual transit relationship is typically between two administrative domains such as small ISPs or universities which are located close to each other and which cannot afford additional Internet services for better connectivity.

Received on June 7, 2004

BGP controls the routing between ASes and allows ASes to apply local policies for selecting routes and propagating routing information, without revealing their policies or internal topology to others. Unfortunately, recent studies have shown that a collection of ASes may have conflicting BGP policies that lead to route divergence[3, 4]. Route divergence can result in route oscillation, which can significantly degrade the end-to-end performance of the Internet. Avoiding these conflicting BGP policies is crucial for the stability of the Internet routing infrastructure. Yet, to be practical any technique for ensuring convergence should not sacrifice the ability of each AS to apply complex local policies.

A natural approach to the route convergence problem involves the use of IRR, a repository of routing policies specified in a standard language. A complete and up-to-date registry could determine if the set of routing policies has any potential convergence problems. RPSL[5], with its form of standard language, allows a network operator to be able to specify routing policies at various levels in the Internet hierarchy. For example, at the ASes level. At the same time, policies can be specified in sufficient detail in RPSL so that the low level router configurations can be generated from them. RPSL has extensive new routing protocols and new protocol features which can be introduced at any time.

Unfortunately, RPSL no longer distinguishes AS relationship due to Internet routing architecture. In the following section, we discuss the basic rule which a router possessing an AS relationship configuration could abide by, and describe the typical policies routing specifications of relative AS in RPSL. Finally we give an example for configuring policies routing using RtConfig.

1 Specifying routing policies in RPSL

Before starting the discussion, we introduce RPSL first.

1.1 Overview of RPSL

RPSL is object oriented; that is, objects contain pieces of policy and administrative information. These objects are registered in the IRR by the authorized organizations. The registration process is beyond the scope of this document. Please refer to [6] for more details on the IRR. RPSL employs class to produce the objects. The "mntner" class defines entities authorized to add, delete and modify a set of objects. The "person" and "role" classes describe technical and administrative contact personnel. ASes are specified using the "aut-num" class. Routes are specified using the "route" class. Sets of objects can be defined AS using the "as-set", "route-set", "filter-set", "peering-set", and "rtr-set" classes. The " dictionary" class provides the extensity to the language. The "inet-rtr" class is used to specify routers. In the following section we focus on the aut-num class that is used for specifying the policies of AS.

Routing policies are specified using the aut-num class. The attributes of the aut-num class are shown in Figure 1. The value of the aut-num attribute is the AS number of the AS described by this object. The as-name attribute is a symbolic name (in RPSL name syntax) of the AS. The import, export and default routing policies of the AS are specified using import, export and default attributes respectively.

Import Attribute: In RPSL, an import policy is divided into import policy expressions. Each import policy expression is specified using an import attribute. The import attribute has the following syntax:

```
import: from <peering-1> [action <action-1>]
        ...
        from <peering-N> [action <action-N>]
        accept <filter>
```

The action specification is optional. The semantics of an import attribute is as follows: the set of routes that are matched by <filter> are imported from all the peers (may not be peers relationship) in < peerings>; while importing routes at <peering-M>, <action-M> is executed. Policy actions in RPSL either set or modify route attributes, such as assigning a preference to a route, adding a BGP community to the BGP community path attribute, or setting the Multi-Exit-Discriminator (MED) attribute. Policy actions can also instruct routers to perform special operations, such as route flap damping.

Attribute	Value	Type
aut-num	<as-number>	mandatory, single-valued, class key
as-name	<object-name>	mandatory, single-valued
member-of	list of <as-set-names>	optional, multi-valued
import	see **Import Attribute**	optional, multi valued
export	see **Export Attribute**	optional, multi valued
default	see **Default Attribute**	optional, multi valued

Fig. 1 Aut-num Class Attributes

Export Attribute: Similarly, an export policy expression is specified using an export attribute. The export attribute has the following syntax:

export: to <peering-1> [action <action-1>]

...

to <peering-N> [action <action-N>]

announce <filter>

The action specification is optional. The semantics of an export attribute is as follows: the set of routes that are matched by <filter> are exported to all the peers (may not be peers relationship) specified in <peering>; while exporting routes at <peering-M>, <action-M> is executed.

Default Attribute: Default routing policies are specified using the default attribute. The default attribute has the following syntax:

default: to <peering> [action <action>] [networks <filter>]

The <action> and <filter> specifications are optional. The semantics are as follows: The <peering> specification indicates the AS (and the router if present) is being defaulted; the <action> specification, if present, indicates various attributes of defaulting, for example a relative preference if multiple defaults are specified; and the <filter> specification, if present, is a policy filter. A router only uses the default policy if it receives the routes matched by <filter> from this peer.

1.2 Specifying routing policies of relative AS in RPSL

The key purpose of RPSL is to allow you to specify your routing configuration in the public IRR, so that you can check your policies and announcements for consistency. Moreover, in the process of setting policies and configuring routers, one can take into account the policies and configurations of others.

In this section, we begin by defining the ASes relationship. We classify the relationship between a pair of interconnected ASes into customer-to-provider, peer-to-peer, and sibling-to-sibling relationships. According to ASes relationships, we introduce some rules that govern policies of relative AS and show how to describe the routing policies in RPSL.

1.2.1 AS relationships and selective export policies

The relationships between ASes arise from contracts that define the pricing model and the exchange of traffic between the administrative domains that the two ASes belong to. Two ASes that exchange traffic have a customer-to-provider, provider-to-customer, peer-to-peer, or sibling-to-sibling relationship. In a customer-to-provider or provider-to-customer relationship, the customer typically belongs to a smaller administrative domain that pays a larger administrative domain for access to the rest of the Internet. The provider is an AS that belongs to the larger administrative domain. In a peer-to-peer relationship, the two peers typically belong to administrative domains of comparable size and find it mutually advantageous to exchange traffic between their respective customers. Two ASes have a sibling-to-sibling relationship if they belong to the same administrative domain or to the administrative domains that have a mutual-transit agreement.

The AS relationships translate into the following rules that govern BGP export policies[12]:

(1) **Exporting to a provider**: In exchanging routing information with a provider, an AS can export its routes and the routes of its customers and siblings, but cannot export routes learned from other providers or peers.

(2) **Exporting to a customer**: In exchanging routing information with a customer, an AS can export its routes and the route of its customers and siblings, as well as routes learned from its providers and peers.

(3) **Exporting to a peer**: In exchanging routing information with a peer, an AS can export its routes and the routes of its customers and sibling, but cannot export the routes learned from other providers or peers.

(4) **Exporting to a sibling**: In exchanging routing information with a sibling, an AS can export its routes and routes of its customers and siblings, as well as routes learned from its providers and peers.

Note that although exporting policies are the same for providers and peers(or customers and siblings), provider-customer relationships are asymmetric and peer-peer(or sibling-sibling) relationships are symmetric, which is the key to distinguishing provider-customer relationships from peer-peer(or sibling-sibling) relationships. To sumup, an AS selectively provides transit services for its neighboring ASes. Let the (r.as-path) denote the first AS in r.as-path. An AS sets up its export policy according to the rule that follows.

Selective export rule: an AS does not provide transit services between any two of its providers and peers. Consider AS u and AS v $\in$ provider(u) $\cup$ peer(u). For each best route r of u, if first(r.as-path) $\in$ provider(u) $\cup$ peer(u), then export(u,v)[{r}]={}.

1.2.2 Peer- peer policies

The peering policies of an AS are registered in an aut-num object which looks something like that in Figure 2. We will focus on the semantics of the import and export attributes in which peering policies are expressed.

Now consider Figure 3. Assume that AS1 and AS2 are in the peer-peer relationship and that AS2 and AS3 are in the provider-customer relationship as well (AS4 and AS5 in the figure will be discussed later). The peering policies expressed in the AS2 aut-num object in Figure 2 are typical for a small service provider providing connectivity for a customer AS3 and using AS1 for transit. That is, AS2 only accepts announcements from AS3, to AS1, AS2 announces only those routes which originate in its AS or in their customer's AS.

```
aut-num:    AS2
as-name:    NEU
descr:      Northeastern University
import:     from AS1 accept ANY
import:     from AS3 accept <^AS3+$>
export:     to AS3 announce ANY
export:     to AS1 announce AS2 AS3
admin-c:    CerNet
tech-c:     CO19-CerNet
mnt-by:     OPS4-CerNet
changed:    neuq@edu.cn
source:     CerNet
```

Fig. 2 Autonomous System Object

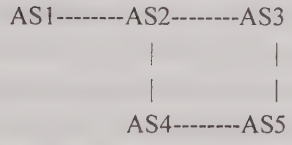

Fig. 3 Some Neighboring ASes

In the example above, "accept ANY" in the import attribute indicates that AS2 will accept any announcements that AS1 sends, and "announce ANY" in the export attribute indicates that any route that AS2 has in its routing table will be passed on to AS3.

Note that with this peering arrangement, if AS1 adds or deletes route objects, there is no need to update any of the aut-num objects to continue the full routing policy. Added (or deleted) route objects will implicitly update AS1's and AS2's policies.

1.2.3 Provider-customer policies

It is not uncommon for an ISP to acquire connectivity from a transit provider which announces all routes to it, which it in turn passes on to its customers to allow them to access hosts on the global Internet. Meanwhile, the ISP will generally announce the routes of its customer networks to the transit ISP, making them accessible on the global Internet. This is the service that is specified in Figure 2 for AS3.

Consider again Figure 3. Suppose now that AS2 wants to provide the same service to AS4. Clearly, it would be easy to modify the import and export lines in the aut-num object for AS2. These changes are trivial to make of course, but clearly, as the number of AS2 customers grows, it becomes more difficult to keep track of, and prevent errors. Note also that if AS1 is selective about only accepting routes from the customers of AS2 from AS2, the aut-num object for AS1 would have to be adjusted to accommodate AS2's new customer.

By using the RPSL "as-set" object, we can simplify this significantly. In Figure 4, we describe the customers of AS2.

Having this set to work with, we can now rewrite the policies in Figure 3 as shown in Figure 5.

```
as-set:     AS2:AS-CUSTOMERS
members:    AS3 AS4
changed:    orange@ripe.net
source:     RIPE
```

Fig.4 The as-set object

```
import:   from AS1 accept ANY
import:   from AS2:AS-CUSTOMERS accept <^AS2:AS-CUSTOMERS+$>
export:   to AS2:AS-CUSTOMERS announce ANY
export:   to AS1 announce AS2 AS2:AS-CUSTOMERS
```

Fig. 5 Policy in the AS2 aut-num object for all AS2 customers

Note that if the aut-num object for AS1 contains the line:

import: from AS2 accept <^AS2+ AS2:AS-CUSTOMERS*$>

then no changes will need to be made to the aut-num objects for AS1or AS2 as the AS2 customer base grows. The AS numbers for new customers can simply be added to the as-set AS2:AS-CUSTOMERS, and everything will work as for the existing customers. Clearly in terms of readability, scalability and maintainability, this is a far better mechanism when compared to adding policy for the customer AS's to the aut-num objects directly. The policy in this particular example states that AS1 will accept route announcements from AS2 in which the first element of the path is AS2, followed by more occurrences of AS2, and then 0 or more occurrences of any AS2 customer (e.g. any member of the as-set AS2:AS-CUSTOMERS).

Because A2 is the provider of A3 and A4, the export policies, an AS2 can export its routes and the route of its customers and siblings, as well as routes learned from its providers and peers (e.g. Figure 5 export: to AS2: AS-CUSTOMERS announce ANY). For AS3 or AS4 it is the customer of AS2, so the export policies, an AS3 or AS4 can export its routes and the route of its customers and siblings, but cannot export routes learned from other providers or peers according to the rule(1). The example is as follows (Figure 6):

```
aut-num:    AS3
as-name:    NEU
descr:      Northeastern University
import:     from AS5 accept ANY
import:     from AS3 accept <^AS2+$>
export:     to AS2 accept <^AS3+$>
export:     to AS4 announce ANY//AS3 and AS4 are a pair of peering
relationship router//
admin-c:    CerNet
```

Fig. 6 Policy in the AS3 aut-num object

1.2.4 Sibling-sibling policies

Now consider Figure 3 again, Suppose AS1 and AS2 are in the sibling-sibling relationship and AS2 and AS3 are in the provider-custom relationship. The sibling policies are expressed in the AS2 aut-num object in Figure 8. The AS2 can export its routes and routes of its customers and siblings, as well as routes learned from its providers and peers according to the rule (4).

Note that if the aut-num object for AS1 contains the line:

import: from AS2 accept <^AS2+ AS2:AS-CUSTOMERS*$>

They are similar to Figs. 4 and 5.

```
as-set:     AS2:AS-CUSTOMERS
members:    AS3 AS4
changed:    orange@ripe.net
source:     RIPE
```

Fig.7 The as-set object

```
import:  from AS1 accept ANY
import:  from AS2:AS-CUSTOMERS accept <^AS2:AS-CUSTOMERS+$>
export:  to AS2:AS-CUSTOMERS announce ANY
export:  to AS1 announce AS2 AS2:AS-CUSTOMERS
```

Fig. 8 Policy in the AS2 aut-num object for all AS2 customers

2 Configuration practice

In this section, we briefly introduce a tool called RtConfig that can be used to configure router according to the policies routing specification.

RtConfig is a tool developed by the Routing Arbiter Project[7] to generate vendor specific router configurations from the policy data held in the various IRRs. RtConfig currently supports Cisco, gated and RSd configuration formats. It has been publicly available since the late 1994, and is currently being used by many sites for router configuration. The next section describes a methodology for generating vendor specific router configurations using RtConfig.

The general paradigm for using RtConfig involves registering policy in an IRR, building a RtConfig source file, then running RtConfig against the source file and the IRR database to create vendor specific router configuration for the specified policy. The source file will contain vendor specific commands as well as RtConfig commands. To make a source file, pick up one of your router configuration files and replace the vendor specific policy configuration commands with the RtConfig commands.

Commands beginning with @RtConfig instruct RtConfig to perform special operations. An example source file is shown in Figure 9. In this example, commands such as "@RtConfig import AS3582 198.32.162.1 AS3701 198.32.162.2" instruct RtConfig to generate vendor specific import policies where the router 198.32.162.1 in AS3582 is importing routes from router 198.32.162.2 in AS3701. The other @RtConfig commands instruct the RtConfig to use certain names and numbers in the output that it generates (please refer to RtConfig manual[7] for additional information).

Once a source file is created, the file is processed by RtConfig (the default IRR is the RADB, and the default vendor is Cisco; however, command line options can be used to override these values). The

result of running RtConfig on the source file in Figure 9 is shown in Figure 10.

```
router bgp 3582
network 128.223.0.0
!
!     Start with access-list 100
!
@RtConfig set cisco_access_list_no = 100
!
!     NERO
neighbor 198.32.162.2 remote-as 3701
@RtConfig set cisco_map_name = "AS3701-EXPORT"
@RtConfig export AS3582 198.32.162.1 AS3701 198.32.162.2
@RtConfig set cisco_map_name = "AS3701-IMPORT"
@RtConfig import AS3582 198.32.162.1 AS3701 198.32.162.2
!
!     WNA/VERIO
neighbor 198.32.162.6 remote-as 2914
@RtConfig set cisco_map_name = "AS2914-EXPORT"
@RtConfig export AS3582 198.32.162.1 AS2914 198.32.162.6
@RtConfig set cisco_map_name = "AS2914-IMPORT"
@RtConfig import AS3582 198.32.162.1 AS2914 198.32.162.6
```

Fig. 9 RtConfig Template File

In Figure 10, you can see the result of running RtConfig on the source file in Figure 9.

```
router bgp 3582
network 128.223.0.0
!
!     NERO
neighbor 198.32.162.2 remote-as 3701
no access-list 100
access-list 100 permit ip 128.223.0.0 0.0.0.0 255.255.0.0 0.0.0.0
access-list 100 deny ip 0.0.0.0 255.255.255.255 0.0.0.0 255.255.255.255
!
no route-map AS3701-EXPORT
route-map AS3701-EXPORT permit 1
 match ip address 100
!
router bgp 3582
neighbor 198.32.162.2 route-map AS3701-EXPORT out
!
no route-map AS3701-IMPORT
```

```
route-map AS3701-IMPORT permit 1
 set local-preference 1000
!
router bgp 3582
neighbor 198.32.162.2 route-map AS3701-IMPORT in
!
!      WNA/VERIO
neighbor 198.32.162.6 remote-as 2914
!
no route-map AS2914-EXPORT
route-map AS2914-EXPORT permit 1
 match ip address 100
!
router bgp 3582
neighbor 198.32.162.6 route-map AS2914-EXPORT out
no ip as-path access-list  100
ip as-path access-list 100 permit ^_2914(((_[0-9]+))*_          \
     (13|22|97|132|175|668|1914|2905|2914|3361|3381|3791|3937|   \
      4178|4354|4571|4674|4683|5091|5303|5798|5855|5856|5881|6083 \
      |6188|6971|7790|7951|8028))?$
!
no route-map AS2914-IMPORT
route-map AS2914-IMPORT permit 1
 match as-path 100
 set local-preference 998
!
router bgp 3582
neighbor 198.32.162.6 route-map AS2914-IMPORT in
```

Fig. 10 Output of RtConfig

3 Conclusion

In this paper, we present a simple model of BGP along with a set of guidelines for ASes that may be applied in configuring their BGP routing policies. These guidelines capitalize on the commercial relationships between ASes, and better guarantee route consistency for all possible initial states with required global coordination. As part of our research work, we are investigating how ASes can verify consistency with this routing policies rule. Since the stability properties can be compromised by human error, we propose to use the route registry that contains the hierarchical interconnection structure of ASes to check for consistency. Using IRR database, each ISP can verify the validity of a route announcement. Although some studies[13] show the global coordination effort faces several impediments, for example, many ISPs may be unwilling to reveal their local policies to others. However it may still be feasible to practice this technique in most of administrative domains.

References

[1] G Huston. Interconnection, peering and settlements-part I. Internet protocol journal, 1999, 45(3): 124-136.

[2] G Huston. Interconnection, peering and settlements-part II. Internet protocol journal, 1999, 45(3): 136-152.

[3] G G Griffin and G Wilfong. An analysis of BGP. Convergence properties. Proc. ACM SIGCOMM, September, 1999.

[4] K Varadnan, R Govindan and D Estrin. Persistent route oscillations in inter-domain routing. Techinical Report 96-631, USC/ISI, February, 1996.

[5] D Meyer, J Schmitz, C Orange *et al.* Alaettinoglu. Using RPSL in Practice. Request for Comments 2650, August, 1999.

[6] A M R Magee. RIPE NCC Database Documentation. Technical Report RIPE-157, RIPE NCC, Amsterdam, Netherlands, May, 1997.

[7] RtConfig as part of the RAToolSet. http://www.ra.net/ra/RAToolSet/RtConfig.html.

Quality Control of ARGO Data Based on Climatological T-S Models

Ji Fengying (纪风颖)[1, 2] Lin Shaohua (林绍花)[2]
1 *College of Environment , Ocean University of China, Qingdao 266003, Shandong, China*
2 *China National Marine Data & Information Service, Tianjin 300171, China*

Abstract By implementing the ARGO program, a large number of T-S profiles can be observed in the world ocean. However, it is very difficult to examine changes of the sensitivity of the sensors equipped at the ARGO floats, because it is difficult to understand their condition in the sea and the reliability of the data. Quality control must be done in order to avoid the wrong conclusion deduced from the wrong data. One of the realistic methods for quality control of the ARGO data is the comparison with the local climatology. High quality climatological T-S models in northwest Pacific have been built based on the Nansen bottle data and CTD data for the quality control in NMDIS. The models are used to check the ARGO data in this area and have got good result.

Keywords ARGO program, Quality control, CTD, Nansen

Introduction

Autonomous CTD profiling floats are free-moving floats that report vertical profiles of salinity, temperature and pressure at regular time intervals. The ARGO program plans to deploy 3000 such floats to observe the upper 2 000 m of the global ocean. It enables high-resolution and real-time observations of the surface and middle layers of the oceans (e.g., Mizuno, 2000). The ARGO program is part of the Global Ocean Observing System (GOOS) and will contribute to the Climate Variability and Predictability Study (CLIVAR) and the Global Ocean Data Assimilation Experiment (GODAE).

It is difficult to directly monitor the conditions of the onboard sensors of the ARGO floats once they are deployed in the ocean. Also, it is extremely difficult to determine the cause of sensor deterioration during the drift of the floats in the ocean. Therefore, to evaluate the quality of the data obtained by the ARGO floats (ARGO data) and, if possible, to obtain high-quality data are important for the program.

Therefore, we can say that the success of the ARGO project depends on the efficiency of the data quality control. Generally, the temperature and salinity in deep layers are considered to be relatively stable [1, 2]. Therefore, the most practical method of making quality evaluations of ARGO data is to compare them for the deep layers to the local climatology. Such a method has been adopted by some organizations. For example, in the University of Washington, Wong *et al.* (2001)[3] is developing a correction method for salinity data using profile data from the World Ocean Database 1998. In the Commonwealth Scientific and Industrial Research Organization (CSIRO) of Australia, salinity data are corrected by using the WOCE-CTD data obtained in the vicinity of floats (CSIRO, 2001).

As a country abut against NW Pacific, China is more interested in the data of this area. Besides the real time quality control method recommended by the international ARGO program, we used NODC

Received on March 2, 2004

salinity-density models for reference, established temperature-salinity models to check ARGO data automatically in northwest Pacific, so that quality control can be carried out on a large amount of ARGO data within a limited period of time.

1 Establishing high quality climatologic T-S models

1.1 The limitation of T-S models by the bivariate frequency distributions method

Our idea about the T-S models comes from the NODC salinity-density models. NODC generated the models for each five-degree square of ocean for which sufficient data were available (10 or more valid stations). Using all valid (non-questionable) data greater than or equal to 100 m in depth, NODC compiled bivariate frequency distributions of salinity versus density (sigma-t) from those derived from the midline and envelope (upper and lower bound) models that define expected values and ranges of salinity as a function of density. Water mass model comparison checks each new station against salinity-density models derived from the historical data in the NODC oceanographic station data file (Fig. 1)[4].

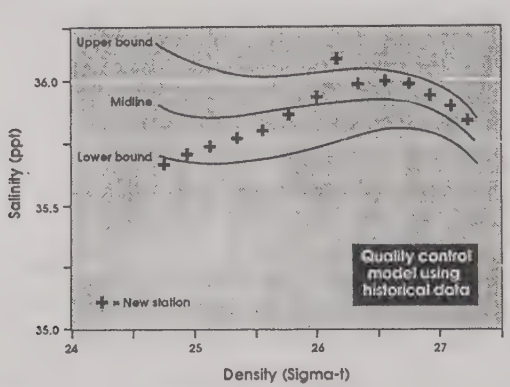

Fig. 1 Ocean Data Quality Control Model by NODC [4]

Because density is derived from temperature, salinity and pressure, wrong salinity can result in wrong density. In this occasion, the salinity-density models will not be effective. Since the two main state variables of the ocean, temperature, T, and salinity, S, are related to each other by definite patterns that represent the mean characteristics of a region[5], the idea of T-S models comes out.

At first, bivariate frequency distributions method was used to set up the T-S models. In a curtain 2° × 2° square (130° - 132° E, 20° - 22° N), temperature was taken as an independent variable, and salinity as an attributive variable and the temperature is divided into a number of sections. In each temperature section, by using the bivariate frequency distributions method we calculate the midline and the envelope value of salinity[5]. In this method, $\triangle T = 0.2$ ℃, $\triangle S = 0.01$, in a certain 2° ×2° square (132° - 134° E, 20° - 22° N), the result is shown in Fig. 2.

Because the number of observation data in each temperature section is different, the envelope of salinity changes acutely (Fig. 3). For example, in the 2.65 ℃ - 2.85 ℃ section, the number of observation data is 47, and the salinity lower bound , middle line and upper bound are 34.51, 34.57, 34. 65 respectively, while in the next section, 2.85 ℃ - 3.05 ℃, the number of observation data is 29, and the salinity lower bound , middle line and upper bound are 34.20, 34.57, 34.65 respectively. The salinity

lower bound changes from 34.51 to 34.20 acutely. Although $\triangle T$ changes, the analogous result appears.

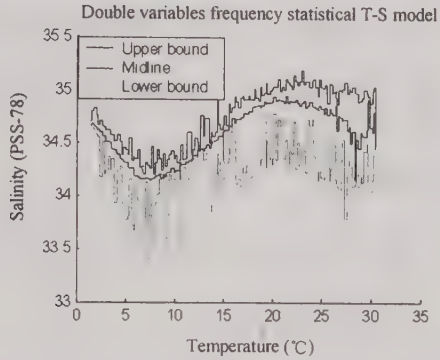

Fig. 2 130° - 132° E, 20° - 22° N, T-S model by bivariate frequency distributions method

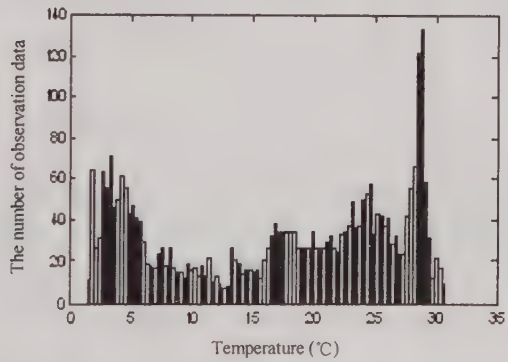

Fig. 3 130° - 132° E, 20° - 22° N, the number of observation data in each temperature section

1.2 Establishing T-S models by multinomial curve fit

A multinomial curve fit was used to define expected values and ranges of salinity versus temperature. The detailed information is as follows.

1.2.1 Historical data amalgamation

Most Chinese ARGO floats have been deployed in Northwest Pacific (0° N, 130° E - 15° N,

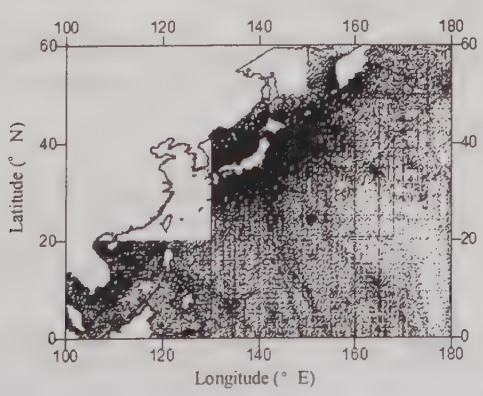

Fig. 4 Northwest Pacific historical temperature and salinity data distribution map

125° E - 23° N, 125° E - 30° N, 145° E - 0° N, 145° E). In this area, a large number of historical temperature and salinity profiles, such as CTD data, Nansen bottle data (Fig. 4) have been collected, processed and quality controlled by NMDIS, so that climatological T-S relationship background can be established by these data.

The northwest Pacific (100° - 180° E, 0° - 60° N) is divided into numerous 2° × 2° subregions by the American navy's square code.

1.2.2 Quality control of historical data

Although CTD data and Nansen bottle data have been processed through general quality control in NMDIS, this idea emphasizes the dataset climatological character, and the singular data are eliminated as follows.

1.2.2.1 Pick out singular data by Pa ¤ T rule [6]

In each 2° × 2° square, for each observed datum x_i, $v_i = x_i - \bar{x}$, , if $|v_i| > 3\sigma$, the datum is regarded as singular, in which $\bar{x} = \frac{1}{N}\sum_{i=1}^{N} x_i$ and N is the number of the observation value, and S is substituted for σ, in which $S = \sqrt{\sum_{i=1}^{N} v_i^2 /(N-1)}$

1.2.2.2 Test singular data by the statistical F method

Because the standard error and deviation in the Pa ¤ T method are influenced by the number of the samples, the singular datum must be tested by the statistical method. Statistical F method is used to check whether the singular datum is remarkably exceptional or not[7].

$$F = \frac{\frac{n+1}{n}(\bar{x} - x_{n+1})^2}{\frac{1}{n-1}\sum_{i=1}^{n}(x_i - \bar{x})^2} \qquad (1)$$

In which, x_{n+1} is the datum whose exceptional character will be checked, and n is the number of the rest data.

F approximately obeys F distribution which freedom is (1, n). Given the upside boundary data α = 0.05, look it up in the F distr ibution table to get the critical value F_α(1, n). When n is greater than 50, the critical value is 4. If F is greater than 4, the datum x_{n+1} will be eliminated, or this datum will be kept in the dataset.

1.2.3 Establishing T-S models by multinomial curve fit

First, in each 2° × 2° square, all historical temperature and salinity data are mapped to the T-S coordinate system, in which temperature T is taken as the independent variable, and salinity S as the attributive variable. A polynomial curve is applied:

$$S = f(T) \qquad (2)$$

which is based on the least square method to fit all the data points. From this curve, the salinity midline was got.

The points (T_i, S_i) above the line are selected to calculate the difference between S_i and $f(T_i)$:

$$\triangle S_i = S_i - f(T_i) \qquad (3)$$

The least square method is again applied to get another polynomial curve equation p

$$\triangle S = p_1(T_i) \qquad (4)$$

to fit the data points (T_i, $\triangle S_i$). For each temperature datum T_i, the salinity upper and lower bounds are

got from the following function:

$$S_{upper} = f(T_i) + g_1 \cdot p_1(T_i) \quad (5)$$

$$S_{lower} = f(T_i) - g_2 \cdot p_2(T_i) \quad (6)$$

S_{upper} is the salinity upper bound versus temperature, in which g_i is the weight coefficient.

In the same way, the salinity lower bound S_{lower} is got. As this model will be used for the quality control of data automatically, the weight coefficients are expanded empirically (Fig. 5).

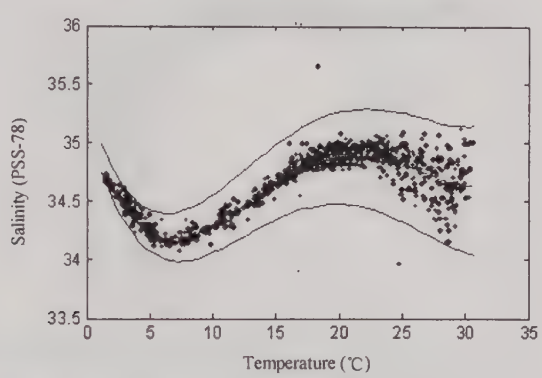

Fig. 5 Temperature and salinity data and the corresponding model in 24° - 26° N, 136° - 138° E

1.2.4 Establishing T-S model for the equatorial area and the high latitude area respectively

In high latitudes, when the temperature is between 0 ℃ and 2 ℃, the salinity varies from 31.5 to 34, while in other temperature sections the range is relatively small. At the same time, the salinity data in the temperature section 0 ℃ - 2 ℃, come from different water masses, and do not vary continuously, so the polynomial curve cant be applied directly (Fig. 6).

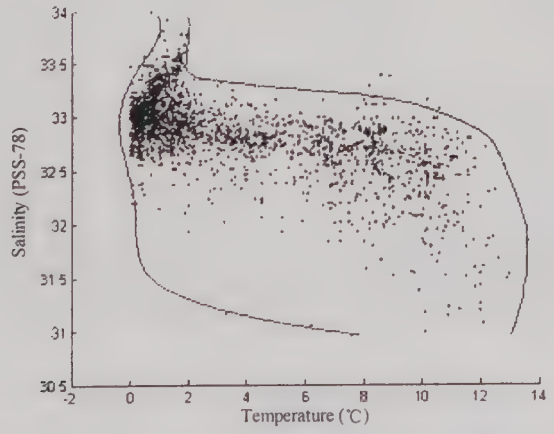

Fig. 6 Temperature and salinity data and the corresponding model in 44° - 46° N, 176° - 178° E

In the equatorial area, the salinity in the temperature section 15.5 ℃ - 23.5 ℃ doesn't vary continuously either. (Fig. 7)

In these areas, the data are divided into two sections. For example, in the equatorial area, the data are divided into two sections, section 1: the temperature below 15.3 ℃; section 2: the temperature above

15.3 ℃. In the section 1, temperature is taken as the independent variable, and salinity as the attributive variable. Then the first part of T-S model is got by the method described in Section 1.2.2. In the section 2, salinity is taken as the independent variable, temperature as the attributive variable and the second part was got, then the two models are combined with the right model in this area (Fig. 8).

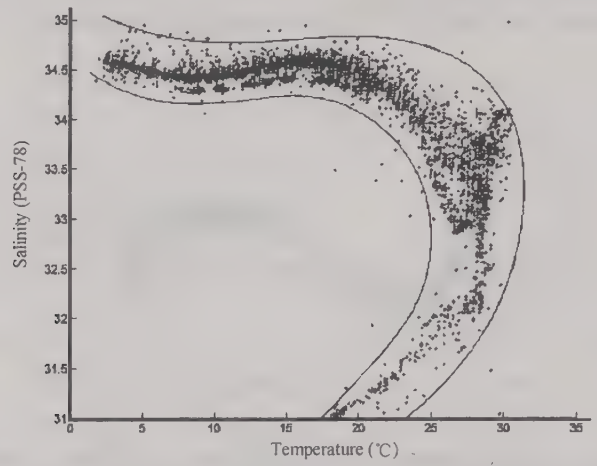

Fig. 7 Temperature and salinity data and the corresponding model in 14° - 16° N, 116° - 118° E

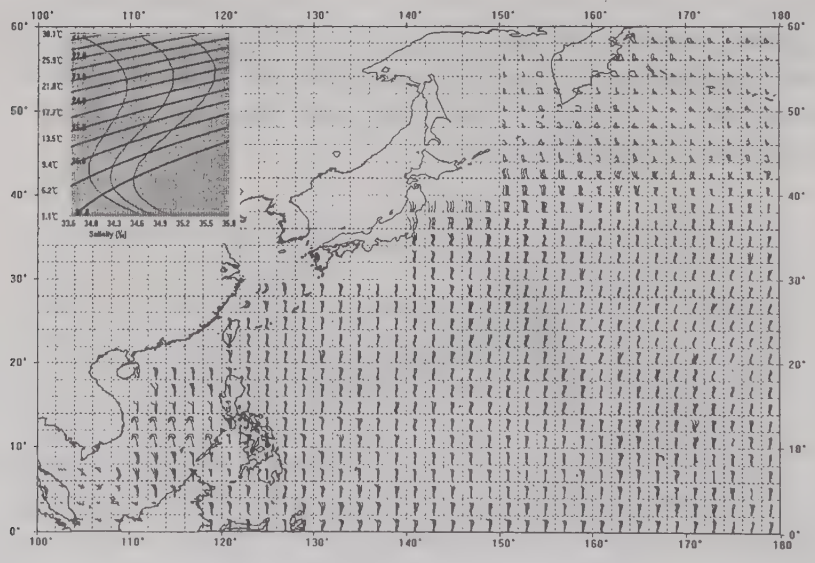

Fig. 8 Northwest Pacific 2° × 2° T-S model

2 Quality control of Argo data by T-S model

Compared with the result of the internationally recommended real-time QC, besides remarkably abnormal data (Fig. 9), some amphibolous data may be picked up (Fig. 10). Salinity measurements of ARGO float may experience sensor drifts owing to biofouling and a variety of other problems. This case

can't be picked up by the regular methods, such as range check, gradient check. As the temperature and salinity relationship is more stable in the ocean bottom, the T-S models can pick up these data (Fig. 10).

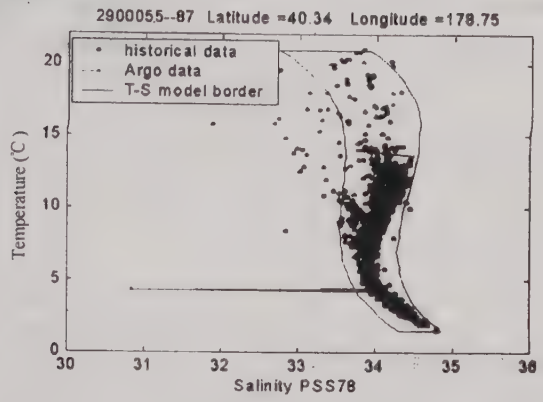

Fig. 9 The 91th cycle of float 2900055 temperature and salinity data, compared with the corresponding T-S model

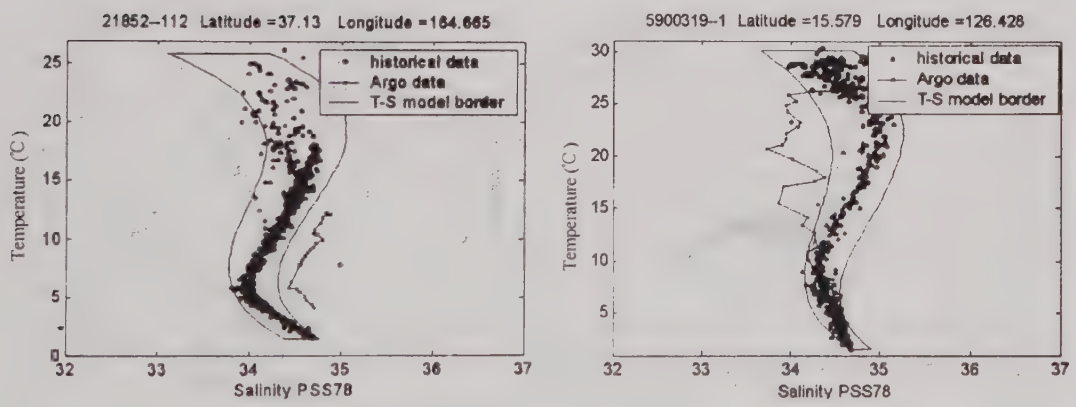

(a) 24th cycle of 21852 (b) The 1th cycle of 5900319

Fig. 10 Temperature and salinity data, compared with the corresponding T-S model

Because the T-S models are the climatological result based on the historical dataset, they can't detect some noise data effectively (Fig. 11). Moreover, because the spatial and temporal coverage of historical data is not dense enough, the scope is relatively small in some areas. ARGO data in good quality have been selected into the dataset and the model is rebuilt again (Fig. 12).

At present, besides the real-time quality control method recommended by the international ARGO program, T-S models are used in the manual quality control system. We check the ARGO data, and at the same time we modify the T-S models. Later, the T-S models will be used in the automatic quality control.

Until now there are 9 413 profiles, 588 802 stations, and Argo data in Northwest Pacific which have been detected by T-S models (Table 1).

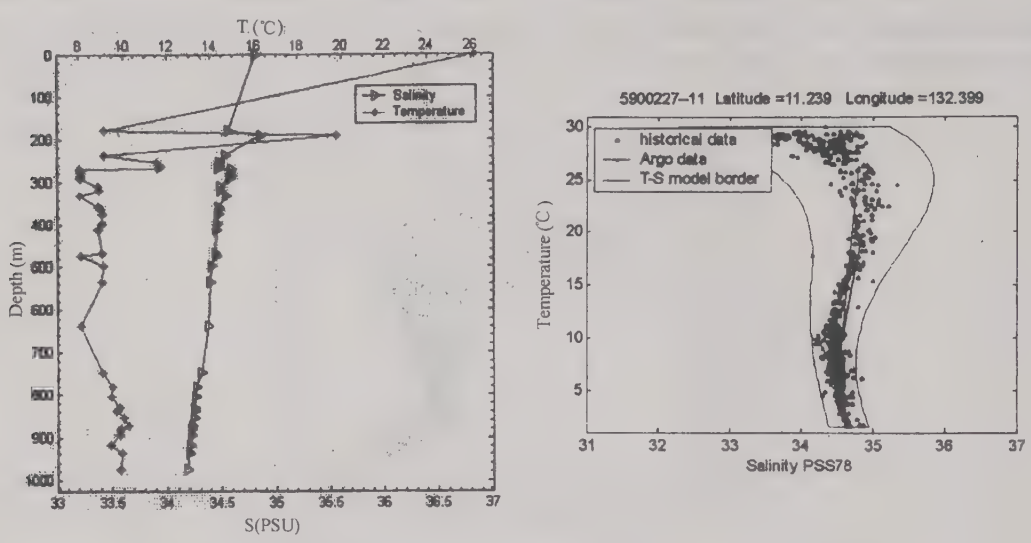

(a) Temperature and salinity profile data (b) Compared with the corresponding T-S model

Fig. 11 The 11th cycle of float 5900227

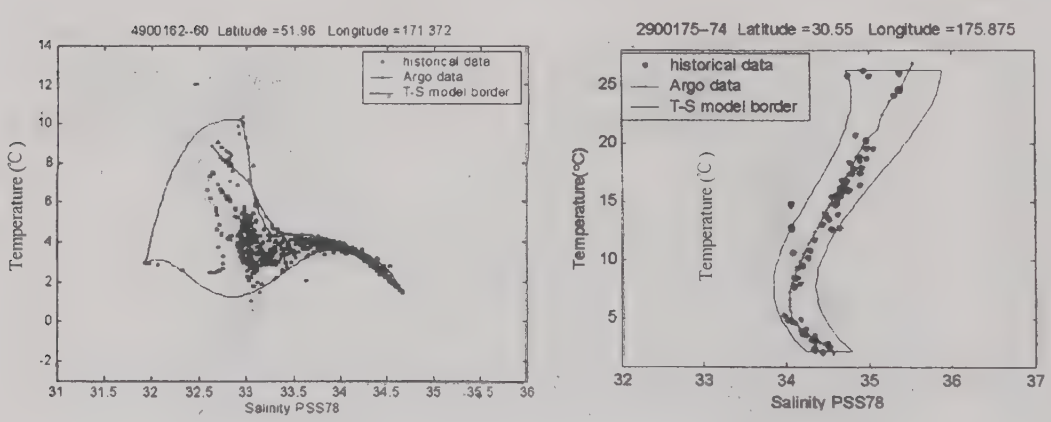

(a) The 74th cycle of float 2900175 (b) The 60th cycle of float 4900162

Fig. 12 Temperature and salinity data, compared with the corresponding T-S model

Tab. 1 The result of data being tested by T-S models in north west Pacific

The sum of the data detected	Error data detected by real-time QC [N]	Error data detected by T-S models	Error data detected by real-time QC and T-S models
566662 data /9162 profiles	24855 data	19031 data	4819 data

Note: Real-time QC is offered by the global Argo program

The result shows in the 19031 error data detected by T-S models, about 25 % (4819) cant be detected by real-time QC. Because the two methods are so different, manual check is done. The final result shows that in the error data detected by T-S models, about 50 % cant be detected by real-time QC,

about 25 % is also detected by real-time QC, and the rest 25 % may be erroeously detected. At present, we have adopted new temperature and salinity data to improve the T-S models. The result shows that the T-S model is more accurate than real-time QC and it is an effective complement to the QC method.

For the error data detected by T-S models, because salinity data are calculated by the temperature, pressure and conductivity data, the salinity data are taken as wrong data first. Then combined with other QC results, the temperature data are checked. For the error data, if they are obviously wrong, we will delete the data directly; if they are constant profile data, the quality control flags are added; if they are the conductivity sensor drift data, the Annie Wong method is adopted to correct the error data, and then the corrected data will be provided to users.

3 Discussion

In general, the T-S model is a useful tool of quality control for the temperature and salinity profile data. But this method is based on the historical data, and the number and the density of the data are critical to the models. The certainty of the estimation will depend on the spatial and temporal variability in the region. We have selected the lately the temperature and salinity profile data to modify the model.

Next, we will set up a new type of T-S model considering the spatial and temporal variations of water-mass structures.

References

[1] Emery W and J Dewar. Mean temperature-salinity, salinity-depth and temperature-depth curves for the North Atlantic and the North Pacific. Progress in Oceanogr., 1982, 11, 219-305.

[2] Li Fengqi, Su Yusong. The analysis of water mass. Qingdao: Qingdao Ocean University Press, 2000.

[3] Wong Annie P S , Gregory C Johnson and W. Brechner Owens. Delayed mode calibration of autonomous CTD profiling float salinity data by θ -s climatology. J. Atmos. Oceanic Technol., 2003, 20, 308-318.

[4] Molinelli E, J Stieglitz R. Specification for an STD/CTD system at the NODC. NODC, U. S., 1981.

[5] Worthington L. The Water Masses of the World Ocean: Some Results of a Fine-Scale Census. Chapter 2 (p. 42-69) of Evolution of Physical Oceanography. Scientific Surveys in Honor of Henry Stommel, B.A. Warren and C. Wunsch, eds., The MIT Press, Cambridge, Massachusetts, 1981, 623.

[6] Chen Shangji, Ma Jirui. Marine Data Processing and Analysis Methods and their Application. Beijing: China Ocean Press, 1991.

[7] Mei Changlin, Zhou Jialiang. Practical Statistical Method. Beijing: Science Press, 2002.

[8] Xu Jianping. Exposure of Argo Global Ocean Observation. Beijing: China Ocean Press, 2001.

Atmospheric Equilibrium Tide Theory

Zhang Deyu (张德宇)[1,2]
1 *China Ocean University, Qingdao 266003, Shandong, China*
2 *Naval Marine Hydrometeorological Center of Qingdao , Qingdao 266003, Shandong, China*

Abstract Based on the equilibrium tide theory of the seawater, a model of long-period variations in air pressure with the lunar motion is derived to advance the climatic tide concept and formulate the climatic tide formula, which provides useful leads for predicting the heavy meteorological catastrophe in Shandong area, even in China, as well as in the whole world.

Keywords air pressure, long period variations, model, climatic tide, atmospheric equilibrium tide

The heavy weather disasters such as heavy drought, rain-storm , tropical cyclone, extra-tropical cyclone, heavy ice year of Bohai Sea and so on have taken place in the Shandong area. They have seriously affected the safety of people's life and fortune in the Shandong area. Researching their periodical laws and characteristics is very important to predict them and prevent their damage as far as possible.

1 The long period of lunar motion

The moon moves from the west to the east of the Earth along an oval orbit, and the average distance between the earth and the moon is 384 401 km. Perigee means that the distance is shortest between the moon and the earth, *i.e.*, 356 400 km, and apogee means that the distance is longest between the moon and the earth, *i.e.*, 406 700 km. The line from perigee to apogee is called arch orbit that moves along the moons path, and its period is 8.8475 a (some tide reference books giving out 8.84732 Julian caledar year) or 3231.48 d. We call it arch orbit period.

The moon moves round the earth, and its orbit is called the moon's orbit. The moon's orbit from south to north intersect ecliptic is called ascending node, and the moon's orbit from north to south intersect ecliptic is called descending node. The ascending node of the moon moves along ecliptic from east to west and its period is 18.6133 a (some tide reference books giving out 18.6129 Julian caledar year) or 6 798.36 d, we call it ascending or descending node period. The ascending node of the moon moving along the ecliptic from east to west causes the variation of the moon's declination. In a period the moon's declination δ variations scope is $18^\circ\ 18' \leqslant |\ \delta\ | \leqslant 28^\circ\ 36'$.

2 The statistic facts between the foundation periods of heavy weather disaster in the Shandong province area and the long period of the lunar motion variations

2.1 Establishment of data samples

Received on June 2, 2003

Tab. 1 Incomplete statistics about the great heavy debacles of the atmosphere in Shandong province

Sample serial number	Disaster name	Occurrence region	Occurrence time	Time interval (a)	Disaster characteristics	8.8475 a multiples	4.4238 a multiples	18.6133 a multiples	9.3067 a multiples	Title of disaster
1A	Tropical storm	Bohai Bay	Apr. 28-29, 1895		Death toll: more than 1 000 people. The water level at Dagu rising to 6.1 m					The biggest tropical storm tide of Bohai Bay
1B	Tropical storm	Laizhou Bay	Apr. 23, 1969	74	Yangjiaogou storm surge, 3.55 m	8.364	16.728	3.976	7.951	The biggest temperate cyclone tide in the world
2A	Heavy ice year	Bohai Sea	winter of 1895							One of the 6 heavy ice years from 1895 to 1992
2B	Heavy ice year	Bohai Sea	Feb. - Mar., 1969	74	Damaging 58 passenger and cargo ships	8.364	16.728	3.971	7.951	The greatest heavy ice year in the 20th century
3A	Drought	Shandong, Henan, Hebei provinces	1876-1878		Death toll: 13 million people					One of the 29 catastrophic events from 1696 to 1920 each with a death toll of 100 000 people
3B	Drought	Shandong, Henan, Shanxi provinces	1920	42 to 44	Death toll: 500 000 people	4.747 to 4 972	9.493 to 9.946	2.256 to 2.364	4.512 to 4.728	One of the 29 catastrophic events from 1696 to 1920 each with a death tol of 100 000 people
4A	Drought	Shandong, Henan, Shanxi provinces	1920		Death toll 500 000 people					One of the 29 catastrophic events from 1696 to 1920 each with a death toll of 100 000 people
4B	Drought	Shandong province, west of Henan province	1992	72	The Yellow River runs out of water flows.	8.138	16.276	3 868	7.736	Great heavy drought in Shandong and the west of Henan province
5A	Great flood	Great waterlogging of Yishu river in Shandong province	1957							
5B	Great flood	Heavy rainstorm in Heze, Linyi, Jining, Zaozhuang, Liaocheng etc. of Shandong province	Aug. 4-5, 1993	36	Death toll: 36 people, with a loss of over 6 billion Yuan	4 069	8.138	1.934	3 868	An average precipitation of 360 mm in Yucheng, and more than 500 mm of precipitation in 12 villages and towns
6A	Typhoon	Shandong peninsula and Qingdao city	Aug. 31-Sept. 1, 1939		Death toll: 17 people, with a loss of 7 96 billion Yen					One of the three typhoons affecting Qingdao most in the 20th century
6B	Typhoon	Shandong peninsula and Qingdao city	Aug. 31-Sept. 1, 1992	53	Losing beyond 24 hundred million Yuan in Shandong province	5 990	11.981	2.847	5.695	One of the three typhoons affecting Qingdao most in the 20th century
7A	Typhoon	Qingdao city	Aug. 29-Sept. 6, 1956							One of the six typhoons affecting Qingdao most after liberation
7B	Typhoon	Qingdao city	Aug. 27-Sept. 1, 1974	18		2 034	4 069	0 967	1.934	One of the six typhoons affecting Qingdao most after liberation
8A	Great flood of the Yellow River	the Yellow River	1117 (Zhenghe 7th year of Emperor Huizon of Song dynasty)		Death toll more than one million people					The greatest death toll caused by the burst of the Yellow River
8B	Great flood of the Yellow River	the Yellow River	Jul., 1958	841		95.055	190 110	45 183	90.365	Greatest flood in the Yellow River in the 20th century

The frequency of heavy weather disaster in the Shandong province area is few, and the frequency of twice occurrence in the same place of the same kind heavy weather disaster is also few, too. Due to all kinds of environmental limits, the author only collects 15 examples of heavy weather disasters having taken place in the Shandong area or having some relationship with this area. The author classifies them into 8 groups (Table 1).

2.2 The foundation period separating and abstracting process of heavy weather disaster in the Shandong area

We calculate every samples time interval of the 8 groups of heavy weather disaster in the Shandong area. Using every time interval, we divide the arch orbit period, half period and the ascending and descending node periods, half period, and then we get the multiple of them. This is the foundation period separating and abstracting process.

2.3 Statistics for the appearing total number of the arch period, half period and the ascending and descending node period, half period of the moon's orbit

There are 5 groups in 8 groups of heavy weather disaster in Shandong area, occupying 62.5 %, whose multiple absolute error dose not exceed 0.1 multiple of the arch orbit period, there are 4 groups in 8 groups of heavy weather disaster in Shandong area, occupying 50 %, whose multiple absolute error dose not exceed 0.1 multiple of the arch orbit half period; there are 5 groups in 8 groups of heavy weather disaster in Shandong area, occupying 62.5 %, whose multiple absolute error dose not exceed 0.1 multiple of the ascending and descending node periods, and there are 4 groups in 8 groups of heavy weather disaster in Shandong area, occupying 50 %, whose multiple absolute error dose not exceed 0.1 multiple of the ascending and descending node half periods.

From the above statistics we can draw the following conclusion: The foundation period of the heavy weather disaster in Shandong area includes the main important period 8.8475 a, or 323.48 d, which is the same as the arch orbit period, and the secondary main important period is 4.4238 a, which is the same as the arch orbit half period; the foundation period of the heavy weather disaster in Shandong area includes the next main important period 18.6133 a, or 6 798.36 d, which is the same as the ascending and descending node period, the next secondary main important period is 9.3067 a, which is the same as the ascending and descending node half period.

3 The physical meaning of foundation period

3.1 According to astronomy, the perigee, the apogee and the south biggest declination and the north biggest declination of the moon's orbit all belong to the strange point of astronomy. In the author's opinion, these strange points of astronomy of the moon's orbit may result in the discontinuous atmospheric movement: At one particular region of the earth the high pressure system sinks strongly, and at the other particular region of the earth the low pressure system rises strongly. At last it causes the heavy weather disaster.

3.2 According to the equilibrium tide theory as well as the similarity in fluid characteristic of the atmosphere and the seawater, especially on monthly, yearly, or more than ten years time scales, we suppose the atmosphere having equal tide with the seawater, which we call the atmospheric equilibrium tide theory. According to the tidal height formula (1) of the equilibrium tide[1].

$$\zeta = \frac{3}{2}\frac{M}{E}\left(\frac{a}{D}\right)^3 a\left(\cos^2\theta - \frac{1}{3}\right) \tag{1}$$

In the formula (1), ζ is amplitude of the seawater, M is the mass of the moon, E is the mass of the earth, a is the radius of the earth, D is the average distance between the earth and the moon and θ is the zenithal distance of the moon. The pressure amplitude P_m of the moon's atmospheric tide and the pressure amplitude P_s of the sun's atmospheric tide equal:

$$P_m = 17.49 \times (3\cos^2\theta - 1) \tag{2}$$

$$P_s = 8.02 \times (3\cos^2\theta_s - 1) \tag{2.1}$$

When the average distance is D = 384 401 km between the earth and the moon; when the average distance is D_s = 149 600 000 km between the earth and the sun. Taking every parameters value we can calculate P_m and P_s (precision arriving at two digits after decimal point), inside formula (2) and (2.1), P_m, P_s unit is hPa, $\rho = P/RT$, ρ is function of pressure P and temperature T, because of $P = P(X, Y, Z, t)$, $T = T(X, Y, Z, t)$ is function of time and space, therefore ρ is function of time and space, too. For the convenience of discussing problems we suppose the air density is the same and take the air density of sea level.

$$\rho = 1.225 \times 10^{-3}\ \text{g/cm}^3 \tag{3}$$

Inside the formula (2), θ is the zenithal distance of the moon; inside formula (2.1) θ_s is the zenithal distance of the sun. Formula (2.2) is the pressure amplitude P of atmospheric tide we get at last, and P unit is hPa:

$$P = P_m + P_s = 17.49 \times (3\cos^2\theta - 1) + 8.02 \times (3\cos^2\theta_s - 1) \tag{2.2}$$

When the shortest distance is D =356 400 km between the earth and the moon, the perigee pressure amplitude,

$$P_{mj} = 21.95 \times (3\cos^2\theta - 1) \tag{4}$$

When the farthest distance is D = 406 700 km between the earth and the moon, the perigee pressure amplitude,

$$P_{my} = 14.77 \times (3\cos^2\theta - 1) \tag{5}$$

the variation,

$$P_{my} - P_m = -2.72 \times (3\cos^2\theta - 1) \tag{6}$$

$$P_{mj} - P_{my} = 7.18 \times (3\cos^2\theta - 1) \tag{7}$$

Inside the formula (7), the variation between the perigee pressure amplitude and the apogee pressure amplitude is $\Delta P_{yj} = P_{mj} - P_{my}$.

The pressure amplitude of the moon perigee enlarges 25.5 % more than the average distance pressure amplitude; the pressure amplitude of the moon apogee reduces 15.6 % as compared with the average distance pressure amplitude. Therefore the variety of pressure amplitude is very observable.

Because the moon moves from the west to the east of the earth along an oval orbit, the line from perigee to apogee is called arch orbit that moves along the moon's path, and its period is 8.8475 a, so inside a period, the pressure amplitude of atmospheric tide is not equal, and there is an amplitude variety

of 21.54 hPa in theory. Owing to the symmetry of the earth, the amplitude variety of 21.54 hPa can finish in half period of arch orbit or 4.4238 a. So, the heavy weather disasters in Shandong area include the main important period 8.847 5 and the sub main important period 4.4238 a. The difference between them is that the land and sea of the earth is not perfectly symmetric. According to the definition that macula 22 a is the main important period and 11 a the sub main important period, we define the main important period 8.8475 a of the heavy weather disasters as the first period and the sub main important period 4.4238 a of the heavy weather disasters as the first half period.

Based on (7) we construct a periodical function P_{yj} Inside formula (7.1), P_{yj} is the variation of the atmospheric tide pressure amplitude in 8.8475 a equaling a period of the moon arch orbit.

$$P_{yj} = 3.59 \times \cos(2 \times 3.14159 / 8.8475 \times t) \times (3\cos^2\theta - 1) \tag{7.1}$$

Inside the formula (2), the atmospheric tide pressure amplitude has relationship with the zenithal distance of the moon, Formula (2) can spread as follows:

$$P_m = 52.47\left[\frac{3}{2}\left(\sin^2\varphi - \frac{1}{3}\right)\left(\sin^2\delta - \frac{1}{3}\right) + \frac{1}{2}\sin 2\varphi \sin 2\delta \cos T_1 + \frac{1}{2}\cos^2\varphi \cos^2\delta \cos 2T_1\right] \tag{8}$$

$$P_{m_0} = 52.47\left[\frac{3}{2}\left(\sin^2\varphi - \frac{1}{3}\right)\left(\sin^2\delta - \frac{1}{3}\right)\right] \tag{9}$$

$$P_{m_1} = 52.47\left(\frac{1}{2}\sin 2\varphi \sin 2\delta \cos T_1\right) \tag{10}$$

$$P_{m_2} = 52.47\left(\frac{1}{2}\cos^2\varphi \cos^2\delta \cos 2T_1\right) \tag{11}$$

$$P_{\delta_{min}} - P_{\delta_{max}} = -3.42 \times (3\sin^2\varphi - 1) \tag{12}$$

The above-mentioned formula T_1 is time angle, P_{m1} and P_{m2} is the variation of the atmospheric tide pressure amplitude in a day or in a half day, and they cant change pressure in a long time period, while only P_{m0} changes with δ declination of the moon in a long time period of 18.613 3 a. Inside the formula (9), the δ declination of the moon changing from $\delta_{min} = 18°\ 18'$ to $\delta_{max} = 28°\ 36'$ needs 9.3067 a, which is just a half period of the ascending and descending node period 18.613 3 a.

In the equator region, φ is zero, the variation of the atmospheric tide pressure amplitude is 3.42 hPa in a half period of the ascending and descending node period in theory, so we define the main important period 18.6133 a of the heavy weather disasters as the second period and the sub main important period 9.3067 a of the heavy weather disasters as the second half period.

About (12) we construct a periodical function $P_{m\delta}$:

$$P_{m\delta} = 1.71 \times \cos(2 \times 3.14159 / 18.6133 \times t_2) \times (3\sin^2\varphi - 1) \tag{12.1}$$

Inside formula (12.1), $t_2 = t_1 + t_0$, t_2 unit is Gregorian calendar year, in the light of the longitude and latitude of a local place, t_0 takes a special value from 0 to 8.8475 a, the scope of t_1 is as follows:

$$0 \leqslant t_1 \leqslant n \times 8.847\,5 \text{ a},\ n = 0, 1, 2, 3, \cdots, n \tag{12.2}$$

Formula (12.1) is the atmospheric tide pressure amplitude formula when the δ declination of the moon changes from $\delta_{min} = 18°\ 18'$ to $\delta_{max} = 28°\ 36'$ next to $\delta_{min} = 18°\ 18'$ in the whole period of 18.613 3 a. We combine formulas (7.1) and (12.1) into the formula (13), which is our model of long

period variations in air pressure, and is called the climatic tide formula.

$$P_{yj\delta'} = 3.59\times\cos(2\times3.14159/8.8475\times t)\times(3\cos^2\theta-1)+1.71\times\cos(2\times3.14159/18.6133\times t_2)\times(3\sin^2\varphi-1) \quad (13)$$

Inside formula(13), P_{yj} unit is hPa, $t_2 = t_1 + t_0$, t_2 unit is Gregorian calendar year, According to the longitude and latitude of a local place, t_0 takes a special value from 0 to 8.8475 a, and the value scope of t_1, t is as follows:

$$0 \leqslant t_1 \leqslant n\times 8.847\,5 \text{ a}, \ n = 0, 1, 2, 3, \cdots, n \quad (12.2)$$

$$0 \leqslant t \leqslant n\times 8.847\,5 \text{ a}, \ n = 0, 1, 2, 3, \cdots, n \quad (12.2)$$

4 Conclusion

In this paper, we have found out that the heavy weather disaster in Shandong area includes the foundation period: the first mainly important period of 8.8475 a, or 323.48 d, which is the same as the arch orbit period, and the first sub mainly important period of 4.4238 a, which is the same as the arch orbit half period; the foundation period of the heavy weather disaster in Shandong area includes the next main important period of 18.6133 a, or 6798.36 d, which is the same as the ascending and descending node period, the next sub mainly important period of 9.3067 a, which is the same as the ascending and descending node half period. Based on the equilibrium tide theory, the model of long period variations in air pressure with the lunar motion is derived to advance the climatic tide concept and formulate the climatic tide formula, which provides useful leads for predicting the heavy meteorological catastrophe in Shandong area, even in China, as well as in the whole world.

References

[1] Yang Dianrong. Oceanography. Beijing: High Education Press. 1986, 234-236.

[2] Chang Zhengchuan *et al.* Meteorological disaster and countermeasures. Beijing: Meteorology Press. 1992, 216-226.

Evolution of Modern Yellow River Delta Coast

Yin Yanhong (尹延鸿) Zhou Yongqing (周永青) Ding Dong (丁 东)
Qingdao Institute of Marine Geology, Qingdao 266071, Shandong, China

Abstract This paper deals with the development and evolution of modern Yellow River delta and the erosion or deposition rates of its different sections. In June, 1996, Yellow Rivers terminal course was artificially turned eastwards to empty into the sea and then the 11th lobe of the modern Yellow River delta began to form. This course change may mark the beginning of the 3rd subdelta formation. As a result of that, the Yellow River delta advances towards east by north with the 1st, 2nd and 3rd subdeltas arranged in succession. Coast zone in the deltaic area is divided into 7 different sections according to their different erosion or deposition rates: the relatively stable section from Dakou River to Shunjiang Stream; the weakly retreating section from Shunjiang Stream to the Tiaohe River mouth, the strongly retreating section from the Tiaohe River mouth to the station 106, the artificially stable section due to stone dam protection from the station 106 to Gudong Oilfield, the strong deposition section from Gudong Oilfield to Dawenliu Haipu, the weakly deposition section from Dawenliu Haipu to the Zimai Stream mouth, and the stable section from the Zimai Stream mouth to the Jiaolai River mouth. It is predicted that the erosion and deposition situations of the sections will nearly remain the same in 10 years, but the retreating and silting-up rates will tend to become slower gradually. Human activities have an evident influence on the changes of the coastline.

Keywords progression and retreat rates, coast evolution, modern Yellow River delta, subdelta

Introduction

The study area encompasses the Yellow River delta coast and part of the Laizhou Bay coast from the Dakou River mouth in the west to the Jiaolai River mouth in the east, and covers a coastline of more than 300 km (Fig. 1).

The modern delta was formed after the river changed its course from the Yellow Sea to the Bohai Sea in 1855. It is a very young delta of about 147 years old.

The Yellow River delta is a river-dominated delta similar to those of Mississippi River[1], Fraser River [2] and Ganges-Brahmaputra[3], but the Yellow River delta is the fastest aggrading delta in the world because the river contains a high amount of silt and the Bohai Sea is very shallow. Therefore the Yellow River delta coast zone shows a fast progression and coastline change.

There are many factors that influence the coastal evolution of the Yellow River delta such as discharge and sediment load, coastal dynamics, sea-level changes, geomorphic and geologic features, vegetation and human activities. Of course, the coastal change of the area is mainly controlled by the

Received on May 13, 2004
The study is supported by the China National Natural Science Foundation (project No. 49476282) and by the Shandong Province Natural Science Foundation (project No. 98E04075).

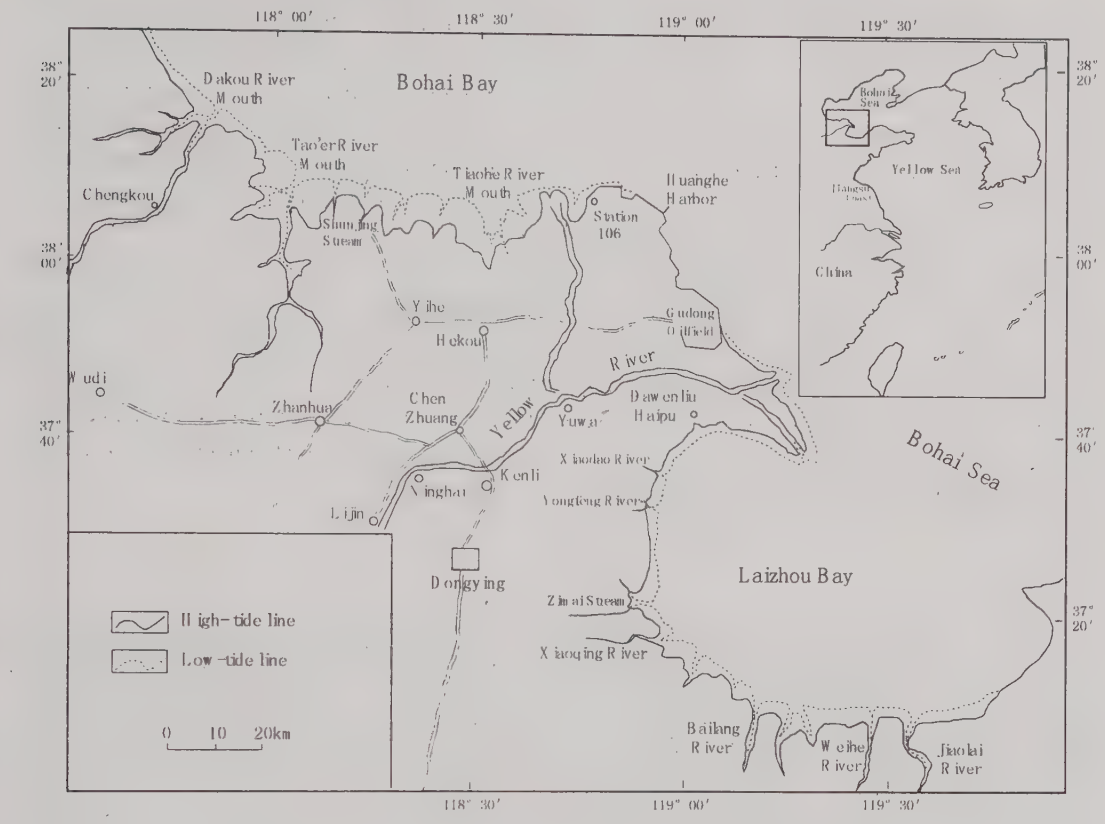

Fig. 1 The geographic location of the modern Yellow River delta

Yellow River. Since 1976, the Yellow Rivers lower reaches have been dry frequently, and the discharge and sediment supply have decreased considerably due to water consumption in the upper and intermediate reaches. According to the measured data from the Lijin station located at the lowest reach of the Yellow River, the mean annual discharge was 344.34×10^8 m^3 from 1950 to 1999. The 1960s had the largest discharge with an annual mean of 501.1×10^8 m^3. The 1970s had an annual mean of 311.0×10^8 m^3, a decrease by 37.9 % when compared to the 1960s due to increase in industrial, agricultural and everyday life water consumption. The 1980s experienced a further decrease by 43.3 % (annual mean 284.1×10^8 m^3) compared to the 1960s, and the 1990s had an annual mean of 145.0×10^8 m^3, a decrease by 71.1 % compared to the 1960s. Annual silt supply has also decreased greatly. From 1950 to 1999, a mean annual silt supply of 8.67×10^8 ton was carried through the Lijin station (the last hydrological station before the Yellow River water into the sea). The 1950s had the largest silt supply with an average of 13.19×10^8 ton per year, and the 1990s had the smallest silt supply with an average of 3.95×10^8 ton per year, a decrease by 70 % when compared to the 1950s. In recent years since 2000, the annual discharge and silt supply of the Yellow River are still quite small, similar to the 1990s.

Many scientists have studied the Yellow River delta, including the coastal sedimentation and its changes [14-14], the river avulsion and the geomorphic features[15-21], and the human impact on the delta[22].

Some of these studies of the Yellow River delta involved some delta coastal evolution, but little research of the present progression and retreat rate in different delta sections in detail was made.

Moreover in recent years, great changes have taken place resulting in diminished silt discharge and river course changes. Recently, the water use of the upper reaches, Xiaolangdi Dam construction and dry weather frequently made the river nearly dry in the lower reaches, and thus less silt was brought to the sea. As a result of the slower deposition at the mouth area, erosion became serious along some coast. Furthermore, in June, 1996, the Yellow Rivers course was artificially turned eastwards to empty into the sea and then the 11th lobe of the modern river delta began to form. Further detailed studies of the coast evolution are necessary in order to develop and control the delta coast.

This paper deals with the development and evolution of the modern Yellow River delta and the erosion or deposition rates of its different sections. We have subdivided the coastal zone into 7 different sections according to their different erosion or deposition rates. It is predicted that the erosion and deposition situations of these sections will nearly remain the same in 10 years, but the erosion or deposition rates will tend to become slower gradually. Human activities have an evident influence on the changes of the coastline. This research will favor predicting the future development and the coastal protection and control of the Yellow River delta.

1 Methods

In recent years, a lot of geological investigations have been made in this research area. In the shallow sea area, some bathymetric surveys were done, and the survey results in different years were compared. Some topographical and geological tidal flat profiles vertical to the coast were also surveyed. The profiles were completed during low tidal periods, and the leveling instrument was used in surveying the tidal flat profiles. According to the measured results of different years in every profile, the erosion or deposition rates along the coast have been obtained. Many samples were collected along the profiles, and sample tests and analyses were made. We also investigated some old fishmen and local villagers along the delta coast in order to understand the coastal changes. In order to analyse the coastline changes in recent years, we have also analyzed many satellite images, especially those taken in 1976, 1978, 1983, 1985, 1988, 1992, 1993, 1994, 1997, 1998, 1999, 2000 and 2001 and some air photographs. Although the Yellow River delta is in a small tidal environment, the tidal influence was also considered in the interpretation of satellite images. For this study, many topographic, geomorphic and geologic data as well as maps in different years have been collected and analyzed. According to all the data, the comprehensive analysis of and the suggestions on the delta coast control have been made.

2 Results and discussion

2.1 Coastline change rates during different periods

Evolution of the delta coastline is closely related to river avulsions. The whole Yellow River delta is characterized by the continuous erosion and deposition, but generally, the deposition dominates, and the coastline progresses gradually. The changes of the modern delta coastline can be summarized in several stages (Fig. 2).

2.1.1 1855—1934

After the Yellow River avulsed in Henan Province in August 1855, the river ran northwards via Shandong Province, and emptied into the Bohai Sea at Ninghai. An extensive fan-shaped accumulation body was formed from Zimai Stream in the east to Taoer River in the west with Ninghai as the apex.

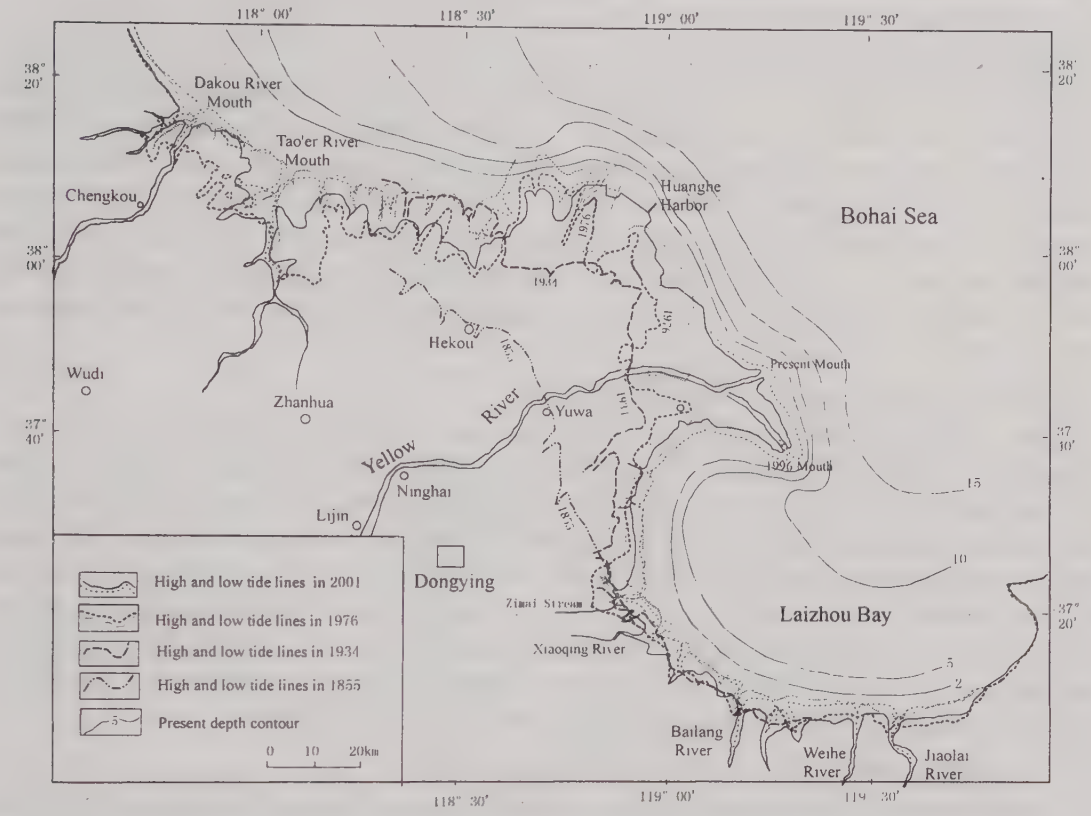

Fig. 2 The coastline changes of the modern Yellow River delta during different periods. The high and low tidal lines in the 4 important stages since 1855 are shown.

From 1855 to 1934, the Yellow River avulsed 6 times, and it swept the deltaic fan surface to form the 1st subdelta. The coastline of 1855 was near Hekou and Yuwa (Fig. 2). During the 49 years from 1855 to 1904, the delta progressed eastwards and extended 20 km into the sea at an average rate of 0.4 km/a. During the 25 years from 1904 to 1929, the delta mainly advanced to the north, to the present Tiaohe River and Taoer River mouths. In 1934, the coastline evidently extended beyond the 5 m depth contour of 1855 and reached the 7 - 8 m water depth. During the period of 1904 to 1934, 18 km progression occurred, 0.72 km/a on average. In the 5 years from 1929 to 1934, the Yellow River avulsed southeast and the coast progressed 4 - 5 km, with an average rate of 0.8 - 1 km/a[23]. From the Xiaodao River mouth to the south, the deposition rate decreased, and near the Zimai Stream even some erosion occurred. In general, it seems that the larger the area swept by the terminal course, the slower the deposition rate, and the smaller the area, the faster the rate.

2.1.2 1934—1976

Since 1934, the apex of the Yellow River delta fan shifted downstream from Ninghai to Yuwa and the 2nd subdelta began to form. During the 42 years from 1934 to 1976, the river avulsed 4 times. The area between the Tiaohe River mouth and Huanghe Harbor received the most of the sediment, resulting in a 20-km progression of the coastline, 0.5 km/a on an average. The area between Dawenliu Haipu and the Yongfeng River mouth progressed fast from 1934 to 1953, but it eroded from 1953 to 1976, and as a result, the coastline shifted seaward by 5 km at an average rate of 0.12 km/a.

2.1.3 1976—2001

Since the Yellow River avulsed to the east at Yuwa in May 1976, the coastline has progressed rapidly. From 1976 to the present, the coastline between Dawenliu Haipu and Gudong Oilfield advanced over 40 km, at an average rate of 1.6 km/a. This occurred because silt supply and deposition became concentrated in this area. The terminal part of the course shifted in a small scope in June 1996, the delta lobe still continued to progress in this area, and the new coastline has extended about 8 km. To the contrary, the coast between the Tiaohe River mouth and Huanghe Harbor suffered strong erosion. The coastline retreated 5 to 7 km at an average rate of 0.2 - 0.3 km/a. Human activities during this period made the coast from Dakou River to Taoer River move seaward. The other coast sections remained nearly unchanged.

2.1.4 Summary of developments between 1855—2001

Since 1855, the Yellow River built up a wide deltaic plain. In 1855, the coastline was near Hekou-Yuwa (Fig. 2). The present coastline is located from Huanghe Harbor to the Gudong Oilfield, about 40 km to the northeast of the former coast at an average rate of 0.27 km/a. The largest advance occurred from Yuwa eastwards to the river estuary of 1996 (about 52 km, on the average 0.36 km/a). The coast near the Yongfeng River moved 10 km seawards at a rate of 0.07 km/a. The Laizhou Bay coast south of the Zimai Stream changed little, and eroded slightly. In the north of the Yellow River delta near the Tiaohe River mouth, the coast progressed 15 - 20 km at an average rate of 0.1 - 0.14 km/a[24]; The coast from Dakou River to Taoer River remained nearly unchanged, but in recent years human activities of coast protection and harbor construction have made some part advance to the sea.

2.2 Development tendency of the modern Yellow River delta

The modern delta was formed after the river changed its course from the Yellow Sea to the Bohai Sea in 1855. The delta between Zimai Stream in the east and the Taoer River mouth in the west (Fig. 1), with Ninghai as its apex, stretches to the 16m depth contour in the sea. It is a very young delta about 147 years old. The sediments mainly consist of the rivers silt and clayey silt in the form of successively growing lobes superimposed on one another. The lobes were formed because of successive avulsions. The newly formed channels followed the maximum gradient into low-lying areas. Therefore, simultaneously formed lobes are very probably not neighbors in space. Several lobes with nearly the same apex made up a subdelta[24]. The modern Yellow River delta is made up of several subdeltas. From 1855 to 1934, the 1st fan-shaped subdelta was formed with Ninghai as the apex (Fig. 3, see channels 1 - 6). From 1934 to 1996, the 2nd fan-shaped subdelta was formed with Yuwa as the apex. Thus, the avulsion node shifted downstream (channels 7 - 10). In June 1996, the most recent avulsion took place and the new river channel (channel 11) turned east into the sea at about 7 km northeast of Dawenliu Haipu (Fig.3).

As a result of embankments, the Yellow River didnt change its course since 1976 until June 1996 when the river was artificially turned to the east near Dawenliu Haipu, and the 11th lobe of the modern delta began to form (Fig. 3). We suppose that this course change marks the beginning of the 3rd subdelta formation. This is supported by the length of the time intervals between formation of the subdeltas. As can be seen from Fig.3, it took nearly 80 years (1855—1934) to form the 1st subdelta. The 2nd subdelta was formed in 62 years (1934—1976). It was formed in a shorter time than the 1st one, and the 2nd subdelta area is also smaller. There is a distance of 35 km between the 1st apex (near Ninghai) and the 2nd one (east of Yuwa), and of 40 km between the 2nd apex and the supposed 3rd one (near Dawenliu Haipu). The distances are more or less the same. Therefore, we think that the avulsion of June 1996

marked the beginning of the 3rd subdelta deposition. If correct, this means that in the future, the terminal part of the river will shift around Dawenliu Haipu as the apex. The new subdelta in the future is expected to progress to the northeast (Fig. 4). We infer that the 3rd subdelta will have a smaller area than that of the 2nd one and grow in a few decades, probably 40 - 60 years.

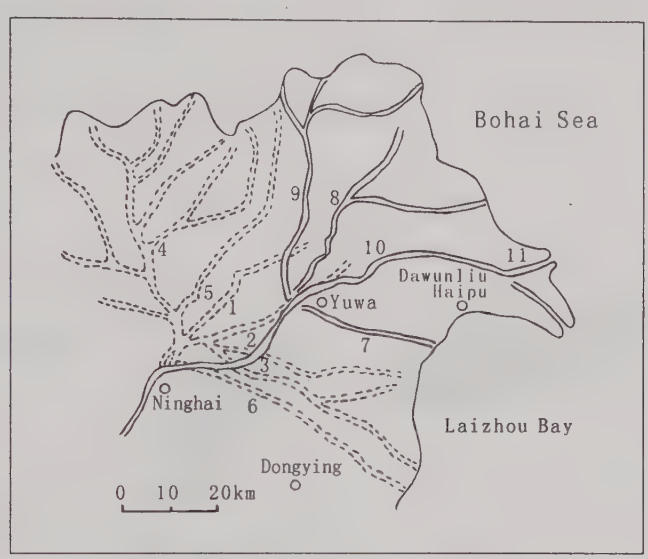

Fig. 3 Avulsions of the river channels in the modern Yellow River delta

Period of existence of channels:

1: 1855-06—1889-03; 2: 1889-03—1897-05; 3: 1897-05—1904-06; 4: 1904-06—1926-06; 5: 1926-06—1929-08; 6: 1929-08—1934-08; 7: 1934-08—1953-07; 8: 1953-07—1964-01; 9: 1964-01—1976-05; 10: 1976-05—1996-06; 11: 1996-06—present

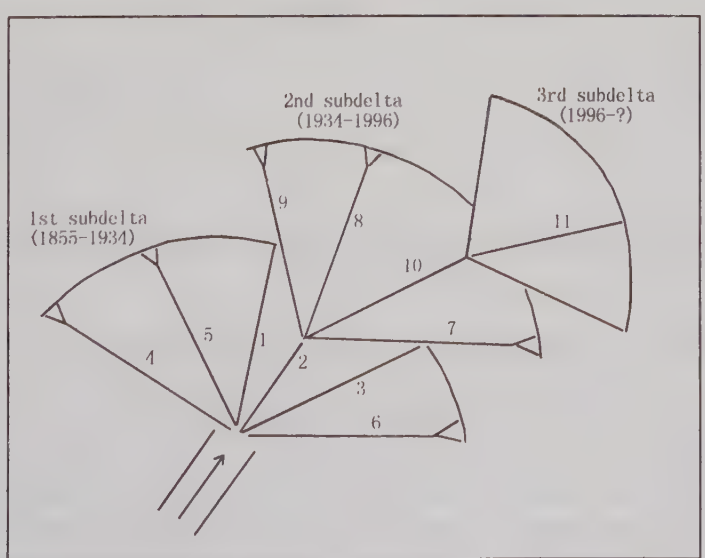

Fig. 4 The development of the modern Yellow River delta (compared to Fig. 3)

2.3 Present coastline change rates and prediction of development in the next 10 years

Based on bottom materials, landforms, geomorphic features, hydrodynamic characteristics and progression and retreat rates, the coast can be subdivided into 7 different sections: a relatively stable section, a slow retreat section, a strong retreat section, an artificially stable section due to stone dam protection, a strong progression section, a slow progression section, and a stable section (Fig. 5). Generally speaking, the river mouth may not be changed in a large scope in the next 10 years since it shifted in 1996. According to the present situations of the different coastal sections, we can predict their development tendency over the next 10 years, and make some suggestions for coast protection.

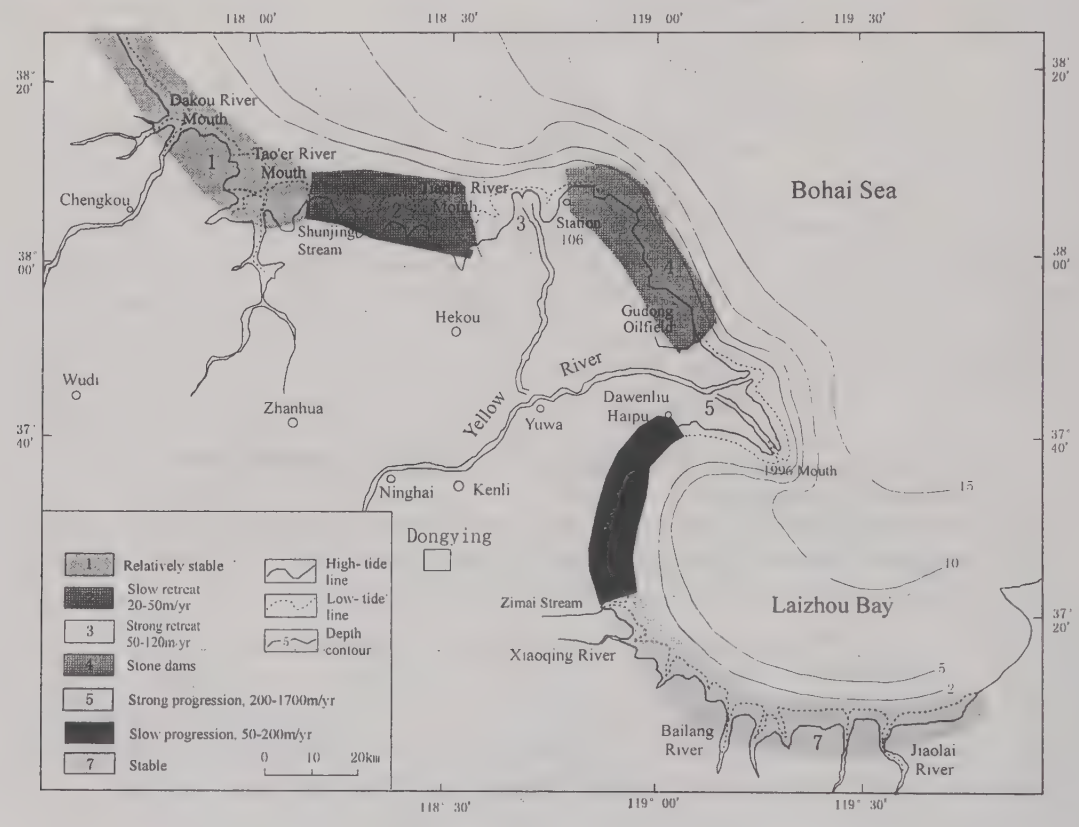

Fig. 5 The division of 7 different coastal sections and predictions of progression or retreats in the next 10 years

2.3.1 Coastal Section from the Dakou River Mouth to Shunjiang Stream (Section 1)

This section is relatively stable. During the period of 1048—1128, the Yellow River flowed into the sea around the mouth of Taoer River and the mouth of Dakou River. This course was abandoned in 1128 AD. Now, the coastal section has a winding high-tide line, a relatively smooth low-tide line, and an intertidal zone of 5 - 15 km in width with an average gradient of 0.032 %. From the late 1970s to the early 1980s, the section was stable or eroded slightly. Since 1983, construction of shrimp ponds, fish ponds and salt fields has resulted in fast progression. The coastline at the Dakou River has advanced 8 km. In the area around the Taoer River mouth and west of the Shunjiang Stream, harbor construction and

a highway to link the harbors that cuts across the tidal flat have caused the coastline to advance rapidly to the sea. The maximum advance is approximately 10 km. Some areas are perennially water-logged. If human activities are disregarded, the coastal section should be relatively stable over the next 10 years. Whether the coast advances or not totally depends upon human activities. To protect farmland from occasional storm surges, dikes should be built to protect the coast near the high-tide line. Actually, such work has already been undertaken in some areas.

2.3.2 Coastal Section from Shunjiang Stream to the Tiaohe River Mouth (Section 2)

The Yellow River emptied into the sea here during the 1909—1926 period. This section now is characterized by slow retreat. In the 1980s, the retreat rate was about 50 - 80 m/a. From 1976 to now, the coastline has retreated 1 km at an average rate of 50 m/a. The present retreat rate is about 30 - 50 m/a. Over the next 10 years, the coastal section will tend to retreat at a little slower rate (maybe 20 - 50 m/a) if human influences are not taken into account. However, due to the human influence, the coastline will probably remain stationary. In the field survey, we saw that some coastal parts protected by dikes and some oilfields by stone dams.

2.3.3 Coastal Section from the Tiaohe River Mouth to the station 106 (Section 3)

This section is characterized by strong retreat. The Yellow River debouched here from January 1964 to May 1976 and then avulsed to another place. The fluvial deposits at the coast are over 13 m thick, and the coastline advanced 17.5 km in this period. After the river avulsed, the coast suffered strong erosion because silt supply stopped. Since 1976, the coastline has retreated 5 - 7 km (0.2 - 0.3 km/a). Especially during the early years (1976—1984) after avulsion, the coastline eroded very fast (0.4 - 0.6 km/a). After constructions of the Yellow River Harbor in 1988, erosion slowed down between 1989 and 1991. At present, the retreat rate is about 50-150 m/a. Without human activities, the coastal section would erode over the next 10 years, and the retreat rate is estimated to be a little less than the present one (maybe 50 - 120 m/a). The construction of the Feiyantan Oilfield will surely lead to steps to stop the erosion. Local areas are protected by stone dams.

2.3.4 Coast Section from the station 106 to Gudong Oilfield (Section 4)

This section is stable because it is protected by stone dams. It is closest to the amphidromic point and has a small tidal range but strong currents. The Yellow River flowed into the sea here from 1953 to 1976, resulting in rapid progression. After the river avulsed, the coast was strongly eroded. Because this area was rich in hydrocarbons, stone dams were built to stop the erosion. Most of the stone-protected coast lies near the low-tide line such as the Yellow River Harbor and Gudong Oilfield. Some erosion still occurs in the offshore area and below the slope of the protected coast. In the next 10 years, the coast section will remain stable. Because fierce storm surges and typhoons can sometimes destroy the dams, attention should be paid to the maintenance of the dams. The Gudong Oilfield is now located closer to the estuary after the avulsion in 1996, and therefore erosion will probably become weaker there and some deposition will occur instead.

2.3.5 Coastal Section from Gudong Oilfield to Dawenliu Haipu (Section 5)

This coastal section is characterized by strong deposition or quick progression. Since 1976, the Yellow River has emptied into the Bohai Sea and experienced very rapid deposition in this area. The fastest advance to sea is about 40 km at an average rate of 1.6 km/a. The new river mouth has advanced about 8 km since 1996 with an advance rate of over 1 km/a. The Yellow River mouth that existed before June 1996 has beeen eroded because of its evident protrusion into the sea and lacking sediment supply.

Generally speaking, in the next 10 years, the present river mouth maybe will keep the progression rate between 1 000 m/a and 1 700 m/a, and the flank coast will be marching at the speed of over 200 m/a. In general, the coastal section is predicted to advance towards the sea at the rates between 200 m/a and 1 700 m/a in the next 10 years. Of course, the progression rate will gradually slow down when the river mouth becomes more protruded into the sea. The dikes of the river should be maintained to prevent the river from flooding.

2.3.6 Coastal Section from Dawenliu Haipu to Zimai Stream (Section 6)

Generally, this section is characterized by slow progression as a result of silt moving southwards in the sea. The northern part has a comparatively fast progression. The southern part is characterized by less deposition. In the next 10 years, this section is will slowly progress (maybe 50 - 200 m/a). Coast protection can be limited to the construction of earth dikes that should be built near the high-tide line to protect the coast from storm surges.

2.3.7 Coastal Section from Zimai Stream to Jiaolai River Mouth (Section 7)

The Yellow River has little influence on this coastal section, which is basically stable though there is local erosion and deposition. It will remain stable over the next 10 years. Occasional storm surges may harm farmlands and constructions. Therefore, we suggest that earth dikes be built near the high-tide line. In fact, this work is now under way in some places.

4 Conclusions

(1) Progression and retreat rates are different in different sections during different periods. From 1855 to 1934, the delta progressed eastwards at a rate of 0.4 - 0.72 m/a. From 1934 to 1976, the coast progressed fastest between the Tiaohe River mouth and Yellow River Harbor, and the coastline shifted 20 km to the north at a speed of 0.5 km/a. Between 1976 and 2001, artificial control made the Yellow River shift less, concentrating sediment supply in a small area. Therefore, the fastest deposition occurred between Gudong Oilfield and Dawenliu Haipu. The coastline shifted about 40 km (1.6 km/a). From 1855 to 2001, the largest shift occurred in the area between Yuwa and the estuary in 1996 (about 52 km, on average 0.36 km/a).

(2) In June, 1996, the Yellow River artificially changed its course about 7 km northeast of Dawenliu Haipu, and the 11th lobe of the modern Yellow river delta began to form. This avulsion probably marks the beginning of the 3rd subdelta formation. As a result of that, the Yellow River delta advances towards east by north with the 1st, 2nd and 3rd subdeltas arranged in succession. It is expected that the future 3rd subdelta will have a smaller area than the 2nd one and its development will take 40 - 60 years.

(3) The coast in the study area can be subdivided into 7 different sections, namely: a relatively stable section from the Dakou River Mouth to Shunjiang Stream, a slowly retreating section from Shunjiang Stream to the Tiaohe River Mouth, a strong retreating section from the Tiaohe River Mouth to the station 106, a stable coastal section from the station 106 to Gudong Oilfield (controlled by stone dams), a strong progression section from Gudong Oilfield to Dawenliu Haipu, a slow progression section from Dawenliu Haipu to Zimai Stream, and a stable coastal section from the Zimai Stream mouth to the Jiaolai River Mouth. It is expected that over the next 10 years, the coastal sections will show a similar behavior, but the progression or retreat rates will have a slower tendency. Of course, human activities will have a strong influence on the coastline.

References

[1] Coleman J M, Roberts H H and Stone G W. Mississippi River Delta: an overview. Journal of Coastal Research, 1998. 14(3): 698-716.

[2] Barrie J V and Currie R G. Human impact on the sedimentary regime of the Fraser River Delta, Canada. Journal of Coastal Research, 2000, 16(3): 747-755.

[3] Allison M. A. Historical change in the Ganges-Brahmaputra Delta Front. Journal of Coastal Research, 1997, 14 (4): 1 269-1 275.

[4] Milliman J D and Meade R H. World-wide delivery of river sediment to the oceans. Journal of Geology, 1983, 91: 1-21.

[5] Qin Yunshan and Li Fan. Study of influence of sediment loads discharged from the Huanghe River on sedimentation in the Bohai Sea and the Huanghai Sea. In: Proceedings of International Symposium on Sedimentation on the Continental Shelf with Special Reference to The East China Sea. Beijing: China Ocean Press. 1983, 83-92.

[6] Xue Chunting, Cheng Guodong and Zhou Yongqing. Early Holocene tidal flat deposits in Huanghe River Delta area. Marine Geology and Quaternary Geology, 1987, 7 (suppl.): 29-40.

[7] Wang Qi, Cao Lihua, Yang Zuosheng *et al.* Characteristics of sedimentary dynamics in Yellow River subaqueous delta. Science in China (Series B), 1991, 21: 660-665.

[8] Xue Chunting, Zhu Xionghua and Lin Hemao. Holocene sedimentary sequence, foraminifer and ostracoda in west coastal lowland of Bohai Sea, China. Quaternary Science Review, 1995, 14: 521-530.

[9] Keller G H and Prior D B. Sediment dynamic of the Huanghe River (Yellow River) Delta and the neighboring Bohai. Bay Geo-marine Letter, 1986, 6: 63-66.

[10] Wright L D *et al.* Processes of marine dispersal and deposition of suspended silts off the modern mouth of the Huanghe. Continental Shelf Research, 1990, 10(1): 1-40.

[11] Wang Y, Aubrey. The characteristics of the China coastline. Continental Shelf Research, 1987, 7: 329-349.

[12] Xue Chunting. Historical changes in the Yellow River delta, China. Marine Geology, 1993. 113: 321-329.

[13] Wang Ying and Wu Xiaogen. Sea level rise and sea beach erosion. Acta Geographic Sinica, 1995, 50(2): 118 -127.

[14] Geng Xiushan, Wu Shiying. Preliminary approach to the dynamical geomorphical conditions of Huanghe seaport. Acta Geographic Sinica, 1988, 43(4): 297-309.

[15] Liu C and Walker H J. Sedimentaru characteristics of cheniers and the formation of the chenier plains of east China. Journal of Coastal Research, 1989, 5, 353-368.

[16] Yoshihi Saito, Wei Helong, Zhou Yongqing *et al.* Delta progradation and chenier formation in Huanghe (Yellow River) delta, China. Journal of Asian Earth sciences, 2000, 18: 489-497.

[17] Zhao Xitao. Development of cheniers in China and their significance to coastline shift. In: Gardiner V (ed.), international Geomorphology, Wiley, London. 1987, 1 253-1 268.

[18] Yang Zuosheng, Keller G H, Lu Nianzu *et al.* Bottom morphology and instability of the modern Huanghe (Yellow River) subaqueous delta. Journal of Ocean University of Qingdao, 1990, 20(1): 7-21.

[19] Shi Z and Chen J Y. Morphodynamics and sediment dynamics on intertidal mudflats in China (1961—1994). Continental Shelf Research, 1996, 16: 1 909-1 926.

[20] Yin Yanhonghong, Cheng Guodong and Fan Shunting *et al.* The characteristics of morphology and hydrodynamics of tidal channels in Yellow River delta. Research of Marine Geology and Mineral Resourcses, Dedicated to the 30th international geological congress. Qingdao: Qingdao Ocean University Press, 1996, 156-160.

[21] Yin Yanhong, Wang Yurong and Liu Xianqi. Types and distribution patterns of modern tidal channels along the Yellow River Delta coast. Chinese Journal of Oceanology and Limnology, 1999, 17(4).

[22] Ren Meie. Human impact on coastal landform and sedimentationthe Yellow River example. Geojournal, 1992, 28: 443-448.

[23] Shandong Scientific and Technological Committee. The comprehensive investigation report of Yellow River mouth area. Beijing: China Science and Technology Press, 1991, 1-324.

[24] Cheng Guodong. Modern sedimentation and its model of the Huanghe Delta. Beijing: Geological Publication House. 1991, 110.

Reducing Environmental Impact of Aggregate Excavation in Small Tropic Pacific Islands

Xue Chunting (薛春汀)
Qingdao Institute of Marine Geology, Qingdao 266071, Shandong, China

Abstract Excavating sands and gravel on land in combination with constructing reservoirs for storing fresh water is an ideal approach in atolls. Appropriate mining of gravel from the prograding gravel beach is acceptable. Digging reef rock close to the edge of the wide ocean reef flat without surface loose sediments on it or sand beach can be accepted. Excavating sand from some depths in lagoon is a scientific approach particularly important for urbanized atolls. However, selecting appropriate sites for mining sand other than at some depths in lagoon is suitable to rural islands without dense populations. These sites include up drift side of long groin on the reef flat, partly filled access channel-port, outlet of artificial channel and lagoon margin on the prograding coast.

Keywords aggregate mining, quarry pit, prograding coast, reservoir construction, atoll

Before the Second World War aggregate excavation had not caused evident impact on the coastal environment since the population was not so large as at present and the houses were built with wood. After the War with the population increasing and the living standard rising, more and more infrastructure facilities and houses using more aggregate and cement are built. Rapid increasing of aggregate excavation has become one of the most significant coastal erosion causes such as in Kosrae, a volcanic island in Federated States of Micronesia[1, 2] and Majuro Atoll, the Marshall Islands[3].

A Pacific-wide sea-level stillstand about 40 000 years ago which resulted in the formation of coastal terraces with significant sand beaches at the depth of about 70 m. It is proposed that such deposits, in water depths of 50 - 100 m and seaward of the reefs, will serve as resources for sustainable development[4]. This may be a good idea. But this dredging needs advanced technology with higher cost. Present attention focuses on mining in lagoon for atolls[5]. Geologic-geophysical investigation has been made in some islands. Reasonable mining area is not only related with optimum depth, wave, current, living corals, but also the whole ecosystem. Geologic-ecological investigation is needed for mining in lagoon.

The above two ways of mining sand are suitable for densely populated islands. They cannot provide gravel and rock. In this paper, suggestions on mining sand, gravel and rock from shallow lagoon margin to land are proposed. This paper sums up my field experience in 1995—1997, when I observed that many excavations had induced erosion in small Pacific islands and that some aggregate mining is acceptable.

1 Negative environmental impact of some existing aggregate excavations

Received on July 6, 2003

Beach sediment extraction directly causes coastal erosion in small Pacific islands[6]. This negative impact has been recognized long before. However, secretly excavating is still often occurring since this is the simplest and low cost excavation. Loose sediment extraction from the reef flat reduces sediment supply to beach and increases wave energy arriving at the shore, resulting in shore erosion, such as in Kosrae Island and Nukufetau Atoll in Tuvalu. Not only this, aggregate excavation on the reef flat can induce blocking-up of small river mouths, changing ecosystem and greatly reduce sand-building organisms (foraminifera and mollusk)[1] (Fig. 1).

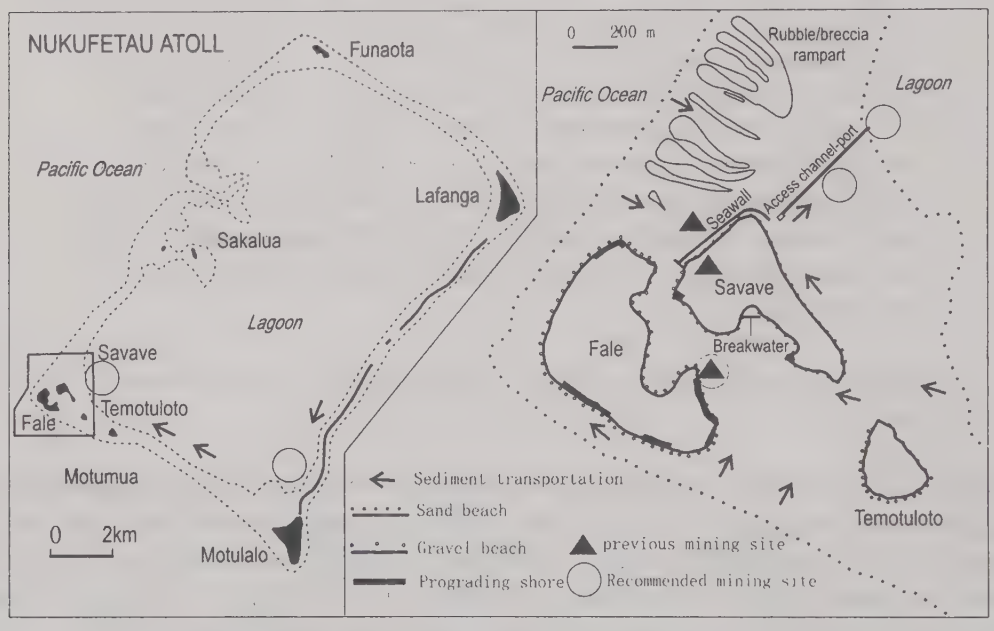

Fig. 1 Sediment transportation, previous aggregate mining sites and recommended appropriate mining sites in Nukufetau Atoll, Tuvalu

Quarry pits are excavated on reef flats in many islands such as Kosrae Island, Majuro Atoll and Tarawa Atoll (Kiribati). Most of these pits trap sediments from reef flats and beaches particularly from sandy shores, thus causing erosion. The large quarry pits excavated in the 1980s are the most significant cause of north coast erosion of Kosrae Island[1].

Commercial aggregate excavation at the east and southeast Majuro Lagoon margin has been conducted for many years (Fig. 2). A mole extends from shore to reef flat edge and an excavator dredges aggregate from lagoon bottom. The interviewed workers told us that some hours after excavation a pit would be formed at the lagoon margin and the pit would be filled naturally in half day. It is quite evident that this pit was filled by the sediment transported by wave and longshore current. The dominant winds are E-NE in Majuro Atoll. The westward longshore sediment transportation is important for the formation, stability and growth of the south long islet. The over-excavation at the lagoon margins reduces sediment supply to the reef flat and beach, and interrupts the sediment dynamic equilibrium along the coast. This is one of the important causes of the lagoon coast erosion approximately 50 km long in Majuro Atoll[3] (Fig. 2).

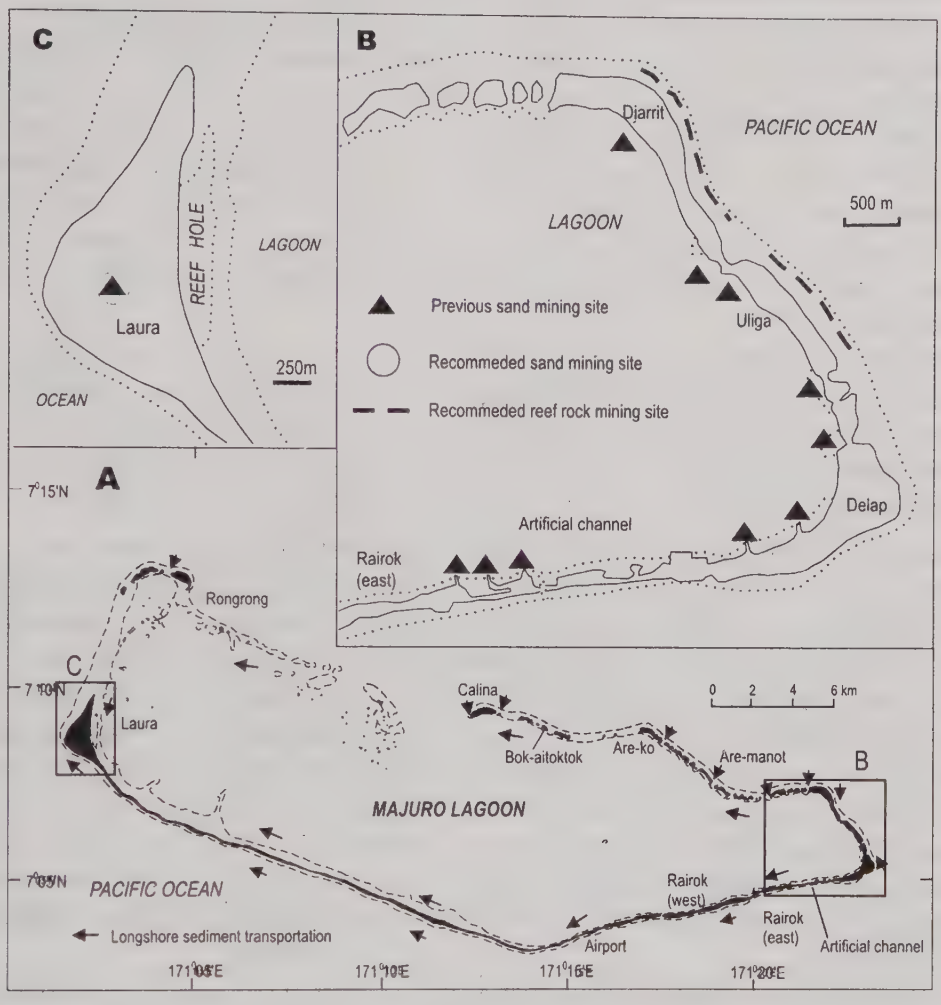

Fig. 2 Longshore sediment transportation, previous aggregate mining sites and recommended appropriate mining sites in Majuro Atoll, Marshall Islands

2 Reducing negative impact of aggregate excavation

Excavation of aggregate from some places in the lagoon is a scientific approach. But selection of the potential mining site in lagoon has to make a detailed geologic-ecological field survey. For many rural atolls such survey may be made some years later. Actually the aggregate extraction volume in rural atolls is not great. Except the deeper lagoon, scientifically selecting some other potential mining sites without significant environmental impacts may be a simple way and easily acceptable by the islanders, particularly local residents in rural islands.

2.1 Excavation of sand and gravel from land

The islanders excavate sand on land recent years in many islands. Excavating sand from land is still a relatively good way for the reef-top islands and some volcanic islands, since there are no lagoons. In comparison with digging sand from beach and reef flat, this is much better since it avoids shore erosion

and destruction of houses along the shore although the excavation leaves some useless pits.

If aggregate (sand and/or gravel) mining in land can be combined with the fresh water reservoir engineering, such mining is a very good option — to kill two birds with one stone. Such reservoirs are really necessary. The fresh water collected from roofs of buildings is reserved in tanks in most atolls at present. When it is dry for a long time, the tank-stored water cannot meet the need. To dig reservoirs for storing surface runoff is particularly suitable to Laura, Majuro Atoll, which has relatively a large area and the subsurface sand is about 20 m thick and Vaitupu Island (a reef-top island). Small-scale excavation of aggregate can link up with reclamation of taro farmlands, which need to be excavated lower than ground.

The Chinese engineers and workers dug volumes of gravel and sand in land for upgrading the runway of Tarawa Airport, Kiribati in 1994. This type of excavation avoided coastal erosion although it left a huge pit without vegetation. The extracted sand was far from the demand. They ground gravel into sand graded rock fragments, which is simple and of low cost since the poor cemented reef rock is easy to be ground. This method for getting sand can be accepted in some islets composed of gravels.

2.2 Excavation of gravel from the prograding gravel beach and sand from special sites

On 21 October, 1972, Cyclone Bebe struck Funafuti Atoll (Tuvalu). The rubble was tossed from the ocean reef front onto the southeast ocean reef flat, forming a 18 km long nearly continuous rubble rampart with a mean height (above the reef flat) of 3.5 m and a width of 37 m[7, 8]. After the cyclone, the rubble rampart on the ocean reef flat migrated shorewards[9], and almost all of the rubble had combined with the ocean beach by 1995. Under the dominant wave action, the beach gravel of the southeast coast of Fongafale Islet slowly moved southwestwards and accumulated on the southwest end. This movement has been going on since the ocean shore existed. The south end of Fongafale Islet, Funafuti Atoll extended 122 m from 1943 to 1973 and another 36 m from 1973 to 1995. A wide gravel beach had accumulated on the ocean side of the southwest end of the islet by 1995. In recent years, the islanders have excavated gravel from there, which has not induced adverse effects although the extending rate has slowed down (Fig. 3).

Cyclone Bebe also tossed the rubble onto the ocean reef flat of the south rim of Nukufetau Atoll, Tuvalu. This rubble filled a natural passage, which previously allowed access for small fishing boats. Some rubbles gradually migrated to the shore and resulted in shore prograding in some sections of Fale Islet. Since 1972, the east shore of Fale Islet has prograded 3-15 m. Some rubbles are still on the reef flat and will continue moving to the beach. Excavating gravel at a corner of Fale Islet has not induced erosion (Fig. 1).

The mining volume at both sites mentioned above did not exceed the sediment accumulation volume. It means that mining on the evidently prograding gravel beach is acceptable and the excavation volume should be less than the sediment accumulation volume.

However, excavation from the prograding sand beach should be prohibited except a few special places, since it has a frequent supplement relation with the neighboring sand beach (much different from the gravel beach). If volumes of sand have accumulated on the up drift side of a long groin extending close to reef flat edge, sand can be mined. If the groin is short (less than half of the reef flat width) do not mine sand since the sand would move to the down drift side of the groin.

Some artificial access channel-port excavated on the reef flat have been partly filled by sediments, so to dredge sand from the channel is useful for improving channel navigation without negative impact, for example, in the access channel-port on the southwest Nikufetau Atoll (Fig. 1).

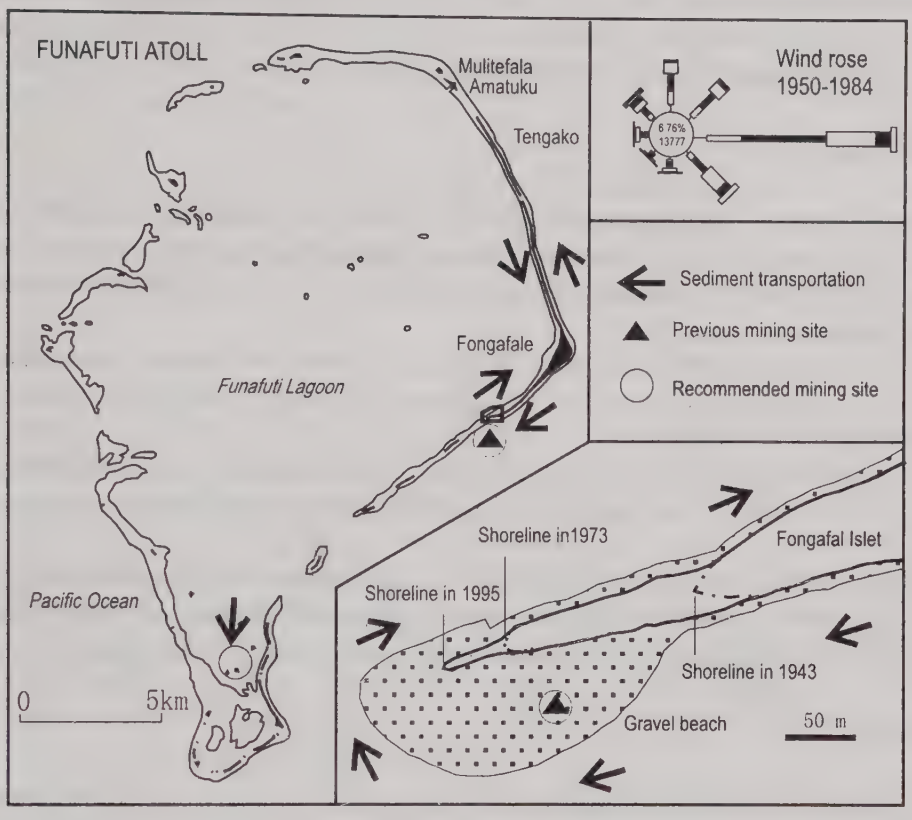

Fig. 3 Sediment transportation, previous aggregate mining sites and recommended appropriate mining sites in Funafuti Atoll, Tuvalu

2.3 Excavation of reef rock from appropriate sites on reef flat

Some quarry pits have not trapped sediment and corals are living well there -- producing aggregate. Such pits are dug close to the ocean and distributed along some artificial ocean shores east of the airport in Majuro Atoll, where no loose sediments on the beach and reef flat can be trapped and coral live in the pit covered by flowing water even in low tide (Fig. 2).

If there are no loose sediments on the wide reef flat and the beach is gravelly such as on the ocean reef flat on the east rim of Majuro Atoll, the quarry pits can be dug close to the ocean for getting big reef rock or rock fragments (Fig. 2).

2.4 Excavation of sand from appropriate sites at the lagoon margin

Many atolls, have their sand accumulating areas at the concave lagoon margin, such as the south ends of Funafuti Atoll and Nukufetau Atoll. There are growing islets or prograding lagoon coasts. If the nearby islets are sparsely populated, appropriate sand mining can be accepted although this would reduce or stop growth of the islets (Figs. 1, 3). The mining volume should not exceed the sand accumulation volume. This way of getting sand is suitable for the outer rural atolls, where the population is not dense.

The access channel-port traps sediment and transports pat of it out of the channel. If the outlet is at

lagoon, sediment accumulates there, such as on the outlet of the channel-port on the southwest reef flat of Nukufetau Atoll. Appropriate mining there can be accepted (Fig. 1).

3 Discussion

Modern coral reef contributes 900 million tons of carbonate production each year[10]. The present aggregate excavation volume is much less than that production. The problem is that the present excavation concentrates in small limited and inappropriate areas. To select appropriate sites can dispel or reduce the negative impact.

The above recommended mining sand sites are only suitable to the rural atoll without a dense population. To meet the need of the densely populated atolls, it is necessary to mine sand from appropriate places in the lagoon.

It is easy to select places for mining gravel with a little environmental impact. Grinding the semi-cemented reef rock or gravel into sand-size rock fragments may be a good alternative, for replacing sand mining.

The bases of some houses are as high as 1 m. Such construction greatly increases the need of aggregate. To improve building structure for reducing requirement of aggregate and meet challenge of storm wave and future sea level rise, the houses should be constructed on concrete piles.

References

[1] Xue Chunting. Coastal sedimentation, erosion and management on the north coast of Kosrae, Federated States of Micronesia. Journal of Coastal Research, 1999, 15: 927-935.

[2] Xue Chunting. The impact of human activities on mangrove coast of Kosrae Island, the Federated States of Micronesia. Transactions of Oceanology and Limnology, 2002, 2: 17-23.

[3] Xue Chunting Coastal erosion and management of Majuro Atoll, Mashall Islands. Journal of Coastal Research, 2001, 17: 909-918.

[4] Cruickshank M. J. Development of aggregate resources in Pacific tropic islands. Marine Georesources and Geotechnology, 1999, 17 (2): 101.

[5] Mallik T K. Calcareous sands from a coral atollshould be mined or not? Marine Georesources and Geotechnology, 1999, 17 (1): 27-32.

[6] Gillie R D. Causes of coastal erosion in Pacific island nations. Journal of Coastal Research Specal Issue, 1997, 24: 173-204.

[7] Maragos J E, Baines G B R and Beveridge P J. Tropical Cyclone Bebe creates a new land formation on Funafuti atoll. Science, 1973, 181: 1 161-1 164.

[8] Baines G B K, Beveridge P J and Maragos J E. Storm and Island Building at Funafuti Atoll, Ellice Islands. In Proceedings of the Second International Coral Reef Symposium. 1974, 485-495.

[9] Baines G B K and McLean R F. Sequential studies of hurricane deposit evolution at Funafuti Atoll. Marine Geology, 1976, 21: M1-M8.

[10] Smith S V and Kinsey D W. Calcium carbonate production, coral reef growth, and sea level change. Science, 1976, 194: 937-939.

Distributional Feature of Detrital Minerals in the Superficial Sediment of South Yellow Sea

Wang Hongxia (王红霞)[1,2], Lin Zhenhong (林振宏)[2], Guo Yugui (郭玉贵)[3]
1 *Qingdao Institute of Marine Geology, Qingdao 266071, Shandong, China*
2 *Ocean University of China, Qingdao 266003, Shandong, China*
3 *Qingdao Municipal Seismological Bureau, Qingdao 266071, shandong, China*

Abstract The composition of detrital minerals with grades of 0.063 - 0.25 mm in the superficial sediment of South Yellow Sea is mainly studied in the paper. The research result shows that the minerals can be divided into more than fifty sorts. The light minerals are mainly feldspar, quartz, mica, *etc.* The heavy minerals are mainly composed of amphibole, epidote, mica, autogeny pyrite, magnetite, hematite, garnet, zircon and so on, which mainly distribute in the sediments of silty clay and lutaceous silt. According to the content and distribution of the main minerals, the research area is divided into five mineral combination provinces. The assembled types of minerals in every province have close relationship with its hydrodynamic conditions and sedimentary environment. And the sorts of detrital minerals also show that the detrital substances in the sedimentary areas mainly originate from the drainage areas of rivers, bedrock weathering, and transformed sediment, *etc.*

Keywords detrital mineral, superficial sediment, zoning of assembled minerals, South Yellow Sea

Introduction

The survey area is located in the west part (between 32° N - 36° N and 120° E - 126° E) of South Yellow Sea , which belongs to the Nantong Sheet under the standard topographic map divisions of 1:1 000 000 scales. The total survey area is about 246 200 square kilometers. A lot of geological survey and research work was carried out around the area in the past[1-7]. The research area was a blank area on a geological survey map. To further probe into the sources, transport mechanism, depositional setting, and sedimentary law of the sediments in South Yellow Sea, a lot of bottom-surface sediment samples were gathered in 62 sites in the area in September 2002. The analysis on the mineral assemblage was carried out. It will be helpful to the systemic study about the sedimentary law in the area.

1 The sample and research method

Using the standard heavy placer analytic technological process, about 239 sediment samples collected from South Yellow Sea were examined. Firstly dry the original samples over heat. Then immerse the dried samples in the fresh water for two days. Use the copper riddle with an aperture of 0.063 mm in diameter to wash out the component with the grain size less than 0.063 mm in diameter.

Received on May 11, 2004
The study is supported by the program: the Regional Marine Geological Survey Project of Nantong Sheet (1:1 000 000) [200011000011021].

Re-dry the samples over heat and separate them with riddle. The samples are divided into two grain grades, which grain sizes are separately > 0.25 mm and between 0.25 - 0.063 mm. Next, use heavy liquid ($CHBr_3$, which density is 2.89) to separate, dry over heat, and weigh the light and heavy minerals from the samples which grades are between 0.25 - 0.063 mm. By means of binocular stereoscope, polarizing microscope and micro-chemical analysis, samples of light and heavy minerals are identified respectively. Adopt the Grain Counting Method in Strip to count 300 to 500 grains and respectively calculate the grain percent content of each light mineral and heavy mineral in the samples.

2 Composition content and distribution of detrital minerals

2.1 Light mineral

More than 95 % of light minerals are made up of feldspar, quartz, mica, carbonate (which is mainly calcite). Besides, there are also some graphite and very little glauconite.

2.1.1 Feldspar

Feldspar is the most abundant and extensively distributed mineral, which distribution is more uniform in the superficial sediment. The average content of feldspar in the superficial sediment is 35.7 %. The maximum content is 57.3 % at the site YNB-60, and the minimum content is 6 % only. The content of feldspar in most sites is between 33 % and 40 %. On the whole, the percentage content of feldspar in the north is higher than in the south (Fig. 1-A).

2.1.2 Quartz

Quartz is the second most abundant mineral, which distribution features are similar to that of the feldspar. Its average percentage content is about 18.9 %. The maximum content is as high as 38 % at the site YNB-86; the minimum content is only 1.3 % at the site YNB-34. Its distribution tends to be higher in the north and lower in the south in the whole survey area (Fig. 1-B). Its vertical distribution is more even in the section.

2.1.3 Calcite

Calcite is mainly distributed in the area to the south of 34° N (Fig. 1-C) and concentrated in the coarser silty sand in the south. Its average content is about 0.29 %. It disappears at some northeastern sites of the research area.

2.1.4 Graphite

The distribution feature of Graphite is opposite to that of calcite. It mainly distributes in the area to the north of 34° N and in the area to the west of 123° E. It is mainly concentrated in the finest clay silt. Its average content is about 0.18 %. It is almost nonexistent in the area to the south of 34° N (Fig. 1-D).

2.2 Heavy mineral

The heavy minerals in the superficial sediment mainly include more than ten kinds of minerals such as hornblende, epidote, pyrite, mica, and garnet. The average content of the heavy minerals is about 2.06 %. The area is divided into three parts which are the high content area, the middle content area and the low content area according to the contents of > 4 %, 4 % - 2 % and < 2 % (Fig.2-A). This clearly shows that the high content area is located to the east of 123° E, and the low content area to the west of 122° E. The percentage content of heavy minerals decreases from east to west in the whole survey area.

Fig. 1 Distribution of percentage contents of light minerals in the superficial sediments of South Yellow Sea
A. Feldspar B. Quartz C. Calcite D. Graphite

2.2.1 Amphibole family

Amphibole family includes: hornblende, actinolite, tremolite, anthophyllite and glaucophane. Among them, the content of hornblende is the highest. It has the following features: most extensive distribution, dark green or blackish green (few brown) in color, and prismatical, granular and tabular in shape (while the crushed ones are in acicular shape). Actinolite, which assumes fibrous aggregate, is lighter than the common hornblende in color. Tremolite is colourless and transparent. Anthophyllite assumes very fine needle fibrous-bunchiness. Glaucophane is in dark blue columnar grain.

The average content of amphibole is about 35.7 %. Most of them are common hornblende with an average content of 32.4 %. The maximum content of amphibole is as high as 56.7 % at the site YNB-35. Its minimum is 2.1 % at the site YNB-79. On the whole, the high content area lies in the middle-southern survey area to the south of 34° 30′ N, and the rest belongs to the middle-low content area. The high content area lies to the east of 122° E, the content being higher in the east and lower in the west; Hornblende is basically distributed in the fine clay silt (Fig. 2-B).

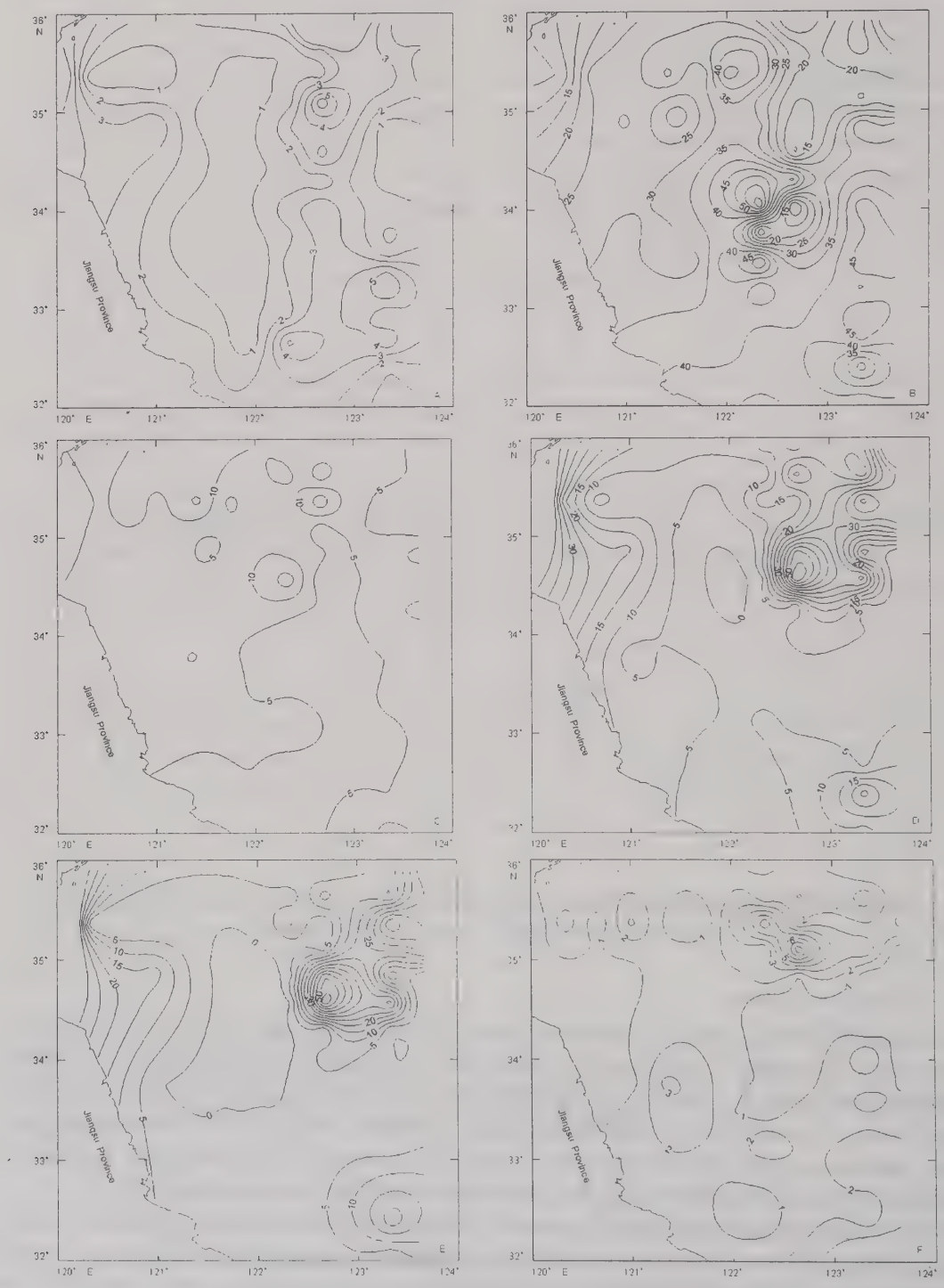

Fig. 2 Distribution of percentage contents of heavy minerals in the superficial sediments of South Yellow Sea

A. Heavy minerals B. Amphibole C. Stable minerals
D. Metal minerals E. Authigenic pyrite F. Magnetite

2.2.2 Epidote family

Epidote family is mainly constituted by epidote. It has more extensive distribution and higher content in the surface sediments of South Yellow Sea. Epidote assumes yellow-green of different shade and a granular shape. Some grains has undergone a weathering process, and their color and feature under a microscope are not obvious. The average content of epidote is about 12.8 % in the whole area. Its maximum content is 26 % at the site YNB-52 that locates in the area to the north of 34° N and the area to the east of 123° E. In the whole area, the content of epidote increases in the north and decreases in the south, but stays stable from the east to the west. The average content of allanite is 0.71 %, which mainly distributes in the sea area to the south of 34° N and to the west of 123° 30′ E. Its distribution is consistent with that of glaucophane. Although the average content of zoisite is only 0.60 %, its distribution scope is more extensive. Its distribution trend is consistent with epidote.

2.2.3 Mica family

Mica family includes biotite, muscovite and weathering mica, which is found everywhere in the survey area. The average content of mica is about 9.18 % in the area. Its distribution law is opposite to that of amphibole and epidote. In the area where amphibole and epidote have the lowest contents separately, the content of mica is highest, 83.3 % at the site YNB-34. This is also the maximum point for the contents of all heavy minerals in the area. The high content area corresponds to the fine sediments in the central area. Because the landform is even, the hydrodynamic conditions are weaker, and the sediment is mainly composed of the fine minerals, the flaky mica with low specific gravity that is easily broken is especially concentrated there. In addition, the content of mica tends to be less vertical from top to bottom in the north of the survey area.

2.2.4 Stable minerals

Stable minerals include garnet, sphene, zircon, apatite, tourmaline, leucoxene, rutile, and staurolite. Its average content is about 6.55 %. By the contents of stable minerals, > 15 %, 5 % - 15 % and < 5 %, the area is correspondingly divided into the high content, middle content and low content areas. Fig. 2-C indicates that the high content area lies to the north of 34° 20′ N and to the west of 122° 30′ E, and the low content area is located in the area to the south of 34° 20′ N. In the whole area, the distribution feature of stable minerals shows that it increases in the north and decreases in the south, which is similar to epidote. There is also a long and narrow low content zone in the area to the north of 35° N and to the east of 123° 30′ E. Garnet is the most abundant mineral and more extensively distributed in the stable minerals. It is found in every sample and appears in granular or euhedral crystal shape with different shades of pink color. Its average content is about 3.94 %. Its maximum content is 14.7 %. The average content of tourmaline is about 0.41 %, which distribution is more extensive. The average content of leucoxene is about 0.36 %, and the average content of phosphorite is 1.05 %. Their distribution tends to decrease from north to south just like epidote. For the sphene, its average content is about 0.29 %, which maximum content area is located in the sea area to the west of 122° 30′ E. It is higher in the west than in the east. The average content of rutile is 0.27 %, which distribution tends to be high toward south just like orthite. Rutile is concentrated at several isolated sites. The average content of zircon is 0.25 %, which belongs to the lowest content-mineral among the stable minerals with the similar distribution law to amphibole. The rutile and staurolite are found only in several samples. In addition, there are some topaz and monazite too in the area. Although the content of monazite is not high, it is more extensively distributed. The topaz is mainly distributed at the northwestern corner of the southern sea area, which

has the similar distribution feature to pyrite.

2.2.5 Metallic minerals

Metallic minerals include hematite, limonite, magnetite, authigenic pyrite, and ilmenite. Its total content is about 12 % (Fig. 2-D). As indicated in the figure, the metallic minerals concentrate in the finer sediment of clay silt in the area to the north of 34° N, and the distribution is almost zero in the south. It can be seen from Fig. 2-E and Fig. 3-F that authigenic pyrite and magnetite are mainly distributed in the northern sea area, and they decrease to zero in the south. The average content of authigenic pyrite is about 8.22 %, and the maximum content is 64.7 %. The minimum content of authigenic pyrite is only 0.3 % at the site YNB-57 in the south. The content distribution is very uneven. The authigenic pyrite is enriched in the fine clay silt sediment with high-organic matter in the area to the north of 34° N, which has been formed in a special sedimentary environment. The authigenic pyrite appears as the shape of biocrust or nonbiocrust. The biocrust shape represents that pyrite has replaced and filled in all kinds of biocrust and rhizome. The nonbiocrust shape has more types such as ball-grain, botryoidal and irregular granular ones, *etc.* The nonbiocrust shape resumes the color of light brass, dark black, indigo and so on, and has been formed in the weak hydrodynamic reducing environment, which belongs to the authigenic mineral. The magnetite mainly emplaces the clay silt by the site YNB-79 and distributes extreme unevenly with the maximum content as high as 27.5 %, and the average content of only 2.04 % and the popular content of 0.3 % The average content of ilmenite is about 0.88 %, which mainly distributes in the sea area to the west of 122° E. The average content of bloodstone and magnetite is about 0.86 %, which mainly distribute in the sea area to the east of 122° E.

The cosmic dust resumes color of black or brown, shape of pellet, metallic luster and little magnetism. It is distributed in the individual sites, which should belong to the production of the end of the Late Pleistocene Epoch[15]. Besides, there are augite, disthene, brookite, chromite, staurolite, barite and so on.

3 Mineral zoning and material sources identification

The survey area can be divided into 5 mineral association provinces according to the distribution law of detrital minerals, diagnostic mineral association, type of sediment, landforms, and hydrodynamic condition, *etc.* (Table 1 and Fig. 3).

Tab. 1 Mineral contents of mineral assemblage provinces in South Yellow Sea

Mineral zoning	Number of sites	Name of minerals									
		Hornblende	Epidote	Micas	Garnet	Pyrite	Apatite	Magnetite	Ilmenite	Tremolite	Actinolite
I	10	34.12	15.15	6.97	5.02	4.5	2.48	2.35	2.08	0.95	0.78
II	7	25.04	11.96	4.8	3.49	21.31	1.25	2.81	0.61	0.59	0.51
III	21	25.86	12.27	5.1	3.52	19.53	1.19	2.93	0.62	0.57	0.53
IV	13	35.87	10.54	15.62	3.05	0.22	0.37	1.25	0.79	1.16	1.84
V	11	41.03	13.75	6.64	3.15	1.23	0.97	1.98	0.83	1.22	1.05

3.1 The northwest mineral province of South Yellow Sea (I)

This province lies in the littoral area of Qingdao to the north of 35° 15′ N and west of 122° 30′

E (Fig.3). Sediments mainly contain fine-grained sandy silt and clay silt. The landform has a gentle slope, which varies slightly. The mineral association is feldspar quartz - hornblende - epidote. The metal minerals such as ilmenite, and the stable minerals such as garnet, sphene, leucoxene, zircon and topaz have higher concentration. The content of authigenic pyrite is less than 5 %. The sediments are mainly derived from the transformed sediment and the coastal washing materials.

There is a sedimentation-transformation area around the site No. 59 and the site No. 60, where the content of stable minerals is more than 15 %. The paleontologic association is relict ancient littoral sediment, which sediment is mainly coarser sandy silt.

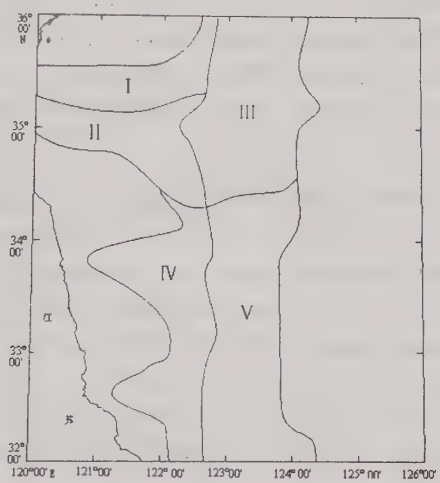

Fig. 3 The zoning sketch map on detrital minerals in the superficial sediment of South Yellow Sea

3.2 The sub-aquatic delta mineral province of Old Yellow River (II)

This province lies in the area to the west of 122° 30′ E between 35° 15′ N and 34° 20′ N (Fig. 3). The grains of the sediment change from fine in the northwest to coarse in the southeast, which are clay silt, sandy silt, to silty sand in turn. The mineral association is quartz - hornblende pyrite - stable minerals-graphite - actinolite - garnet. The diagnostic mineral is authigenic pyrite. The sediments mainly come from the coastal materials and materials from the old Yellow River, which latter were transformed by all kinds of hydrodynamic actions[8].

There is also a transformed sedimentary area, where the content of stable minerals is more than 15 %. The paleontologic association is relict ancient littoral association, which sediment is mainly silty sand.

3.3 The middle mineral province of South Yellow Sea (III)

This province lies in the area to the north of 34° 20′ N and to the east of 122° 30′ E (Fig. 3). The main component of the sediments is clay silt that distributes in strip from south to north. The mineral association is feldspar - quartz - hornblende - epidote - authigenic pyrite - magnetite. The diagnostic minerals are authigenic pyrite and magnetite, which are related to the material component from the Shandong Peninsula and the Korean Peninsula. Therefore, the contents of feldspar, quartz, hornblende and epidote are high[9]. The high content of authigenic pyrite corresponds to the following special sedimentary environment of more than 70 m in depth, low landform, fine sediment, reduction

condition, and high concentration of organic matter[10]. Magnetite is mainly derived from the high magnetite-bearing metamorphic rock and the ultrabasic rock extensively distributed in the Shandong and Liaodong Peninsulas, which were carried to such lower place to deposit passing through each marine hydrodynamic action[9].

3.4 The southwest mineral province of South Yellow Sea (Ⅳ)

This province lies in the area to the south of 34° 20′ N and to the west of 122° 30′ E (Fig.3), The sediments are constituted by coarse silty sand in the middle of the area and sandy silt that distributes in strips from north to south on both sides of the area. The mineral association is hornblende - epidote - mica -carbonate - rutile - sphene - hematite - limonite - allanite - tremolite - glaucophane. The diagnostic minerals are mica and carbonate, which contents rank number one in whole area. The high concentration of mica and other flaky minerals represents the environment of gentle topography and weaker hydrodynamic condition[11, 12]. The old Yellow River mainly supplies sediments for the province, which are reformed by sea current[8].

3.5 The southeast mineral province of South Yellow Sea (Ⅴ)

This province lies in the area to the south of 34° 20′ N and to the east of 122° 30′ E (Fig. 3), which belongs to the shelf relict sedimentary area. The sediments are constituted by clay silt that distributes in strips from north to south. The mineral association is hornblende - anthophyllite - tremolite - epidote - zoisite - monazite - zircon. In the whole area, the content of heavy minerals in the province is the highest. The diagnostic mineral is hornblende. The sediments mainly came from the Yangtze River and were formed in the late period of the Late Pleistocene Epoch. The macrograined minerals were concentrated after the flaky minerals and fine-grained minerals were carried away by sea current.

4 Results

The analysis on sedimentary minerals shows that the sediments contain more than 50 minerals. The mineral associations and their zoning are closely related to the characteristics of rock in the provenance, sedimentary environment and sand transportation of river. The light minerals are mainly constituted by feldspar and quartz. In addition, there are a few calcite and graphite and few glauconite. The heavy minerals are mainly constituted by hornblende and epidote, and there are also a few authigenic pyrite, mica and so on. The heavy minerals are mainly derived from the Old Yellow River, Shandong Peninsula, Liaodong Peninsula, Yangtze River and Korean Peninsula. Because the granite and granodiorite are extensively distributed along the coast of Shandong Peninsula, the contents of feldspars and amphiboles are higher in the sediments of sedimentary area.

The zones of heavy minerals successively assume the trend of medium content zone low content zone medium content zone high content zone from the coast to the sea. The medium content zone nearby the coast reflects the environment where the velocity of stream at the estuary into the sea suddenly slows down and the sand carrying ability of current reduces, which is helpful to the sedimentation of clastic materials. The low content zone reflects the stronger hydrodynamic state, which is the screening result of waves. Along with the deepening of sea water and the weakening of hydrodynamic condition, the heavy minerals successfully deposited and formed the medium content zone and high content zone that distributed toward deep water. The heavy minerals with high contents such as magnetite are mainly derived from the basic rock, ultra-basic rock and metamorphic rock in north Jiangsu Province.

The authigenic pyrite is the main authigenic minerals in the superficial sediments of South Yellow Sea, which mainly distributes in the area to the east of 122° E and the partial sea area at the old estuary of Yellow River (Haizhou Bay). After the diversion of Yellow River course, the flaky minerals concentrated and formed abundant microsphere crystal authigenic pyrite because of weakening of hydrodynamic condition at the old estuary of Yellow River, hightening of organic matter content in sediments, and the reducing reductive sedimentary environment.

According to the variation of mineral contents and their distribution characteristics, the investigation and research area is divided into five mineral association provinces, which are the northwest mineral province of South Yellow Sea (Ⅰ), the sub-aquatic delta mineral province of Old Yellow River (Ⅱ), the middle mineral province of South Yellow Sea (Ⅲ), the southwest mineral province of South Yellow Sea (Ⅳ), and the southeast mineral province of South Yellow Sea (Ⅴ). Thereinto, the partial transformation sedimentation zones are respectively contained in Province Ⅰ and Province Ⅱ . The different mineral sedimentation provinces reflect different sources of matter and special sedimentation environments. There are different sources of matter, landforms and reliefs in the sea, which hydrodynamic conditions are different. This results in the different mineral association provinces.

References

[1] Lee H J, Chough S K, Jeong K S *et al.* Geo-technical properties of sediment cores from the southeastern Yellow Sea: effects of depositional process. Marine Geo-technology, 1987, 7 (1): 55-64.

[2] Lee H J, Jeong K S, Han S J *et al.* Heavy minerals indicative of Holocene transgression in the southeastern Yellow Sea. Continental Shelf Research, 1988, 8 (3): 255-266.

[3] Chough S K, Kim D C. Dispersal of fine-grained sediments in the southeastern Yellow Sea: A steady state model, Journal of Sedimentary Petrology, 1981, 5 (3): 721-725.

[4] Li S Q, Liu J, Wang S J *et al.* Sedimentary sequence and environmental evolution in the eastern South Yellow Sea during the last deglaciation and the Holocene. Chinese Science Bulletin, 1998, 43 (9): 757-761.

[5] Zheng G Y *et al.* Quaternary Geology of the South Yellow Sea. Beijing: Science Press. 1991.

[6] Li S Q, Liu J, Wang S J *et al.* The comparative study on stable isotopic records since deglaciation in east and west parts of the South Yellow Sea. Marine Geology & Quaternary Geology, 1997, 17(4): 1-2.

[7] Zhao Y Y, Park Y A, Qin Y S, *et al.* Material sources for the Eastern Yellow Sea Mud: evidence of mineralogy and geochemistry from China Korea joint investigation. The Yellow Sea, 2001, 7(1): 22-26.

[8] Qin Y S, Zhao Y Y, Chen L R *et al.* Geology of the Yellow Sea. Beijing: China Ocean Press. 1989.

[9] Liu M H, Wu S Y, Wang Y J. Late Quaternary Sediments in the Yellow Sea. Beijing: China Ocean Press. 1987.

[10] Peng H C. A discussion on the sedimentary environment in the western domain of the North Yellow Sea in the light of distribution regularities of authigenic pyrite and its correlation factors. Geological Review, 1979, 25 (2): 53-57.

[11] Jiang X J, Li S Q, Shen S X. Features of heavy minerals in the YSDP 102core on the southeast continental shelf of the South Yellow Sea. Marine Geology & Quaternary Geology, 2002, 20 (2): 29-30.

[12] Lin X T, Li W R, Shi Z B. Characteristics of mineralogy in the clastic sediments from the Yellow River provenance, China. Marine Geology & Quaternary Geology, 2003, 23 (3): 17-21.

[13] Zheng G Y. Quaternary Stratotype Stratigraphic Correlation of the South Yellow Sea. Beijing: Science Press. 1989.

Optimized Composition of Functional Bacteria for Bioremediation of Sediment Environment of Shrimp Culture

Li Qiufen (李秋芬), Xin Fuyan (辛福言), Zou yuxia (邹玉霞), Chen Minshan (陈民山), Tang qisheng (唐启升)
Yellow Sea Fisheries Research Institute, CAFS, Qingdao 266071, Shandong, China

Abstract After the single-strain abilities of organic-pollutant-degrading bacteria in bioremediation of sediment environment of shrimp culture are determined, the multi-strain degrading effect of the compositions of different strains is measured. The results indicate that the multi-strains groups have higher degrading ability than the single-strain groups. Three-strain groups are better than two-strain groups, and four-strain groups are better than three-strain groups and five-strain groups, the groups composed of strains Lt7222, Lt7511, Fc6308 and Gy7018 has the best degrading effect, the CODMn removal rate is 73.2 % in 66 h, and gets to 82.7 % in 114 h, 30 % higher than that of the best single-strain group; Groups of Lt7222, Lt7511, Lt7451 and Gy7018 are the second, whose COD_{Mn} removal rate is 82.1 % in 114 h. It is suggested that multi-species bacteria be used as functional bacteria in bioremediation of mariculture environment.

Keywords optimized composition, functional bacteria, biodegradation, bioremediation, shrimp culture environment

Introduction

In nature, most organic matter is decomposed to little molecular organic matter by extra cellular enzyme of microorganisms[1]. The degrading ability of single strain is limited by the species of their extra cellular enzymes[2]. At the same time, the biodegradation of organic matters are always carried out step by step, and different enzymes play roles in different steps. The products of one enzyme or bacterium might be the substrate of another enzyme or bacterium. Therefore, the thorough mineralization of organic matter is the result of cooperation of many enzymes secreted by many bacteria. The activated sludge in bio-treatment of industrial and domestic wastewater always includes several kinds of bacteria, fungi and Protozoa. The combined effect of several species of Photosynsetic bacteria in degrading organic wastewater is better than that of the single strain[3, 4]. The organic pollutants in sediments environment is composed of several organic matters, such as protein, cellulose, lipid and carbohydrate and so on. In order to improve the remediating effect of selected functional bacteria strains, we have determined the remediating effect of the combinations of different strains, and have selected the best combination.

1 Material and methods

1.1 Source of bacteria strains

Received on August 6, 2003
The paper is supported by the national high-technology development project (819-02-07) and the project of NSFC (30200209).

The organic-pollutant-degrading bacterial strains have been selected by us. According to their degrading ability, enzyme activity and the regularity of no antagonisty to each other, 7 strains [Lt7132 (shown as 1, the same below), Lt7222(3), Lt7451(6), Lt7511(7), Fc6308(8), Gy7017(17), Gy7018(18)] are selected in the experiments.

1.2 Preparation of medium

20 g artificially formulated shrimp diet is added into 1L seawater, immersed over night, and then filtered. The residue is rejected. 20 % distilled water and 0.05 % yeast extract are added, pH is adjusted to 7.6, and then is autoclaved for 20 min. After cooling, the medium is delivered into Erlenmeyer flasks, 150 mL per flask.

1.3 Preparation of bacteria suspension

Bacteria cultures are washed down from plants with sterile physiological saline, rinsed two times by centrifugation to release adhered medium, and weighted, and then the sterile physiological saline is added to make a suspension with a final concentration of 20 mg wet culture per mL.

1.4 Composition of bacteria strains and measurement of degrading abilities

The suspensions of the seven strains are mixed as single-strain groups, two-strain groups, three-strain groups, four-strain groups and five-strain groups, 250 μ L mixed suspension of each group is inoculated into the liquid shrimp feed medium (as shown in Table 1), and each group is inoculated two flasks. The concentration of protein and COD of medium are determined before inoculation. After inoculation, sample are taken every 24 h, centrifuged at 5 000 r/min, and the COD_{Mn} of the supernatant is measures with the alkaline $KMnO_4$ method. The COD removal rate is calculated using the following formula:

$$C = (COD_{t0} - COD_{ti})/COD_{t0} \times 100\ \%$$

COD_{t0} means the COD at the beginning of experiments; COD_{ti} means the COD at sometime after starting

Tab. 1 Inoculation volume of the strains in different groups (μ L)

No.of groups	Lt7132 (1)	Lt7222 (3)	Lt7451 (6)	Lt7511 (7)	Fc6308 (8)	Gy7017 (17)	Gy7018 (18)
1		250					
2				250			
3						250	
4		125		125			
5		84		84			84
6		84		84	84		
7		84		84		84	
8		84	84	84			
9	63	63		63	63		
10		63	63	63	63		
11		63		63	63		63
12	50	50	50	50		50	
13		50	50	50	50		50

The COD_{Mn} of the culture are determined 5 times. At the end of experiments, the COD, the concentration of protein and inorganic nitrogen (NH_3-N, NO_2-N, NO_3-N) are determined too. The

concentrations of protein are determined with the Folin-phenol method, and other indexes are determined with the methods in "Standards of Oceanographic Survey"[5].

2 Results

2.1 Degrading ability of groups composed of different number of strains

As demonstrated in Fig. 1, the results of degradation by different strain combinations indicate that most multi-strain groups have higher degrading ability than the single-strain groups. The three-strain groups are better than the two-strain groups, and the four-strain groups are better than the three-strain groups, but the five-strain group is not better than the four-strain group, which COD_{Mn} removal rate increases to over 80 %, 30 % higher than the best single-strain group. The results indicate that there is synergetic effect between these strains, but not the more strains the better.

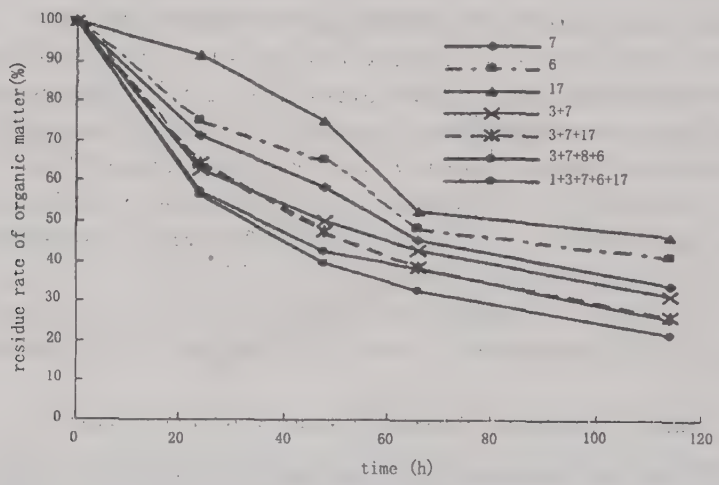

Fig. 1 Degrading ability of groups composed of different number of strains

2.2 Degrading ability of groups composed of the same number of strains

As demonstrated in Fig. 2, in the three-strain groups, the degrading ability has no significant difference in the first 24 h. But they become different since the 72nd h, in the 6 selected groups, the group composed of Lt7222, Lt7511 and Gy7018 is the best, with the COD removal rate of 80 % in 114 h. The group composed of Lt7222, Lt7511 and Fc6308 was the second, with the COD removal rate of 76.3 %. The group composed of Lt7132, Lt7511 and Fc6308 has the poorest effect, and other groups have the effect in between.

In the four-strain groups, the group composed of strains Lt7222, Lt7511, Fc6308 and Gy7018 (3 + 7 + 8 + 18) has the best degrading effect, which COD_{Mn} removal rate is 73.2 % in 66 h, and gets to 82.7 % in 114 h; the group of Lt7222, Lt7511, Lt7451 and Gy7018 (3 + 7 + 6 + 18) is the second, which COD_{Mn} removal rate is 71.8 % and 821.1 % in 66 h and 114 h, respectively. The group of Lt7312, Lt7511, Lt7451 and Gy7018 (1 + 7 + 6 + 18) is the poorest group, with a COD_{Mn} removal rate of 55.4 % in 114 h (see Fig. 3).

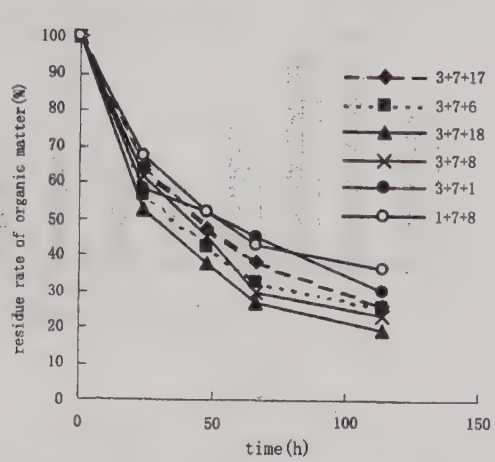

Fig. 2 Degrading ability of three-strain groups

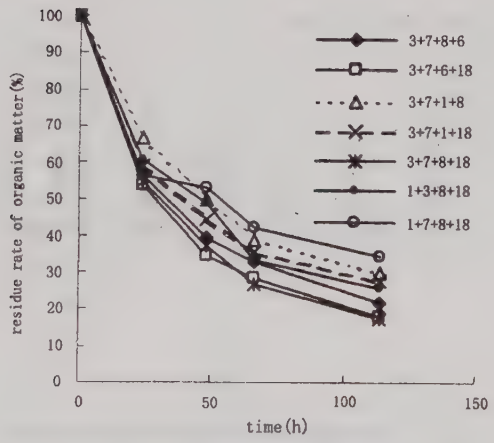

Fig. 3 Degrading ability of four-strain groups

2.3 Protein and total organic matter degrading of different groups

As shown in Fig. 4, most multi-strain groups have higher protein degrading ability than single-strain groups, with the similar regularity as that of the total organic matter degradation. But the group composed of Lt7222, Lt7511, Lt7451 and Fc6308 (3 + 7 + 6 + 8) has the highest protein-degrading rate, although its COD removal rate is not the highest.

2.4 Degrading products of organic nitrogen in different groups

At the end of experiments, the concentrations of NH_4-N, NO_2-N, NO_3-N in the culture liquids are determined. As shown in Fig. 5, the final products of single-strain groups and multi-strain groups are different. The final products of strain Lt7222 are NH_4-N and NO_2-N, and NO_2-N is the main product; The final products of strain Lt7511 included NH_4-N, NO_2-N and NO_3-N; Those of strain Lt7451 are NO_2-N, NO_3-N, and NO_3-N is the main product. While the final product of multi-strain groups is mainly NO_3-N, it has the highest ratio in the groups of Lt7222, Lt7511, Fc6308 and Gy7018. The above result indicates that the multi-strain groups can degrade the organic nitrogen more thoroughly than the single strains by synergetic effect.

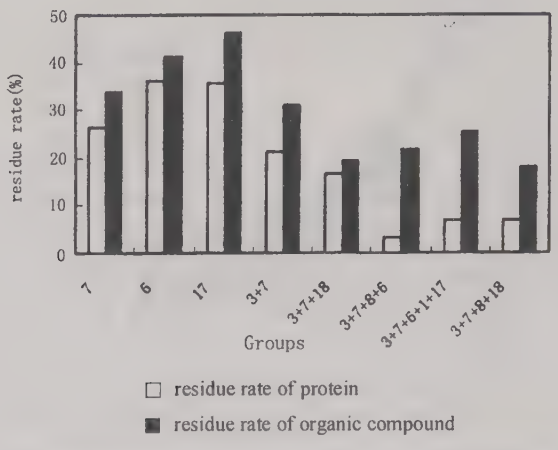

Fig. 4 Protein and total organic matter degrading of different groups

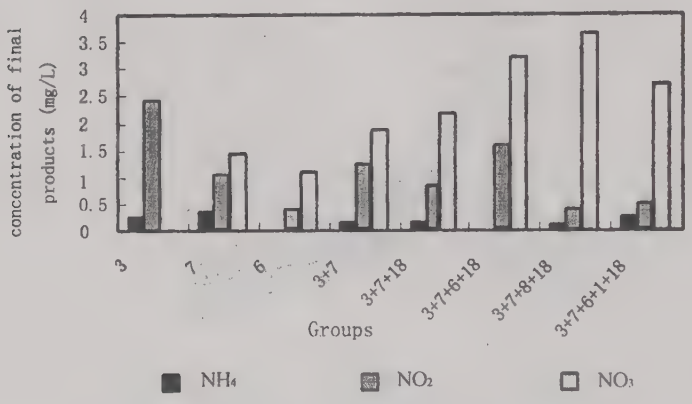

Fig. 5 Degrading products of different groups

3 Discussion

It can be seen from the result of composing experiments, the multi-strain groups have a better degrading effect than the single-strain groups, and the groups composed of different strains have different effects. In order to inquire into the mechanism, the enzyme activities of every strain are analyzed, the result indicates that the strain Lt7222 shows high activity of amylase and lipase; the strain Lt7511 shows activity of urease and lecithinase, besides amylase and lipase; the strain Gy7018 shows activity of amylase and lipase, but no activity of protease; the strain Lt7132 only has amylase activity; while the strain Fc6308 shows high activity of protease, so, the group composed of Lt7222, Lt7511, Fc6308 and Lt7451 has a lower total organic matter degrading rate, but a higher protein degrading rate. When different strains are composed together, the total degrading rate of shrimp feed is increased because of the complementary action of enzymes. Furthermore, the stronger and the more kinds of the enzyme of single strain, the higher of the COD removal rate of the group.

In the natural ecosystem, the indigenous flora has stable complementary and symbiotic relationships, and it can thoroughly mineralize the organic matter. In many engineerings of

bioremediation, indigenous mix cultures from polluted environment are used[6, 7]. So, in bioremediation through bioaugmentation, we should also optimize the composition of functional bacteria in the light of the pollutant removing rate, thoroughness of degradation, no hazardous intermediate and final product accumulation. According to the above, the two compositions are selected in this paper.

Reference

[1] Austin B, *et al.* A probiotic strain of *Virbio Alginolyticus* effective in reducing disease caused by *Aeonomas salmonicida*, *Vireo anguillarum* and *Vibrio ordalii*. Journal of fish disease, 1995, 18: 93-96.

[2] Ma W Y, Yang L Y *et al.* Environmental Microbiology Engineer. Nanjing: Press of the University of Nanjing. 1998.

[3] Jiang X P, Chen S Y. Study on Treatment of Fish Processing Wastewater with High Concentrate by Red Nonsulfur Photosynthetic Bacteria. J ocean university of Qingdao. 1989, 19(2): 134-142.

[4] Zhang Z M, Liu J X, Wang Y F. Study on the Purple Nonsulfur Photosynthetic Bacteria II. Purification of organic waste solutions with high concentration by rhodopseudomonas spheroids. J Shanxi University, 1985 (2): 103-110.

[5] State Ocean bureau. Standard of oceanography monitoring. HY003.5-91, 1991, State Ocean bureau. Standard of oceanography investigation. Beijing: Ocean Press. 1991.

[6] Banerjee D K *et al.* Monitoring the biological treatment of anthracence-contaminated soil in a rotating-drum bioreactor. App. Microbiol Biotechnol. 1995, 43: 521-528.

[7] Corseuil Henry X *et al.* Implications of the Presence of Ethanol on Intrinsic Bioremediation of BTX Plumes in Brazil. Hazardous waste & hazardous material, 1996, 13(2): 213-221.

Investigation of Macrobenthos in the Intertidal Zone of Tianjin and Discussion on Bioremediation

Hu Guikun (胡桂坤), Zhang Qingtian (张青田)
Marine Science & Engineering College, Tianjin University of Sci. & Tech., Tianjin 300450, China

Abstract An investigation of macrobenthos in the littoral zone was carried out in Tanggu District, Tianjin City in June 2003. This investigation was the only integrated one since 1983 there. Something about macrobenthos investigation was reported in this paper. The results showed that the biomass of macrobenthos of that area was almost at the same level as that of 1983, and the density of macrobenthos increased a little. The biomass of *Mactra veneriformis* has great effect on the average biomass of that area. The diversity of macrobenthos has changed obviously, and 5 or 6 kinds of macrobenthos have become extinct or decreased greatly. So the ecological structure of macrobenthos has become simpler and unstable. In addition, some ecological methods to remedy the area are discussed in this paper.

Keywords macrobenthos, bioremediation, intertidal zone, Tianjin

Introduction

Bohai Sea is a nearly enclosed sea, and the exchanging ability of water is poor. So the pollution condition of Bohai Sea is more serious than other seas in China. Tianjin City is an important city that lies by the Bohai Bay, and the pollution of Tianjin seashore zone is also serious. All kinds of wastewater from Beijing city and Tianjin city are the main pollution for the seashore zone of Tianjin. Both marine petroleum exploitation in the Bohai Bay and transportation of Xin'gang Harbor have an impact on the condition of this area. These kinds of pollution have made many marine organisms die out or their quantity decrease greatly. And fisheries of Tianjin have been affected badly because the Bohai Bay has been very short of fisheries resource.

Because of these reasons above, more and more studies about the Bohai Bay have been carried out. However, most of these studies were on the neritic zone of Bohai Bay, and the integrated study on the intertidal zone of Bohai Bay has not been carried out since 1983[1]. So it is very important to make an integrated investigation of this intertidal zone. The results of the investigation will make people know what the condition is at present, and will play a great role in the management and bioremediation of this zone. Supported by the National 863 Program, an integrated investigation in this area was carried out in Tanggu District, Tianjin City in June 2003. The results of macrobenthos investigation are mainly reported in this paper, and the corresponding data are analyzed and compared with that of 1983. Because the scope of this investigation is smaller than that of 1983, the data of near sites, such as Gaoshalings and Lvjuhes, are selected and compared.[1)]

Some information about the intertidal zone of Tianjin is as follows: The intertidal zone is very broad. It has a plain topography with a small slope. The type of tide in this area is irregular semidiurnal,

Received on August 8, 2003
The paper is supported by the National 863 Program under the contract No. 2002AA648010.
1) Investigation of marine biological resources in the coastal zone of Tianjin. 1986. Unpublished data.

i.e., there are two high tides and two low tides per lunar day, and the current velocity of ebb tide is slower than that of flood tide.

1 Investigation design

1.1 Investigation scope

According to the requirement of this investigation, many surveys and field prospecting were carried out. And about 20 km^2 of this intertidal zone was finally selected as demonstration zone of bioremediation. The actual zone was from Lüjuhe to the outdoor bathing beach of Tanggu. According to the Specifications for Marine Monitoring (SFMM, its edition number is GB 17378.7-1998)[2], 16 sites in the demonstration zone were selected to make the investigation of macrobenthos. The actual locations of these sites are listed in Table 1. These sites were arranged in 4 lines, which were vertical to the bank, and 4 sites were arranged in each line. The 4 sites of line 1 were marked as 1-1, 1-2, 1-3, 1-4 in proper order from the bank to the Bohai Sea, and the sites in other lines were also marked according to the same rule.

Tab. 1 Sites of the investigation of macrobenthos in the intertidal zone

Site	1-1	1-2	1-3	1-4	2-1	2-2	2-3	2-4
38° N	51′ 54″	51′ 47″	51′ 38″	51′ 31″	52′ 21″	52′ 12″	52′ 04″	52′ 00″
117° E	38′ 14″	38′ 27″	38′ 40″	38′ 54″	38′ 38″	38′ 51″	39′ 04″	39′ 17″
Site	3-1	3-2	3-3	3-4	4-1	4-2	4-3	4-4
38° N	52′ 47″	52′ 39″	52′ 31″	52′ 22″	53′ 24″	53′ 16″	53′ 07″	52′ 59″
117° E	39′ 02″	39′ 16″	39′ 28″	39′ 41″	39′ 36″	39′ 49″	40′ 01″	40′ 14″

1.2 Investigation methods

The investigation and analysis were carried out according to SFMM (GB 17378.7-1998)[2].

1.3 Investigation time

The basic investigation was carried out on the 4 lines at the same time on June 17, 2003. The samples were taken when ebb tide occurred. After being processed according to the requirement of SFMM, the samples were taken quickly to the laboratory of Marine Science and Engineering College, Tianjin University of Science and Technology for further indoor analysis.

2 Results and analysis

2.1 Biomass and density of macrobenthos in the intertidal zone

The investigation results of the biomass and the density of macrobenthos are showed in Figs. 1 and 2. The weight of macrobenthos in Figure 1 was wet weight after macrobenthos were soaked in formaldehyde for 3d, and the weight of shell was also included. The average biomass of this area was 661.45 g/m^2, and the average density of this area was 359.38 $ind./m^2$. The biomass and the density of the 16 sites were different greatly, and the macrobenthos were not well-distributed over this area. Something about biomass could be seen from the figure 1, the highest and the lowest values of biomass appeared in the sites 1-3 and the sites 2-1 in sequence. The highest value of biomass was about 75 times larger than

the lowest value of biomass. The values of biomass in each line increased progressively from the coastline to the sea, but the value became less at the 4th site, which was the furthermost site to the bank.

The corresponding trend of the density could be seen in Fig. 2, and the highest and the lowest values of density appeared in sequence in the sites 4-3 and the sites 3-4. The difference of the two values was about 17 times.

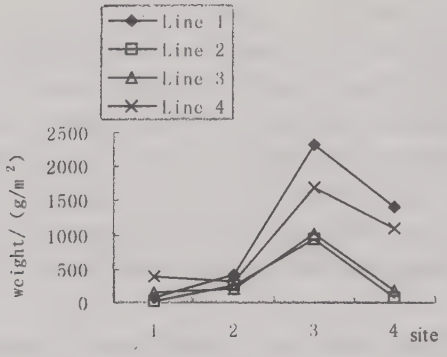

Fig. 1 Results of the biomass of macrobenthos in the investigation sites

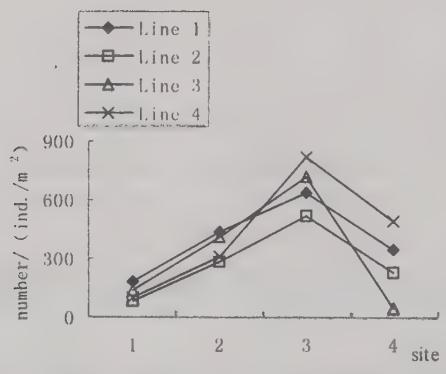

Fig. 2 Results of macrobenthos density in the investigation sites

The trend was maybe caused by the distribution of *Mactra veneriformis*. The percentage of biomass of *M. veneriformis* varied from 0 % to 95.17 % in these sites. The biomasses of line 1 and line 4 were obviously larger than those of line 2 and line 3, which was mainly caused by the difference in the biomass of *M. veneriformis*. The sediments of high biomass sites were suitable for *M. veneriformis* to grow[13]. In addition, the biomass of very few sites affected the average biomass of the whole investigation zone greatly.

The trend of results was similar to that of 1983. In 1983, the annual average biomasses of Gaoshaling and Lüjuhe were 211.09 $g/m^2 \cdot a$ and 201.60 $g/m^2 \cdot a$ in sequence. And the highest average value of biomass was 638.55 g/m^2 in the middle of the intertidal zone of Gaoshaling. To compare the values of biomass only, the results of this investigation were larger obviously than those of 1983. But it must be pointed out that the Haifang Road built several years before affected the structure of the

intertidal zone greatly, and most of the investigation sites were in the middle of the intertidal zone in which the biomass was always larger than other areas. In addition, the value of biomass in 1983 was the average value of the whole year, and the results showed that the biomass of macrobenthos changed seasonally. After integrated analysis with these reasons above, it could be concluded that the biomass of this investigation was almost the same as that of 1983.

The annual average density of 1983 was 599.40 ind./m^2 • a, and the corresponding value in the sand zone was 117.70 ind./m^2 • a. To analyze in terms of biomass, the density of this investigation was a little larger than that of 1983.

2.2 Components of macrobenthos

About 22 kinds of macrobenthos and 12 kinds of macrobenthos shell have been gathered in this investigation zone. The main species of macrobenthos are showed in Table 2[4-7].

Tab. 2 Components of macrobenthos in the area

Number	Macrobenthos	Number	Macrobenthos
1	*Anthopleura xanthogrammica*	18	*Periophthalmus* sp.
2	*Cerinathus* sp.	19	*Diopatra neapolitana*
3	*Lingula anatina*	20	*Glycera chirori*
4	*Morella iridescens*	21	*Goniada* sp.
5	*Nassarius succinctus*	22	*Nereis* sp.
6	*Mactra veneriformis*	23	*Neverita didyma**
7	*Umbonium thomasi*	24	*Siliqua pulchella**
8	*Nassarius* sp.	25	*Barnea davidi**
9	*Nassarius varicifera*	26	*Potamocorbula amurensis**
10	*Palaemon* sp.	27	*Arca (Anadara) subcrenata**
11	*Philyra pisum*	28	*Dosinia japonica**
12	Grapsidae	29	*Epitunium* sp.*
13	*Diogenes edwardsii*	30	*Meretrix meretrix**
14	*Macroplithalmus japonicus*	31	*Solen* sp.*
15	*Eriocheir leptognathus*	32	*Cerithium* sp.*
16	*Acetes chinensis*	33	*Ostrea* sp.*
17	*Exopalaemon* sp.	34	*Balanus* sp.*

Note: "*" means for that only the shell was found.

The percentages of different kinds of macrobenthos in each site are listed in Table 3. As seen from Table 3, polychaeta, mollusk and crustacean are the main components of macrobenthos, and the percentages of the 3 kinds of macrobenthos are almost equal, but the mollusk (*M. veneriformis* especially) plays an important role in the ecosystem because its individual weight is bigger than that of others. The percentages are almost consistent with the results of 1983, but the effect of crustacean has decreased a little.

Ninety-five kinds of macrobenthos were gained in 1983, and about 20 kinds of macrobenthos among them lived in Gaoshaling. For example, there were *M. veneriformis*, *Arca (Anadara) subcrenata*,

Tab. 3 Percentages of different macrobentho species

Site	Coelenterata	Polychaeta	Mollusca	Crustacea	Others
1-1	0	20	20	60	0
1-2	0	25	25	33.33	16.67
1-3	0	28.57	28.57	21.43	21.43
1-4	0	20	33.33	33.33	13.33
2-1	0	16.67	33.33	50	0
2-2	0	30	20	30	20
2-3	0	33.33	22.22	33.33	11.11
2-4	0	10	30	40	20
3-1	0	11.11	33.33	33.33	22.22
3-2	0	16.67	33.33	33.33	16.67
3-3	0	11.11	33.33	33.33	22.22
3-4	7.14	42.86	14.29	21.43	14.29
4-1	0	28.57	28.57	14.29	28.57
4-2	10	20	30	30	10
4-3	20	0	60	0	20
4-4	0	25	37.5	12.5	25

M. iriddescens, *N. varicifera*, *Stenthytra glabra*, L. *anatine*, *G. chirori*, *Lumbrinereis heteropoda*, *Ceratonereis* sp., *Portunus trituberculatus*, *M. japonicus*, *P. pisum*, *A. xanthogrammica*, *etc.*. The difference between the two investigations showed that the main components of macrobenthos changed obviously. Four or five kinds of dominant macrobenthos, such as *S. glabra, M. iriddescens*, have become extinct or decreased greatly although there were a lot of them before, and almost only *M. veneriformis* was left as the dominant macrobenthos.

The diversity index (Shannon Weaver index) of this area is about 2.215, the diversity of macrobenthos has decreased a little as compared with that in 1983. And the diversity indexes of several sites are much smaller. So the ecological structure of this area is becoming worse and unstable. So some proper bioremediation methods should be taken to prevent the ecosystem from collapsing.

3 Discussion

3.1 The Situation of macrobenthos in the intertidal zone

The results of this investigation show that the biomass of macrobenthos of that area is almost at the same level as that of 1983, and the density of macrobenthos increases a little. They are more than what someone has imagined. Perhaps it owes to the fact that the government has attached importance to the pollution and has managed energetically. The biomass of *M. veneriformis*, which should be paid attention to, has great effect on the average biomass of that area, and the ecological structure of macrobenthos of this area is becoming worse and unstable. The dominant macrobenthos and food web of this area are becoming simpler. It may be predicted that the ecosystem would collapse without proper bioremediation.

3.2 Handling methods against the limiting factors

The results of this investigation show that the water of this area is in the middle or poor nutrient levels, and is polluted mainly by oil and some heavy metals. The results also show that the sediment in this area is mainly polluted by oil and arsenic, a highly poisonous element[2]. These kinds of pollution have become the key factors of bioremediation, so these limiting factors must be controlled first.

In the light of the current situation, the following methods and techniques should be taken to mitigate the pollution, and to increase the carrying capacity of environment. (1) The high tolerance and the supernormal accumulations of plant for some chemical materials such as heavy metal could be made use of to mitigate the environmental pollution. So some proper alga and *Spartina anglica* that exist near by could be transplanted for the purpose[8-10]. This method would not only mitigate the environmental pollution, but also increase the primary production of this area, and it also has an advantage for bioremediation. Such transplantation should be carried out referring to the methods of bioremediation that are discussed in the following section (Section 4.3) of this paper. (2) Based on protecting and utilizing the existing microbe such as bacteria, proper bacteria group should be selected to decompose the pollution[11-13]. Furthermore, in bioremedying the marine culture eco-environment, the marine biotechnology mainly uses gene engineering bacteria and algae to degrade organic pollutants efficiently, uptake, accumulate and transform pollutants, accumulate and fix heavy metal, e.g., toxic materials, clean or transform toxic pollutants in culture environment, recover those degraded or destroyed ecosystem. Some bacteria strains have been used to clean up oil pollution, and their efficiency is ten thousand times that of natural bacteria. The recovery of oil-polluted Alaska is a successful example[14, 15]. And this method could be applied with the transplantation of the bore animals, e.g., polychaeta, in order to improve the physical and chemical qualities of the sediment and accelerate the material cycle and energy flow.

At the same time, management must be strengthened, and the pollution source should be controlled in order to prevent the pollution from emerging again later. Management is the essential method to decrease pollution, and it is also the key link in protecting the results of improvement.

3.3 Discussions on bioremediation methods for this area

Not only the limiting factors should be controlled, but also the ecological form of the biocoenosis in this intertidal zone should be improved, because only the proper ecosystem could bring about good material cycle, good energy flow, and good information transfer. And only this kind of ecosystem has a high self-controlling power. The results of this investigation show that the ecosystem form of this area is becoming simpler, and the ecosystem is becoming unstable. So the proper methods should be protecting original species, and transplanting proper new species here which are near this area. It would make a self -controlling ecosystem quickly. Certainly, the niche of different species should be paid attention to before the transplantations are carried out. The species that have the same niche should not be transplanted in order to prevent direct competition. So the following measures could be taken:

(1) Microbe is the most important decomposer of the ecosystem, so the function of marine heterotrophic bacteria in nutrient cycle and the regeneration of other inorganic elements should be paid more attention to. After this, the microbial food loop would be formed, which would be beneficial to raising the species diversity and keeping the ecosystem stable[13].

(2) Taking advantage of the symbiosis of *S. anglica* and clamworm (*Polychaetes*), *S. anglica* and *Polychaetes* e.g. *P. aibuhitensis* could be transplanted to this area. This method would not only increase

2) Assessment report of this investigation. 2003. Unpublished data.

the primary production, but also modify the structure of the sediment here. At last, the physical and chemical characters would become better than before, and the diversity index would increase certainly. More importantly, it would provide a good condition for raising the carrying capacity of this area[16-19]. Furthermore, some kinds of *Polychaetes* have high tolerance for oil, so it is very beneficial for us to carry out bioremediation with *Polychaetes* here[20, 21].

(3) According to the niche principle, the existing species e.g. *M. veneriformis etc.* would be protected and other mollusk and so on that have different niches could be transplanted here. For example, *A. subcrenata, Potamocorbula laevis, etc.* would be transplanted because they have different space niches with the main existing species here, and there were a lot of them before in this area. These bivalves would play an important role in the material recycle in the benthic-pelagic flux course. Biological subsidence could make nutrient be detained and a lot of nutrient would form the nutrient pool. This would strengthen the effects of microbe, and would accelerate the release of inorganic material from the sediment to the waters. It has been proved that N, P, Si could release faster, and the release of ammonia is most obvious[22-24]. In a word, the mollusk affects not only the plankton system, but also the benthic system[24, 25].

(4) Artificial ecological fishery reef would be set in the proper shallow sea zone where depth is about 5 m, it would provide a good environment for marine organisms to live in, reproduce, and migrate. After summarizing the experience and lessons of artificial multiplication of *Fenneropenaeus japonicus*, the method of artificial multiplication could be applied again. Some existing or migrating marine organisms, for example, *F. japonicus, F. chinensis, Portunus*, *Paralichthys olivaceus, etc.*, could be selected for this purpose. So, a concentrated resource zone about 10 km^2 would be formed in this zone later, and it would be beneficial for ecological restoration on a larger scale.

By using these methods, not only the pollution of this area could be lightened, stable ecosystem could be formed, ecosystem could be recovered, but also enormous economic value could be obtained gradually. It is predicted that the best mode of ecological-economic benefit could be established and a fine recycle among coastal ecosystems, marine biology and economy could be realized in 4 - 5 years. Furthermore, the operable technical scheme and standard of bioremediation for the similar intertidal zone could be formed and the reference data could be provided.

Acknowledgements

This investigation received the support of many teachers of Tianjin University of Science and Technology, such as Chen Huibin, Li Haiming, Dong Jinggang, Zhang Fu, Yi Lixia, Liu Xianbin, Cui Qingfa, and some senior students of marine science major in this university. It is also supported by the Tanggu Fisheries Bureau. Thanks to all of them.

Reference

[1] Xu L M. Character and analysis of the alluvial shoal zone in the west of Bohai Bay. Harbor & Engineering Technology. 1996, 2: 9-14.

[2] State Quality and Technical Supervision Administration. The Specifications for Marine Monitoring, Part 7: ecological survey of offshore pollution and biological monitoring (GB 17378.7-1998). 1998, 42-54.

[3] Li Z J, Zhang Q, Zhang H H, *et al.* Mollusk culture. Guangzhou: Guangzhou Science and Technology Press. 1999, 163-165.

[4] Li M D. Ichthyography. Beijing: Ocean Press. 1998, 50-200.

[5] Qi Z Y. China Economic Mollusk. Beijing: China Agriculture Press. 1998, 45-500.

[6] Liang X Q, Fang J Z, Yang H Q. Aquatic Biology. Beijing: China Agriculture Press. 1996, 169-364.

[7] Yang D J, sun S C. Ocean Invertebrate. Qingdao: Ocean University of Qingdao Press. 1999, 90-437.

[8] Yang J P, LU J B. Technology for ecological restoration. Beijing: Chemical Industry Press. 2002, 1-58.

[9] Chang X L, Wang W H, Feng Y M, *et al.* Investigation of cadmium (II) biosorption on *Sargassum kjllmanum.* Marine Science Bulletin, 2003, 22(4): 26-31.

[10] Marine monitoring quality guarantee handbook editor group. Marine monitoring quality guarantee handbook. Beijing: China Ocean Press. 2000, 249.

[11] Hu G K, Zhang Q T. Role of marine bacteria in the ecological recovery. Marine Information, 2002, 4: 20-22.

[12] Cai M G, Qian A H, Wang X, *et al.* Study on the condition of oil pollution and self-purification at Dapengao, Daya Bay. Marine Science Bulletinm, 2003, 22(5): 34-37.

[13] Ning X R. Microbial food loop. Donghai Marine Science, 1997, 15(1): 66-68.

[14] Zhang S C, Fan X, Ma Y J. The principle and application of marine biology technology. Beijing: China Ocean Press. 1997, 1-5.

[15] Prichard P H. Oil spill bioremediation experiences, lessons and results form the Exxon Valdex oil spill in Alaska. Biodegradation,1992, 3(2-3): 315-335.

[16] Zhang Z N, Sun W L, Yu Z S, *et al.* Large scale transplant of the *Neanthes japonica* (Izuka) population. Oceanologia et Limnologia Sinica, 1993, 24(5): 520-526.

[17] Zhao Q L, Zhao Q. Effects of *Spartina anglica* on the soil habitats of *Perinereis aibuhitensis.* Chinese Journal of Ecology, 1997,16(2): 28-30.

[18] Jiang F X, Wang W Z, huang Y S, *et al.* Preliminary study on interactions between *Spartina anglica* C. E. Hubbard and *Perinereis aibuhitensis* Grube. ACTA ECOLOGICA SINICA, 1992, 12(1): 84-88.

[19] Wang S H, Zhang Z N. Study of *Neanthes japonica* feeding on natural sediment. Journal of Ocean University of Qingdao, 2002, 32(3): 409-414.

[20] Dekker R, Moorsel V W N M. Effects of different oil doses, diapersant and dispersed oil on macrofauna in model tidal flat ecosystems. In: Fate and effects of oil in marine ecosystem. Kuiper J. Holland: Nijhoff Publishers. 1987, 117-131.

[21] Tang S M, Chen X L, Zhuang D F, *et al.* Simulating ecological study on the effects of Polychaetes on diesel oil pollution. ACTA OCEANOLOGICA SINICA, 1993, 15(4): 85-90.

[22] Han J, Zhang Z N, Yu Z S. Effects of Manila clam (Ruditapes philippinarum) on the benthic-pelagic particle flux in Xuejiadao intertidal zone. Journal of Ocean University of Qingdao, 2001, 31(5): 723-729.

[23] Davis W R. The role of bioturbation in sediment resuspension and its interaction with physical shearing. Journal of Experimental Marine Biology and Ecology, 1993, 171: 235-249.

[24] Ji R B, Mao X H, Zhu M Y. Impacts of coastal shellfish aquaculture on bay ecosystem. Journal of Oceanography of Huanghai & Bohai Seas, 1998, 16(1): 21-27.

[25] Hatcher A, Grant J, Schiield B. Effects of suspended mussel culture (*Mytilus* spp.) on sedimentation, benthic respiration and sediment nutrient dynamics in a coastal bay. Marine Ecology Progress Series, 1994, 115: 219 -235.

Study on the Characteristic Organic Compounds in Red Tide by Factor Analysis Method

Zhao Mingqiao (赵明桥), Li Gongke (李攻科), Zhang Zhanxia (张展霞)
School of Chemistry and Chemical Engineering, SunYat-Sen University, Guangzhou 510275, Guangdong, China

Abstract Factor analysis is used to study the organic compounds that have high degree of correlation with biomass in algal blooming. Based on this correlation, they are named characteristic organic compounds. The compounds found are sequalene (SQU), cedrol (CED), 2, 5-cyclohexadiene-1, 4-dione, 2, 6-bis(1, 1-dimthylethyl) (PBQ), phenol, 2, 6-bis (1, 1-dimethylethy-4-methyl) (BHT), 3-t-butyl-4-hydroxyanisole (BHA), 1, 2-benzenedicarboxylie acid, bis-(2-methyl propyl) ester (DIBP), dibutyl phthalate (DNBP), respectively. Monitoring the variations of concentration of these characteristic organic compounds in seawater may provide scientific basis for studying and forecasting red tides.

Keywords factor analysis, red tide, characteristic organic compound

Red tide is one of the major disasters in the world oceans today. To explore into the laws of red tide occurrence, people have studied the effect of meteorological factors, hydrological conditions and inorganic nutrients on the red tide[1-3], and determined the key factors contributing to the occurrence of red tides through such numerical analysis methods as cluster analysis, judgement analysis, principal component analysis, multiple regression analysis, *etc.* [4-9], and carried out research on red-tide forecasting.

Factor analysis[10] is a multiple statistical method for studying the correlation among a group of variables (or samples). Based on the variations in the concentration of organic compounds in seawater when the red tide occurs[11] and by applying the factor analysis method, this paper defines several principal factors that are correlated to each other in a certain characterization phenomenon acted upon by many factors, and studies the organic compounds with close relations to the red tide and their possible sources.

1 Factor analysis method

Proceeding from a set of original analysis and test data, factor analysis finds out several principal factors which govern the variables and are not related to each other by studying the internal structure of the data's related matrix (or covariance matrix). Under the precondition that the information loss of original data is reduced as far as possible, a few principal factors are used to replace the large amount of original variables, which have some relations to each other so as to reveal the internal relations among original variables and explain rationally the relation between the environmental phenomena and principal factors.

Received on September 8, 2003
This work is supported by the National Natural Science Foundation of China (29977029).

1.1 Mathematical model for factor analysis

The relations among the organic compounds in red tide are rather complicated. There may be some correlation among n organic compounds, jointly reflecting certain information on the red tide, or, there may be some organic compounds which are independent of each other and some information on the red tide is only exhibited in a certain organic compound. If the information on each variable (organic compound) D_i is decomposed to represent the linear combination of various information factors in the system (red tide seawater), then

$$D_i = a_{i1}F_1 + a_{i2}F_2 + \cdots + a_{ik}F_k + C_iU_i \quad (1)$$

Where, F_1, F_2, $\cdots$ F_k appear in the expression of each variable, and are called common factors, which reflect certain information common in many variables; a_{i1}, a_{i2}, $\cdots$ a_{ik} are the common factor loads, and U_i is a special factor which is only related to the variable D_i, indicating a certain special character of this variable. It is obtained by using the matrix after standardization processing as follows:

$$R = AA' + CC' \quad (2)$$

R^* ($R^* = R - CC'$) is called approximate correlation matrix. Factor analysis transforms the correlated relations among n variables into those between the n variables and the k common factors, *i.e.*, obtaining the factor load matrix through the approximate correlation matrix R^*.

V_i is the total variance contribution of the common factor F_i to all the variables, so V_i may be used to measure the importance of the common factor F_i, *i.e.*, the larger V_i is, the greater the importance of F_i is. The contribution of F_i to the total variance is expressed by the variance contribution percentage P_i. The larger the P_i is, the more important is this factor, and its accumulated total variance is:

$$Q = \sum_{j=1}^{k} P_j = (\sum_{i=1}^{k} V_j / n) \times 100\ \% \quad (3)$$

When the accumulated contribution of n common factors amounts to over 80 %, it is not necessary to obtain the following common factors. Each common factor is extracted according to the magnitude of variance contribution of each factor, *i.e.*, the variance contributions $r_1 \geqslant r_2 \geqslant r_3 \geqslant \cdots \geqslant r_k$ of the principal factors F_1, F_2, $\cdots$, F_k are extracted one by one in the order of the magnitudes of r_i. The common factors extracted in this order are called the 1st principal factor, the 2nd principal factor, $\cdots$, the kth principal factor respectively.

1.2 Variance maximum orthogonal factor rotation

Factor rotation causes the load on a variable to polarize, *i.e.*, on some variables, a given principal factor has a very high load while on other variables, the sum of its loads is close to zero, thus making it easy to reveal the laws of the factors (variables) and the system information and understand their inherent nature. The common factor rotation method is the variance maximum orthogonal factor rotation method. For any orthogonal matrix T, we have:

$$BB' = AT(AT)' = ATT'A' = AA' = R \quad (4)$$

The matrix $B = AT$ after orthogonal transformation of A is still a factor solution of R.

1.3 Factor score

The common factor is expressed by the linear combination of variables (or samples), *i.e.*,

$$F_j = \beta_{j1}x_i + \beta_{j2}x_2 + \cdots + \beta_{jp}x_k \quad (j = 1, 2, \cdots, m) \quad (5)$$

The factor score on the factor R of each sample is calculated. Factor score may indicate the interrelationship between samples, which is of practical significance to the classification of samples.

According to the factor model, the factor score is:

$$F = A'R^{-1} D \quad (6)$$

A' is the displacement of the factor load matrix after orthogonal rotation, R^{-1} is the inverse matrix of the variable correlation matrix and D is the matrix after the standardization of original data. The k main factor values of m samples obtained from the data matrix computation after the standardization of m samples may indicate the relations among samples and classify them.

2 Experimental

2.1 Analysis of red tide seawater samples

The red tide seawater samples from the Zhujiang River mouth in the South China Sea in Mar.—May, 1998 were chosen to measure the concentrations of organic compounds by using the SPME-GC-MS method. The results of analysis are used to analyze the following data.

2.2 Selection of organic compounds for factor analysis

The organic compounds in the red tide seawater are taken as variables for factor analysis. The selection is made according to the following principles:

(1) Trace organic compounds must be chosen;

(2) The degree of matching between subtrace organic compounds must be above the intermediate level and reference material is defined by contrast upon preliminary qualification by MS;

(3) The detection rate is over 80 %.

Following the above-mentioned principles, 16 organic compounds are chosen as variables for factor analysis, including PDA, HDA, SQU, DDO, CED, PBQ, BHT, BPA, BHA, TDC, HDC, ODC, OEC, DIBP, DNBP and DEHP.

3 Results of factor analysis

3.1 Correlation coefficient matrix

After standardized processing of the analytical data, each organic compound is taken as a variable to the correlation coefficients among various variables and obtain the correlation matrix for the 16 variables (Table 1). The absolute values of these correlation coefficients are mostly larger than 0.3, indicating there is some correlation among these variables, *i.e.*, there exists some relationship of interdependence and inter-constraint among them in the course of red tide occurrence.

3.2 Preliminary results of factor analysis

Based on the correlation matrix obtained from original variables, all the characteristic values and eigenvectors are calculated and the common factors with characteristic values larger than 1 are extracted by using the principal component analysis method. The preliminary results of factor analysis are shown in Tab. 2. It can be seen from Tab. 2 that there are four principal factors with the characteristic values larger than 1 and the accumulated variance of these four principal factors is 87.96 %, indicating that these four factors can better reflect the information in the original data matrix and be used as the cattell for characteristic value-factor number (Fig. 1). It can be seen from Fig. 1 that from the fourth factor downwards, the curve tends to be flat and its variance contribution (characteristic value) rapidly decreases, indicating that the total characteristic value does not change significantly with the increase of

Tab. 1 Correlation coefficient of variance

Variable	PDA	HDA	SQU	DDO	CED	PBQ	BHT	BPA	BHA	TDC	OEC	HDC	ODC	DIBP	DNBP	DEHP
PDA	1	0.713	0.56	0.691	0.581	-0.03	0.721	0.66	0.68	0.13	0.027	0.272	-0.03	0.402	0.205	0.592
HDA	0.713	1	0.687	0.846	0.854	-0.37	0.775	0.699	0.629	0.273	0.322	0.341	0.029	0.599	0.213	0.365
SQU	0.560	0.687	1	0.651	0.614	0.059	0.656	0.574	0.652	0.067	0.246	0.501	0.226	0.628	0.546	0.483
DDO	0.691	0.846	0.651	1	0.937	-0.3	0.749	0.631	0.717	0.158	0.187	0.487	0.205	0.752	0.369	0.58
CED	0.581	0.845	0.614	0.937	1	-0.46	0.572	0.604	0.537	0.125	0.106	0.234	-0.06	0.833	0.415	0.502
PBQ	-0.03	-0.37	0.059	-0.3	0.46	1	-0.1	-0.42	-0.18	0.202	0.167	0.167	0.532	-0.07	0.216	-0.1
BHT	0.721	0.775	0.656	0.749	0.572	-0.1	1	0.697	0.909	0.21	0.419	0.699	0.45	0.329	0.012	0.577
BPA	0.66	0.699	0.574	0.631	0.604	-0.42	0.697	1	0.83	-0.35	0.182	0.324	-0.17	0.223	-0.21	0.681
BHA	0.68	0.629	0.652	0.717	0.537	-0.18	0.909	0.83	1	-0.15	0.251	0.69	0.319	0.261	-0.05	0.745
TDC	-0.13	0.273	0.067	0.158	0.125	0.202	0.21	-0.35	-0.15	1	0.665	0.367	0.569	0.236	0.169	-0.48
OEC	0.027	0.32	0.246	0.187	0.106	0.167	0.419	0.182	0.251	0.665	1	0.641	0.492	9E-04	-0.23	-0.17
HDC	0.272	0.341	0.501	0.487	0.234	0.167	0.699	0.324	0.69	0.367	0.641	1	0.742	0.133	0.022	0.204
ODC	-0.03	0.029	0.226	0.205	-0.06	0.532	0.45	-0.17	0.319	0.569	0.492	0.742	1	0.083	0.117	0.067
DIBP	0.402	0.599	0.628	0.752	0.833	-0.07	0.329	0.223	0.261	0.236	9E-04	0.133	0.083	1	0.756	0.36
DNBP	0.205	0.213	0.546	0.369	0.415	0.216	0.012	-0.21	-0.05	0.169	0.23	0.022	0.117	0.756	1	0.11
DEHP	0.592	0.365	0.483	0.58	0.502	-0.1	-0.1	0.681	0.745	0.48	0.17	0.204	0.067	0.36	0.11	1

Tab. 2 Preliminary results of factor analysis

Variable	Variance contribution	Factor	Characteristic value	Common factor variance	Accumulated variance
PDA	1.000	1	7.239	45.245	45.245
HAD	1.000	2	3.059	19.120	64.365
SQU	1.000	3	2.243	14.019	78.384
DDO	1.000	4	1.533	9.582	87.965
CED	1.000	5	0.663	4.142	92.108
PBQ	1.000	6	0.516	3.222	95.330
BHT	1.000	7	0.362	2.263	97.593
BPA	1.000	8	0.219	1.369	98.962
BHA	1.000	9	0.103	0.646	99.607
TDC	1.000	10	5.298E-02	0.331	99.939
OEC	1.000	11	9.820E-03	6.138E-02	100.000
HDC	1.000	12	5.371E-16	30357E-15	100.000
ODC	1.000	13	3.635E-16	2.272E-15	100.000
DIBP	1.000	14	1.421E-16	8.883E-16	100.000
DNBP	1.000	15	-1.724E-16	-1.078E-15	100.000
DEHP	1.000	16	-3.783E-16	-2.364E-15	100.000

factor number. Factor analysis transforms the 16 variables into four principal factors that are different from each other and the number of variables is greatly reduced. Based on the factor score, the covariance matrix of the regression factor fraction is calculated, *i.e.*, the correlation matrix among factors. The correlation coefficients among various factors are all zero except themselves, showing that these four factors are mutually independent and almost entirely non-correlative. Except PDA and SQU, all the organic compounds have their variances larger than 0.8, *i.e.*, the four factors can explain the most majority of variances, thus indicating that it is appropriate to take the number of main factors as four in the present study.

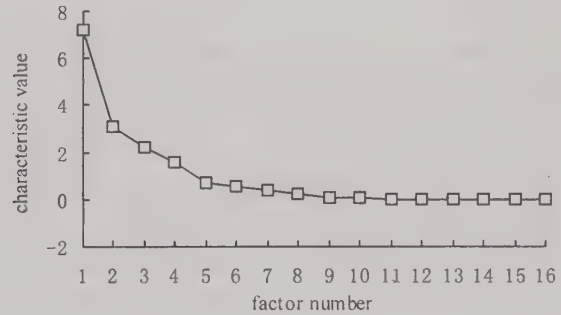

Fig. 1 Cattell for the confirmation of main factors

3.3 Matrix of factor load

Based on the magnitude of characteristic values, four principal factors each with a characteristic value larger than 1 are extracted and their matrix of factor load is shown in Tab.3. From this load matrix, the score expression for each principal factor may be written with various original variables, *i.e.*, Factor 1 = 0.773·PDA + 0.880·HDA + 0.81·SQU + 0.933·DDO + 0.844·CED 0.21·PBQ + 0.892·BHT + 0.772·BPA + 0.867·BHA + 0.1·TDC + 0.296·OEC + 0.584·HDC + 0.246·ODC + 0.647·DIBP + 0.287·DNNBP + 0.664·DEHP. The expressions for the other three factors may be inferred.

3.4 Naming of factors

It can be seen from the matrix of factor load that Factor 1 has larger load coefficients on PDA, HDA, DDO, CED, SQU and PDA, HAD, DDO are mainly the organic compounds resulted from metabolism of red tide organisms, indicating that these organic compounds have stronger links with red tide. When the red tide occurs, the concentrations of these organic compounds increase and their incremental quantity is positively correlated to red tide organisms. Factor 1 also has larger load coefficients on BHT, BHA and BPA, and these organic compounds mainly originate from such antioxidants as food, fat or oil, forage and rubber, *etc.* Their concentrations may vary with the activity of red tide organisms, *i.e.*, when the number of red tide organisms increase, the concentrations of these organic compounds also increase. Factor 2 has larger load coefficients on TDC, OEC, HDC and ODC and these organic compounds are all organic acids, which are mainly resulted from metabolism of red tide organisms or decomposition and release of marine life after their death. But they and PDA, HDA are not in the one and same main factor. PDA, HDA, DDO, CED, SQU, *etc.* are mainly neutral compounds while TDC, OEC, HDC and ODC present weak acidity, thus suggesting that there are differences in source and nature between these two types of matter. Factor 2 shows relations with organic acids. Factor

Tab. 3 Matrix of factor load

Variable	1	2	3	4
PDA	0.773	-0.215	-0.062	0.176
HDA	0.88	-0.052	0.1002	-0.36
SQU	0.81	0.0852	0.2056	0.218
DDO	0.933	-0.049	0.1829	-0.11
CED	0.844	-0.23	0.3386	-0.28
PBQ	-0.21	0.5712	0.1179	0.657
BHT	0.892	0.2131	-0.295	0.02
BPA	0.772	-0.367	-0.443	-0.08
BHA	0.867	-0.009	-0.431	0.181
TDC	0.1	0.8006	0.3156	-0.45
OEC	0.296	0.7258	-0.259	-0.38
HDC	0.584	0.6379	-0.295	0.099
ODC	0.246	0.8481	-0.067	0.299
DIBP	0.647	-0.054	0.7084	-0.002
DNBP	0.287	0.0377	0.8688	0.318
DEHP	0.664	-0.378	-0.203	0.465

Note: Methods of extraction: principal component analysis; Extraction of factor number; extraction of 4 principal factors.

3 has larger load coefficients on DIBP and DNBP, which are mainly the plasticizers of phthalic resin type in the plastics, indicating that this factor is related to these compounds. DIBP, DNBP etc. in the ocean are mainly adsorbed in the bed mud, and when the red tide occurs, the action of marine microorganisms may cause the DIBP and DNBP in the bed mud to release into the sea water, thus increasing their concentrations. Factor 4 has a longer load only on PBQ, which is mainly the oxidized product of the rubber anti-oxidant. In contrast to other compounds, the concentration of PBQ in sea water when the red tide occurs is lower than that before the red tide, which is possibly due to the anoxic or even anaerobic sea water. PBQ mainly originates from the oxidized products of BHT, BHA, EPA and under anoxic conditions, its oxidization speed slows down, thus reducing the concentration of PBQ.

In order to further reveal the relations of these organic compounds with various factors, the matrix of factor load is rotated by the variance maximum rotation method, and the matrix of rotation factor after rotation is shown in Tab. 4. Factor 1 still has larger loads on PDA, HDA, SQU, DDO, BHT, BHA and BPA, Factor 2 has larger loads on CED, DIBP and DNBP, Factor 3 has larger loads on TDC, OEC, HDC, and ODC and Factor 4 has larger loads on PBQ. It can be seen that the matrix of factor load changes little before and after rotation, and therefore, it is appropriate to classify these compounds by using this factor method. However, CED has a larger load on Factor 1 before rotation, while it has a larger load on Factor 2 after rotation, indicating that CED is somewhat different from PDA, HDA, SQU and DDO in source and nature. In fact, PDA, HDA, DDA, *etc.*, mainly originate from marine bacteria while CED mainly comes from terrestrial plants, and the factor analysis points to their difference in source.

Tab. 4 Matrix of rotation factor

Variable	1	2	3	4
PDA	0.754	0.317	-5.115E-02	-8.622E-02
HDA	0.592	0.480	0.345	-0.469
SQU	0.626	0.568	0.167	0.108
DDO	0.668	0.590	0.238	-0.259
CED	0.506	0.681	0.125	-0.474
PBQ	-0.135	3.218E-02	0.118	0.884
BHT	0.845	0.151	0.436	-2.926E-02
BPA	0.879	-3.106E-02	-2.394E-02	-0.400
BHA	0.968	3.030E-02	0.183	-8.500E-03
TDC	-0.315	0.291	0.875	2.919E-02
OEC	0.140	-0.122	0.889	-7.614E-03
HDC	0.542	4.754E-03	0.678	0.302
ODC	0.180	5.609E-02	0.653	0.642
DIBP	0.223	0.927	5.749E-02	-0.100
DNBP	-7.395E-02	0.917	-0.122	0.281
DEHP	0.835	0.158	-0.335	8.588E-02

The organic compounds in the red tide seawater may be classified as follows through the above-mentioned factor analysis:

(1) Metabolic factors: PDA, HDA, SQU, DDO, TDC, OEC, HDC and ODC mainly originate from growth, reproduction, metabolism and decomposition of red tide organisms or other marine organisms. They are named metabolic factors. Based on the differences in their physicochemical character and source, the factor analysis method is used to divide them into two parts. The neutral compounds of PDA, HDA, SQU and DDO are named the metabolic factor Ⅰ and the organic acids of TDC, OEC, HDC and DOC the metabolic factor Ⅱ, so as to indicate the differences in their nature, source and relations to the red tide.

(2) Pollution factor: PBQ, BHT, BHA, BPA, DIBP and DNBP are the industrial pollution organic compounds discharged into the sea. Among them, PBQ, BHT, BHA and BPA are of the redox character and may be subjected to the effect of dissolved oxygen and red tide organisms in the red tide environment. Factor analysis indicates that they are closely related to the activity of red tide occurrence, so BHT, BHA and BPA are named the pollution factor Ⅰ; DIBP, DNBP and DEHP are possibly mainly subjected to the decomposition, transformation, release of marine microorganisms and the factor analysis indicate that they are somewhat different from other pollutants, so they are named the pollution factor Ⅱ.

(3) Terrigenous plant factor: CED mainly originates from the terrestrial plant and also from marine organisms. In the factor rotation matrix, it has not only some load on the factor 2, but also larger load on the factor 1. Factor rotation indicates that there are both links and differences between CED and the metabolic factor Ⅰ, so it is named the terrigenous plant factor.

4 Detection of the red-tide characteristic organic compounds

Based on the above-mentioned factor analysis, we may define the typical red-tide characteristic organic compounds, and provide basis for the monitoring, prediction, prevention and control of red tides by measuring the variations in the concentrations of characteristic organic compounds. The red-tide characteristic organic compounds are defined on the basis of typicality, universality, early-warning nature, convenience in measurement and the principle that they can represent different categories in the factor analysis.

SQU, CED, PBQ, BHT, BHA, DIBP and DNBP are chosen as the typical red-tide characteristic organic compounds. PDA and HDA have lower concentrations and for DDO, TDC, OEC, HDC and ODC, despite larger variations in their concentrations before and after the red tide, the concentration variations lag behind the occurrence of red tide, so they are not chosen as the typical red-tide characteristic organic compounds.

5 Conclusions

The organic compounds in the red-tide seawater are divided into the metabolic, pollution and terrigenous plant factors by using the factor analysis method. Based on the correlation of these organic compounds and the mutually influencing relations between them and the red tide algae and marine microorganisms, they are further divided into the metabolic factor Ⅰ and the metabolic factor Ⅱ; the pollution factor Ⅰ and the pollution factor Ⅱ; and the terrigenous plant factor. The organic compounds of SQU, CED, PBQ, BHT, BHA, DIBP and DNBP, which have closer relations with the red tide, are hosen as the red-tide characteristic organic compounds.

We have made regression analysis with the concentrations of red-tide characteristic organic compounds in seawater as independents and the natural logarithm of the red-tide organism density as a dependent variable, and carried out the research on red tide prediction. The results of prediction are satisfactory [12].

References

[1] Foster P, Voltolina D, Spencer C P, *et al* A seasonal study of the distribution of surface state variables in Liverpool Bay. J. Exp Mar Biol Ecol., 1983, 73: 151-165.

[2] Huang C, Qi Y. The abundance cycle and influence factors on red tide phenomena of noctiluca scintillans (dinophyceae) in Dapeng Bay, the South China Sea. J Plankton Res., 1997, 19(3): 303-318.

[3] Zhong Sisheng, Li Jinrong, Luo Yidan. Analysis of environmental factors contributing to the occurrence of Peridinium pentagonum red tide in the Daya Bay. Marine Environmental Science, 2002, 21(1): 34-38.

[4] Qi Yuzao, Hong Ying, Lü Songhui, *et al.* Outbreak of *Chattonella marina* red tide and its relations to ecological parameters in the Dapeng Bay, South China Sea. Oceanologia et Limnologia Sinica, 1994, 25(2): 132-138.

[5] Wang Anli, Wang Weina. Research on the relationship between the shrimp pond red tide and the environmental factors. Acta Oceanologica Sinica, 1995, 17(2): 128-133.

[6] Wang shousong, Feng Guocan, Xia Zongwan, *et al.* Structural analysis of the essential factors associated with the noctiluca scintillans red tide in Dapeng Bay. Oceanologica et Limnologia Scinica, 1994, 25(2): 146-151.

[7] Qi Yuzao, HuangWeijian and Qiu Xuanhong. Time-series model for the population dynamics of noctiluca scintillans in the Dapeng Bay. Journal of Jinan University (Natural Science), 1991, 12(3): 96-103.

[8] Kaito S, Hirobe H, Maegawa T. On the essential sea water parameters to discriminate between red tide and non-red tide by discriminant analysis. Bull Jap Soc Sci Fish, 1985, 51(1): 1-12.

[9] Quchi A. Prediction of red tide occurrence by means of discriminant analysis. Bull Jap Soc Sci Fish, 1984b, 50(10): 1 647-1 651.

[10] Lu Xiaohua, Chemometrics. Wuhan: Huazhong University of Science & Technology Press, 1997.

[11] Li Gongke, Zhao Mingqiao, Zhang Zhanxia. Rapid detection of organic compounds in seawater during red-tide by SPME-GC-MS. Environmental Chemistry, 2000, 19(1): 73-78.

[12] Zhao Mingqiao, Li Gongke, Zhang zhanxia. Study on the relationship between the concentration of characteristic organic compounds and red tide by multiple regression. Acta Scientiarum Naturalium Universitatis Sunyatseni, 2003, 42(1): 35-38.

Annotation on Mangrove Plants

Wang Bosun (王伯荪)[1], Zhang Weiyin (张炜银)[2], Liang Shichu (梁士楚)[3], Zan Qijie(昝启杰)[4]
1 *School of Life Sciences, Zhongshan University, Guangzhou 510275, Guangdong, China*
2 *Institute of Forest Ecology and Environmental Protection, Chinese Academy of Forestry, Beijing 100091, China*
3 *Institute of Botany, Chinese Academy of Sciences, Beijing 100093, China*
4 *Guangdong Neilingding-Futian National Nature Reserve Administration, Shenzhen, 518040, Guangdong, China*

Abstract This paper reviews and discusses the technical terms and definition of mangrove and mangal, as well as mangrove plant. The word mangrove has been used to refer either to the constituent plant of tropical and subtropical intertidal community or to the community itself, but this usage makes more confusion. Being leaved mangrove in the more limited sense for the constituent plant species, mangal was proposed by MacNae (1968) as a term for mangrove community, which has been universally applied to most previous studies and should be adopted now. Mangrove should be therefore defined as a tropical and subtropical tree restricted to intertidal zones, which possesses some morphological specializion and physiological mechanism adapted to its habitat, and mangal as a tropical and subtropical forest community restricted to marine intertidal zones and periodically inundeated by the tides. A new term "consortive plant" is proposed here for herb, liana, epiphyte or parasite, which is restricted in the strict mangrove habitat.

Keywords mangrove, mangrove plant, true mangrove, semi-mangrove, mangal, consortive plant, mangal associates

Mangrove plants are woody plants that grow in the low wave energy intertidal zones and are periodically inundated by seawater in tropical and subtropical regions. They are terrestrial flowering plants entering and evolving in the seashore. They, displaying a huge biodiversity, occupy the ecological critical area (ECA) of seashore, and possess special morphological structures and physiological ecological characteristics due to their adaptation to special environment. The biological peculiarities of mangrove plants have intrigued botanists for a long time. Scientists are making an increasing commitment to broaden our knowledge of this biological community[1].

Nowadays, the total number of publications on mangrove plants exceeds 5 600 titles[2] or 7 000 titles [1]. However, there are no definite answers to what species on the earth belong to mangrove plants or how many families, genera and species exist. Furthermore, there are disputes on the definitions or concepts and technical terms on the mangrove plants.

The objective of this paper is attempting to provide a concise annotation on the related terms or issues, to clarify the existing confusions and thus to benefit the further in-depth studies and facilitate the conservation, ecological restoration and sustainable development of mangrove plants and mangal.

Received on September 7, 2003
This study is supported by the Key Program of National Natural Science Foundation of China (39830310).

1 Technical terms

Mangrove was firstly coined in 1878 by Bowman, a biologist, and originated from *mangue* (Portuguese) and *mangle* (Spanish). It was transliterated from the name of a mangrove-derived dye in Taino, a language of American Indian. In Taino, it was named the dyes of mangrove plants. In 1753, Carolus Linnaeus, a Swedish botanist who established the binomial system of nomenclature, used mangle as an epithet to name the American mangrove species *Rhizophora mangle* Linn., and used the American mangrove as the type species of *Rhizophora* Linn.

The word "mangrove" has been used to refer either to the constituent plants of tropical intertidal forest communities or to the community itself. However, mangrove should be strictly or in a narrow sense, used only for a species of the mangrove plants[3, 4], rather than broadly as a name for the mangrove trees, mangrove forest or mangrove community. Now, mangrove has become the name specifically for the constituent plant species. Moreover, *mangal*, once proposed by MacNac (1968), has been pervasively adopted as the technical name for mangrove forest or mangrove community[4, 5].

It is proper to use *mangrove* to refer to a specific mangrove plant and to use *mangal* or mangrove forest for mangrove trees so as to avoid unnecessary confusions. In addition, the term of *mangal* has been widely used in the international academic circle. Therefore, it should also be adopted domestically, thus making it convenient to do academic exchanges internationally.

2 *Mangal*

Mangal possesses the unique features of wetland ecological system and has the characteristics of both terrestrial and marine ecology. Although mangal had been attracting much public interest and attention, its definition or concept was not defined until the end of the 19th century, by A.F.W.Schimper (1856—1901) and E.Warming (1841—1924), in 1885 and 1886, respectively.

Mangrove vegetation, the 'mangrove formation' of Schimper, is "a complex of plant communities covering large areas fringing sheltered tropical shores. It varies in character from forest 30 m high or more to a poor scrub barely 2 m high"[6]. Warming[7] thought that mangal is a plant community that forms a low forest or a shrub with rich pneumatophores, inhabits at the tropical seashore wetland, such as seacoast, port or estuary, with tranquil water, and is inundated, permanently or during high tide, by seawater, and whose species usually grow and extend to the mainland along the river. Although both the definitions reflect some of the features of mangal, neither is succinct or clear. Moreover, both the definitions derived due to the limited knowledge are focusing on the tropical region and thus limited to the use for zonal vegetation.

Recent researchers have more concise understandings of the concept of mangal. For example, "Mangroves are an azonal vegetation confined to the saltwater of tidal regions"[8], "It is a tidal forest"[5], "… littoral woody plant communities that naturally distributed in the intertidal zone of tropical and subtropical" [9], "Distribution of mangal is restricted to low latitude saltwater tidal regions"[10]. Mangal refers to the woody plants of the arbores and shrubs that grow in the tropical and subtropical intertidal zone between the sea and the mainland[11]. According to the relationship between the growing zone and the tide level, mangal can be defined as the woody plants that grow in a tropical and subtropical low energy seashore zone between slightly above mean sea-level and mean higher tide level. They undergo exposure to and inundation by seawater periodically, the former longer than the latter[12]. Obviously, these definitions are more precise and concise, emphasizing the azonal distribution of mangal in tropical

and subtropical regions and the fidelity of mangal to the tide-related environment[4].

To conclude, *mangal* can be defined as a woody community that grows in the tropical and subtropical intertidal zones and is periodically inundated by the tides. The definition proposed by Zhang (1997)[12] and emphasizing the tidal relationship can also be adopted.

3 Mangrove Plants

Mangrove plants are an ancient group of plants. The results of the study of fossil pollens and other remains have confirmed that some modern genera of mangrove plants, such as *Avicennia*, *Sonneratia*, *Rhizophora* , *Bruguiera* , *Ceriops* , *Excoecaria* and *Pellicera*, occurred in early Tertiary[5]. *Rhizophoraceae* , appearing in Eocene, became the dominant of mangrove plants in Miocene and Pliocene. *Sonneratiaceae* occurred in Eocene and Early Oligocene[13, 14]. In East Hemisphere, *Nypa* appeared in Late Cretaceous, while in Europe, it appeared in Lower Eocene[5], even in Paleocene[15]. *Acrostichum*, called mangrove ferm, occurred in early Eocene[4].

The predominant plants in a mangrove swamp are the trees, and it is these species that are generally listed. In the past, the researchers have varied in their interpretation of what can be included as a mangrove (these are the tree species) when one is considering the landward edge of a swamp or the transition to freshwater conditions[16].

Recently, there are some relatively uniform standards by which to determine the mangrove plants [11], or categorizing the mangrove plants is becoming more and more identical all over the world[9]. Yet, disagreements still exist. Davis[17] thought that mangrove plants are all the plants growing on the tropical coastline intertidal muddy and soft soil, including the true mangroves that grow in the intertidal zone, and the semi-mangroves that grow either in the intertidal zone or on the seashore. Researchers of Indian Ocean and Pacific Ocean mangal, MacNae[3] and Walsh[18] pointed out that mangrove plants are trees and shrubs that grow on the tropical seashore between the highest tide level and the mean tide level, and that exclude the semi-mangrove growing either in the intertidal zone or on the seashore[19]. One of the obvious disagreements is that the former includes "all the plants"[17], while the latter[13, 18] only includes "trees and shrubs"; the other is that the former includes "semi-mangrove", while the latter excludes "semi-mangrove".

Most Chinese researchers recognize that mangrove plants are woody plants species in mangal, excluding herbs, lianas and epiphytes. They divide the mangrove components into true mangrove (eu-mangrove) and semi-mangrove[10, 19-22]. Tomlinson stressed the fidelity of mangal to the environment affected by tide, and divided the mangrove plants into major components (major elements of mangal) or strict or true mangrove, and minor components (minor elements of mangal), while the term of "semi-mangrove" was not proposed[4]. Emphasizing the *exclusive* and *non-exclusive* property, Saenger *et al.* categorized mangrove plants into the "exclusive species" (true mangrove) and the common "non-exclusive" species (semi-mangrove)[23]. It should be pointed out that Lin (1993) held the viewpoint that most of researchers who studied mangal indeed regarded mangrove plants specifically as the true mangrove, and true mangrove had to be differentiated from semi-mangrove[24]. As a result, semi-mangrove was excluded from mangrove plants.

To conclude, *mangrove* plants may be concisely defined as woody plants that grow in the tropical and subtropical intertidal zones subjected to tidal influences, and possess special morphological structures and physiological mechanisms. They can be divided into true mangrove and semi-mangrove components.

3.1 True mangrove(eu-mangrove, strict mangrove)

True mangroves are the woody plants that specifically grow in the intertidal zone. Growing and reproducing in the intertidal zone, they cannot reproduce naturally in land habitats[19]. Characteristically, they have vivipary, respiratory roots, stilt roots, halodrainage tissues, and high osmotic pressure within the cells[20, 21]. They are the plants that can only grow and reproduce in the intertidal zone subjected to frequent inundation by tide water, and they have pneumatophores, stilt roots and vivipary that are exclusive morphological organs for growing in the intertidal zone[11]. Major elements of mangal (strict or true mangroves) proposed by Tomlinson possess all or most of the following features[4]:

(1) Complete fidelity to the mangrove environment; that is , they occur only in mangal and do not extend into terrestrial communities.

(2) A major role in the structure of the community and the ability to form pure stands.

(3) Morphological specialization that adapts them to their environment, the most obvious are aerial roots, associated with gas exchange, and vivipary of the embryo, whose functional significance is not clear.

(4) Some physiological mechanism for salt exclusion so that they can grow in sea water, and frequently excrete salt.

(5) Taxonomic isolation from terrestrial relatives, separated from their relatives at least at the generic level and often at the subfamily or family level. These constitute the criteria for recognizing a true mangrove.

So, we consider that the true mangrove refers to those plants growing in the typical mangrove habitats, where seawater salinity is often 17.0 - 36.4, and not those in the zone subjected only to irregular spring high tides or storm high tides. Their terrestrial taxonomic relatives are family, subfamily, tribes or genera. They are separated from their relatives at least at the generic level and often at the subfamily or family level.

3.2 Semi-mangrove

As early as the beginning of the 20th century, the concept of *semi-mangrove*, although not defined clearly, was suggested by Tansley *et al.*[25]. It refers to those plants that are found mainly in the "back mangal" and on the landward side of the true mangal. Emphasizing the amphibious features of semi-mangrove, some Chinese researchers held that semi-mangrove can not only grow in intertidal zone (sometimes become predominant species), but also, as amphibious woody plants, grow and reproduce naturally in land habitats[26]. They are amphibious and able to grow and reproduce both in land and in intertidal zone, and are occasionally inundated by spring tide while growing in the terrestrial marginal zone, and do not have the exclusive morphological features of adapting to intertidal zone[11]. Minor elements of mangal proposed by Tomlinson are inability to form a conspicuous element of the vegetation[4]. They may occupy peripheral habitats and only form pure communities. Their terrestrial taxonomic relatives are family, genera or species, and the isolation is mostly at the generic level. Minor elements proposed by Tomlinson are not equally semi-mangrove, since some of them are true mangrove but some are even not mangrove plants. However, the idea can be referred to when it tends to decide what semi-mangrove is.

Semi-mangrove plants grow on the landward fringe of mangrove habitats or in the terrestrial marginal zones subjected to irregular high tides where seawater salinity can be as low as 0.114 %. Their terrestrial taxonomic relatives are family, genera or species. Semi-mangrove plants are separated from their terrestrial relatives mostly at the generic level.

It should be pointed out that semi-mangrove plants also have the specially adapted morphological structures and physiological mechanisms, such as *Heriterie littoralis* with respiratory roots, *Nypa fruticans* with crytovivi parous, and *Acanthus ilicifolius* with the ability to excrete the salt. Semi-mangroves can grow in terrestrial marginal zones. In fact, they are not amphibious woody plants, although some species can grow in inland river banks affected by tides or in the seashore formed by mangrove epeirogenesis.

3.3 Red mangrove and black mangrove

Mangrove plants are divided into red mangrove and white mangrove[8] or into mangrove group and black mangrove[26].

Red mangrove refers to the genera of plants that possess stilt roots and viviparous seedlings[8], or that can provide red dyes, such as *Rhizophora*, and other mangrove plants of Rhizophoraceae: *Ceriops*, *Kandelia*, *Bruguiera etc.* It is inappropriate to include *Sonneratia* and *Excoecaria* proposed by Blasco[26] in the red mangrove group. So is *Avicennia* by Walter[8].

Black mangroves are those genera with crytovivi parous, such as *Avicennia*, *Nypa* and *Oncosperma etc.* It seems unreasonable to incorporate *Pandanus tectoricus* in the black mangrove, which was proposed by Blasco[26].

White mangrove refers to the plants that have thin pneumatophores growing up from horizontal roots spreading radially in the soil from the stem base[8]. For example, *Laguncularia* and *Conocarpus* belong to the white mangrove.

4 Consottive plant and mangal associates

The non-mangrove plants distributing within the mangal community are recognized as consortive plant (consort of mangrove, commensal plant) and mangal associates (associated species).

4.1 Consortive plant (commersal plangt, mangrove commensal)

Lots of non-woody herbs and parasites, epiphytes and lianas of specialized group of dependent plant guild or aerosynusia[10] exclusively grow and distribute in the mangal environment or parasitically on the mangrove plants. However, they are not mangrove plants and differ from the mangal associates that can grow both on the edge of the forest and on the seashore. Therefore, these plants are specially classified into consortive plants or mangrove commensals. Called mangrove fern, *Aerostichum*is the most typical representative. The plants of this kind were once regarded as true mangrove or semi-mangrove, even mangal associates. They are, in fact, the herbs and simply grow in the mangal environment. So, it is not precise to classify them into true mangrove, semi-mangrove, or mangal associates.

Thus, consortive plants refer to the herbs that specifically grow in the mangal environment and to the parasitic, epiphytic and liana plants whose existences are exclusively associated with the mangrove plants. Besides the three known species in *Aerostichum* , other seven species: *Hamata parvnla*, *Deudrobium rhizophoreti*, *D. prostralum*, *D. callibotrys*, *Bulbophyllum xylocarpi*, *Plethiandra sessilifolia*[27] and *Amyema gravis*[11] have been identified.

4.2 Mangal associates (associated plant)

Mangal associates are defined as the woody species that appear in the mangal or its borders occasionally, but cannot become predominant species, and the epiphytes, lianas and herbs that grow in the mangal environment[9]. Tomlinson[4] proposed the name of mangal associates, and brought about a

list of mangal associates covering 27 families, 46 genera and 60 species that exist all over the world. However, he didnt provide a clear definition or concept and merely foot-noted it on the table according to the availability of aerial roots and vivipary. As a result, the list cannot be considered as a strictly defined but an arbitrarily prepared one. The namelist includes the woody plants growing in the mangal environment in salt marsh, seashore, wetland, rain forest, and coastal beach. Except the disputable *Acanthus*, *Conocarpus*, and *Oncosperma*, the others listed are explicitly determined, of which some are semi-mangrove or true mangrove plants, such as *Cerbera*, *Barringtonia*, *Cynometra*, *Dalbergia*, *Derris*, *Pongamia*, *Myristica*, *Brownlowia* and *Dolichandron*.

To be exact, the plants of mangal associates are seashore, seacoastal, halophilous, halotolerent and even terrestrial plants occasionally found on the landward edge or fringe of mangal environment that is inundated by irregular high tides. They are called fringe species or non-typical species of mangal and distribute on the edge of mangal environment[126]. While being parasitic or epiphytic plants, they can grow deep into the mangal plants.

5 Epilogue

(1) The word "mangrove" shall refer to a specific mangrove plant but not to the broad mangrove plants and/or mangal. Mangal is widely used all over the world and shall be applied in China as well.

(2) Mangal can be defined as a woody community that grows in the tropical and subtropical intertidal zones and is periodically inundated by seawater. The definition proposed by Zhang[119] and emphasizing the tidal relationship can also be adopted.

(3) Mangrove plants are woody plants that grow in the tropical and subtropical intertidal zones subjected to tidal influences, and possess specially adapted morphological structures and physiological mechanisms. They are isolated from taxonomic relatives, and can be divided into true mangrove and semi-mangrove.

(4) Represented by *Aerostichum*, consortive plants or mangrove commensals refer to the non-woody plants that strictly grow in the mangal environment.

(5) Mangal associates are halophilous, halotolerent even terrestrial plants occasionally found on the landward edge or fringe of mangal environment that is inundated by irregular high tides.

References

[1] Snedaker S C. Snedaker J G. The mangrove ecosystem. Snedaker S C. Snedaker J G. The mangrove ecosystem: Research methods..Paris: UNESCO. 1984, 85-93.

[2] Rollet B. Bibliography on mangrove research. Paris: UNESCO.1981,1 600-1 975.

[3] MacNae W. A general account of the fauna and flora of mangrove swamps and forest in Indo west pacific region. Adv. mar.Bive, 1968,6(73): 270.

[4] Tomlinson P B. The Botany of mangroves. New York: Cambridge University Press. 1999. 26-206.

[5] Richards P W. The tropical rain forest (second edition). Cambridge: Cambridge University Press. 1996, 299-312.

[6] Schimper A F W. (Reprinted) Plant-geography upon a physiological basis (English Transl .by.W.R.Fisher 1903), H.R. Engelman and Wheldon & Wesley Ltd., 1960, 395-410.

[7] Warming E. Oecology of Plant. Transl. P. Groom. & I. B. Balfour. Oxford. 1909.

[8] Walter H. Vegetation of the earth. and ecological system of the geo-biosphere (2nd). New York : Springer-

Verlag. 1979.

[9] Lin P, Fu Q. Environmental ecology and economic utilization of mangroves in China. Beijing: CHEP.1995.

[10] Wang B-S. Phytocoenology. Beijing: CHEP. 1987, 298-300.

[11] Fan H Q. MangroveSafeguard of Environment Protection. Nanning: Guangxi Science & Technology Press. 2000, 18-23.

[12] Zhang Qiaomin, Yu Hongbing, Chen Xinshu *et al* . The relationship between mangrove zone on tidal flats and tidal levels, Acta Ecologica Sinica, 1997, 17(3): 258-265.

[13] Jin J H, Han B P. Geohistorical distribution of mangrove and its significance. In: Fan H Q, Liang S C. Research and management on Chinas mangroves. Beijing: Science Press. 1995, 76-79.

[14] Jin J H, Liao W B, WangB S, Peng S L. Paleodiversification of the environment and plant community of Tertiary in Hainan Island. Acta Ecologica Sinica, 2002, 22: 425-432.

[15] ВуЛЬФ Е Р.1943. An introduction to historical plant geography. Zhong C X , Zhang L Z,eds., Beijing: Science Press. 1960, 30-86.

[16] Chapman V J. Botanical surveys in mangrove communities. Snedaker S C, Snedaker J G. The mangrove ecosystem: Research methods. Paris: UNESCO. 1984, 53-80.

[17] Davis J H. The ecology and geologic role of mangrove, in Florida. Washington Publication. 1940.

[18] Walsh G E. Mangroves, A Review in R.T. Reimold and H.Queen (eds.) Ecology of Halophytes. New York: Academic Press. 1974, 51-174.

[19] Zheng D Z, Zheng S F, Liao B W. The dynamic studies on mangrove of Qinglan Harbour in Hainan Island. Guangzhou: Guangdong Science & Technology Press. 1995, 133-137.

[20] Chang H T. Analysis on the mangrove flora of the world. AsiaPacific symposium on mangrove ecosystems. Hong Kong HKUST. 1993, 32-33.

[21] Chang H T. Analysis of the mangrove flora in the world. Editorial Board of Collected Works of Chang Hungta. Collected Works of Chang Hungta. Guangzhou: Zhongshan University Press. 1995, 202-211.

[22] Wang B-S. Mangrove. Editorial Board of Forest of Guangdong. Forest of Guangdong. Guangzhou: Guangdong Science & Technology Press. Beijing: China Forestry Publishing House. 1990, 177-187.

[23] Saenger P, Hegerl E J, Davie J D S. Global Status of Mangrove Ecosystems. Commission on Ecology Papers No.3. The Netherlands: IUCN. 1983, 25-66.

[24] Lin P. Species distribution and type of forest aspect of mangrove in China. Li Z-J. Issue of environment and ecology. Xiamen: Xiamen University Press. 1993, 74-79.

[25] Tansley A G, Fritsch F E. Sketches of vegetation at home and abroad (I). The flora of the Ceylon littoral. New Phytol., 1905. 4: 1-17, 27-55.

[26] Blasco F. Taxonomic considerations of the mangrove species. Snedaker S C, Snedaker J G. The mangrove ecosystem: Research methods. Paris: UNESCO. 1984, 81-90.

[27] Ding Hou. Rhizophoraceae. Flora Malesiana Ser. 1, 1958, 5: 429-493.

Fractal Characteristics of the Distribution Pattern of Mangrove *Bruguiera Gymnorrhiza* Populations in Southern China

Liang Shichu (梁士楚)[1], Dong Ming (董 鸣)[1], Wang Bosun (王伯荪)[2]

1 *Laboratory of Quantitative Vegetation Ecology, Institute of Botany, Chinese Academy of Sciences, Beijing 100093, China*

2 *School of Life Science, Zhongshan University, Guangzhou 510275, Guangdong, China*

Abstract The distribution patterns of mangrove *Bruguiera gymnorrhiza* populations in southern China are analyzed using the box-counting method of fractal theory. The patterns of *B. gymnorrhiza* populations could be thought of as fractals as they exhibit self-similarity within the range of scale considered. Their fractal dimensions are not integer but fractional, ranging from 1.04 to 1.51. The unoccupied dimensions change from 0.49 to 0.96. The combined conditions of population density, pattern type and aggregation intensity together influence the values of fractal dimensions of patterns. The box counting is a useful and efficient method to investigate the complexity of patterns. Fractal dimension may be a most desirable and appropriate index for quantifying the horizontal spatial microstructure and fractal behaviors of patterns over a certain range of scales.

Keywords pattern, fractal, fractal dimension, ecological unoccupied dimension, *Bruguiera gymnorrhiza*

In the 1970s, Mandelbrot introduced a new field of mathematics, fractal geometry, to the world, which extends our usual ideas of classical geometry beyond those of point, line, circle and so on into the realm of the irregular, disjoint and singular. Fractal geometry has the potential to provide us with a new way to understand and analyze such natural spatial phenomena, which are not smooth, but rough and fragmented to self-similarity or self-affinity over a range of scales[1]. A considerable number of applications using fractal geometry have been studied. Fractal geometry is becoming increasingly popular among ecologists[2-5]. Examples in plant ecology include the fractal analyses of leaf shapes, root systems, branches, crown and canopy, biomass, height structure, and pattern[6-11].

Spatial distributions are traditionally described in terms of such basic types as regular, random or aggregated. Each of these patterns is often determined on one preselected scale. It has been universally known that within a habitat, different habitat resources often distribute unevenly, that is, have a characteristics of spatial heterogeneity. Heterogeneity of habitat resources may lead the plant and animal populations to distribute over different scales. Thus traditional pattern analysis methods may fail to explore the mechanisms by which organism size, resource availability and spatial structure of habitats control the microstructure of distribution pattern. Just for these reasons, ecologists have been searching for common principles that predict the responses of species distributions to different factors at different scales. There is a great deal of interest in the potential usefulness in applying the concepts of fractals to the study of spatial structures in ecology[2-5]. The study results have showed that various hierarchical

Received on September 15, 2003

The paper is supported by grants from the NSFC (No. 39825106 and 39860023).

levels of vegetation patterns, from individual, population, community to landscape, often appear to be statistically self-similar over ecologically relevant ranges of scales, which can be better characterized by using fractal theory[12].

Although the concept and rules of fractal geometry have been used in pattern research for several years recently, the relationship between the complex degree of fractal patterns and population density, pattern type and aggregation intensity has been still unclear and the application of fractal geometry to the analysis of mangrove species remains untouched. Mangroves are a woody plant community growing between near mean sea level and the high spring tide mark in the marine intertidal zone along tropical and subtropical coasts. Traditional approaches to describing and interpreting spatial distributions of mangrove species have focused on the patterns either of species zonation or of species diversity. Like other ecological systems, mangroves exhibit many types of spatial and temporal heterogeneity and patchiness on a broad range of scales[13], and this patchiness is fundamental to population dynamics, and to many evolutionary and ecological processes. Do patterns of mangrove species have the similar detail over a range of scales? To address this problem and to measure the complexity of pattern structure, a fractal approach must be used.

1 Materials and methods

1.1 Plant species and study site

Bruguiera gymnorrhiza (L.) Lamarck is widely distributed along the coast of southern China. It is one of the largest trees in the Chinese mangroves, with occasional stems >10 m tall. This species is a common element of mangrove assemblages in the mid-intertidal zone that is inundated by normal high tides, often mixed with *Rhizophora stylosa*, but absent from the area nearest to the seaward edge. *B. gymnorrhiza* can locally be present as the dominant species, but usually as a patch than a zone.

The field work is conducted at the National Shankou Mangrove Reserve (21° 28′ - 21° 37′ N, 109° 37′ - 109° 47′ E) in southern China. It has a subtropical marine monsoon climate. The mean annual air temperature is 22.9 ℃, the absolute maximum air temperature is 38.2 ℃, and the absolute minimum air temperature is 1.5 ℃. Local tides have a semi-diurnal regime with an average of 2.53 m and a maximal range of 6.25 m. The annual mean temperature of sea water is 23.5 ℃, salt content 20 - 23, and pH 7.6-7.8. Mangroves cover an area of about 730 hm^2, and consist mainly of *B. gymnorrhiza*, *R. stylosa*, *Kandelia candel*, *Aegiceras corniculatum*, and *Avicennia marina*.

1.2 Plot design and measurements

Four study plots, Q1, Q2, Q3 and Q4, are chosen in *B. gymnorrhiza* communities of different population densities and aggregation intensities. In addition, these communities have different substrate conditions that represent stages in a successional sequence of tidal flat in the Reserve (Table 1). At each plot, eight contiguous 10 m × 10 m quadrats are established and placed parallel to the coastline because the community occurs in a zone roughly parallel to the coastline with a width of 10 to 25 m. Tree height, DBH, crown size, and the x and y coordinate of individuals are measured. Five soil samples are collected from the top 20 cm layer of the soil, four from the four corners of the plot and one from the center. They are mixed thoroughly to a single composite sample which is dried, sifted to remove particles greater than 3 mm, and analyzed for particle-size distribution, organic matter content, and salinity.

Tab. 1 General conditions of four typical sampling plots of *B. gymnorrhiza* community in the National Shankou Mangrove Reserve in Southern China

Plot number	Q1	Q2	Q3	Q4
Site	Yingluo Dyke	Yingluo Dyke	Yingluo Station	Yingluo Village
Soil physicochemical property				
Texture	Light clay, slightly hardened	Medium clay, semi-hardened	Sandy loam, muddy	Sandy loam, muddy
Sandy particle (1 - 0.05 mm)	14.993	11.809	24.512	25.220
Coarse silt particle (0.05 - 0.01 mm)	21.942	14.535	35.169	22.542
Fine clay particle (<0.001 mm)	31.463	35.215	19.138	18.519
Organic matter (%)	6.42	7.16	4.37	4.85
Salinity	21.56	25.13	12.38	15.42
Community width (m)	12-15	10-14	16-25	13-19
Species importance value				
B. gymnorrhiza	269.4	256.75	265.45	235.67
K. candel	30.6	0	11.47	28.96
R. stylosa	0	43.25	23.08	35.37

1.3 Fractal analysis method

The point pattern map (Fig.1) of *B. gymnorrhiza* individuals is drawn based on their coordinate data. A grid, meshes of which are called r size square boxes, of unit length is superimposed onto the map, and the number of nonempty boxes, $N(r)$, is counted. This step is repeated for different sizes of r, which are respectively 1.00, 1.11, 1.25, 1.43, 1.67, 2.00, 2.50, 3.33, and 5.00 m on the basis of subdividing the plot side length into 2^n equal parts. Fractal dimension (D) is calculated using the following formula of the box-counting method:

$$D = -\lim_{r \to 0} \frac{\ln N(r)}{\ln r} \qquad (1)$$

In a log-log plot of r versus $N(r)$ the linear approximation of the first-degree polynoma ($y = a + b x$) is performed, where the slope (b) of the least square fitted line presents the box-counting fractal dimension. To evaluate the worth of the fit of regression lines, the coefficient of determination is used. The range of data points which provides the value of the coefficient of determination of 0.92 is assumed to be the range in which present pattern shows self-similarity. All these processes are carried out using the software of MATLAB 6.0.

2 Results

Fig.2 shows that each $\log r - \log N(r)$ curve can be subdivided into two sections characterized by different slopes and scale ranges. The scale size of inflexion points for Q1, Q2 and Q3 is 2.0 m, while that for Q4 is 1.43 m. The mean crown sizes of *B. gymnorrhiza* individuals in Q1, Q2, Q3 and Q4 are

respectively 2.2, 1.8, 2.6, and 1.5 m, and the least crown sizes are 1.4, 1.2, 1.9 and 0.7 m. Only in Q4 sapling individuals grow into patches with the mean size of 1.5 m. These indicate that the scale sizes of inflexion points, in fact, correspond with the mean crown size of individuals, the crown size of the least individual or the mean size of sapling patches. As shown in Table 2, at the significance level of 0.05 or 0.01, the fractal dimensions for the distribution patterns of *B. gymnorrhiza* populations in Q1, Q2, Q3 and Q4 are respectively 1.27, 1.36, 1.04, and 1.51, in the order of Q3 < Q1 < Q2 < Q4.

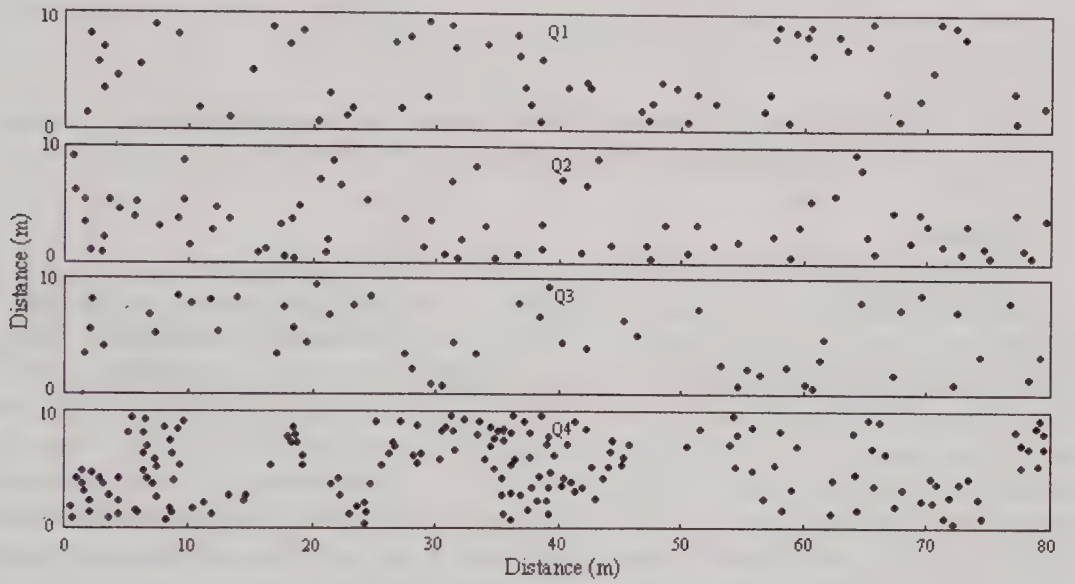

Fig. 1 Point pattern maps of *B. gymnorrhiza* individuals with DBH ≥ 2.5 cm in the four plots, Q1, Q2, Q3 and Q4, each composed of eight contiguous 10 m×10 m quadrats. One blackened circle denotes one individual

Tab. 2 Fractal dimension for distribution pattern of *B. gymnorrhiza* populations in the four plots, Q1, Q2, Q3 and Q4

Plot number	Scale range of r (m)	Box dimension		
		Slope of linear regression	R^2	D_b
Q1	1.00-1.67	−0.11	0.588	
	2.00-5.00	−1.27	0.924*	1.27
Q2	1.00-1.67	−0.11	0.594	
	2.00-5.00	−1.36	0.991**	1.36
Q3	1.00-1.67	−0.15	0.738	
	2.00-5.00	−1.04	0.982**	1.04
Q4	1.00-1.25	−0.44	0.876	
	1.43-5.00	−1.51	0.985**	1.51

Note: *, ** Significant at the 0.05 and 0.01 probability levels, respectively.

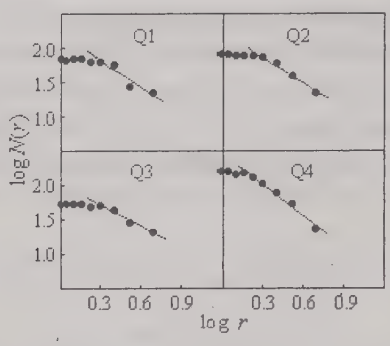

Fig. 2 $\log r - \log N(r)$ relations for distribution patterns of *B. gymnorrhiza* populations in the four plots, Q1, Q2, Q3 and Q4

3 Discussion

The spatial pattern of an object cannot usually be described well enough using methods of Euclidean geometry if it distributes unevenly. As far as an important characteristic of fractal geometry is the property of self-similarity, it should have a constant amount of detail as the pattern is viewed at different range of scale, and cannot be measured with a single characteristic length. This fact has been used for developing methods for the complexity measuring of spatial data[114]. Two hypotheses have been proposed to explain the origin of fractal distribution[115]. First, distribution of species can reflect a distribution of some abiotic factors presenting a template upon which organisms and ecological systems operate. If so, the template should be fractally organized. Indeed, many environmental parameters do display statistical self-similarity over a certain range of scales. Another hypothesis shows that a fractal spatial pattern is the result of community self-organization, which is then transformed into other structures under evident external influences. If so, fractals may be a universal way of biota's self-organization and filling up the space. The spatial distribution pattern of a plant population can be viewed as points on a plane, and the fractal dimension of such a point pattern can be any value between 0 and 2, depending on its complexity.

In a community, each individual must occupy a range of ecological space for the need of environmental resources such as nutrient, water and sunlight during its growing process. Different individuals differ in the occupation degree and utilization ability to ecological space, owing to their different development degrees and spatial positions in the community. These may lead to the occurrence of different patterns. Li suggested that different patterns have different fractal dimensions[116]. The fractal dimensions for patterns of *B. gymnorrhiza* populations range from 1.04 to 1.51. In Q4, the fractal dimension for pattern of small-aged individual group ($\leqslant$15 a) is 1.38, while the middle-aged individual group (16 to 40 a) is 1.18. These results imply that the fractal dimensions for different populations of the same species or for the same population in different development stages may vary, and reflect the variation of function and position of *B. gymnorrhiza* population in different community successional stages. Theoretically, if a population occupies all horizontal spaces of the community, its pattern will have a fractal dimension of 2. But, under natural conditions, any of the plant populations never has a fractal dimension of 2 unless it has enough quantity of individuals that distribute evenly at any spatial scales. It is rather difficult for plant populations to occupy all the community spaces due to intraspecific and interspecific competition and the limitation of habitat conditions. Zhang *et al.* reported that the box

dimensions for the horizontal distribution patterns of *Adenophora lobophylla* and *A. potaninii* populations are positively related to the ability of them to occupy the space in the communities, and closely to the environmental factors[17]. Practically, the fractal dimension measured using the boxcounting method belongs to ecological occupied dimension, which reflects the realized occupation ability of a population to ecological space[18]. The dimension unoccupied can be called as ecological unoccupied dimension, which reflects the potential occupation ability of a population to ecological space, *i.e.*, quantifies how many spaces still leave in the community. The ecological unoccupied dimensions for Q1, Q2, Q3 and Q4 are 0.73, 0.64, 0.96 and 0.49, respectively. But it is noteworthy that not all the ecological unoccupied dimensions reflect the realized conditions of unoccupied spaces in the community. For example, in Q3, there are plentiful rock outcrops that reduce the spatial positions for *B. gymnorrhiza* individuals to occupy.

The combined conditions of population density, pattern type and aggregation intensity together influence the values of fractal dimensions of patterns. As shown in Table 3, both densities and

Tab. 3 Aggregation intensity of *B. gymnorrhiza* populations in the four plots, Q1, Q2, Q3 and Q4

Plot number	Q1	Q2	Q3	Q4
Population density (plant / hm^2)	838	988	650	2250
Variance/mean	0.203	0.591	0.264	6.349
T value	−1.492	−0.765	−1.377	10.007
Type of pattern	Random	Random	Random	Clump
Index of clumping (David & Moore 1964)	7.578	9.466	5.764	27.849
Index of patchiness (Lloyd 1967)	0.905	0.959	0.887	1.238
Morisita's Index (Morisita 1959)	1.034	1.096	1.013	1.415

aggregation intensities of *B. gymnorrhiza* populations change in the order of Q3 < Q1 < Q2 < Q4, which is consistent with the size order of their fractal dimensions. This suggests that the variation in the fractal dimensions reflects the scale variation degree of pattern intensity, discloses the uneven degree of individual distribution, and reveals the natural regenerative situation of *B. gymnorrhiza* populations. In terms of the four plots, seedlings and saplings are mostly aggregated around their parent trees or occur in distinct, separated patches. In Q1 and Q2, community soils have been more or less hardened, which are not beneficial to the dispersal and development of viviparous seedlings and thus directly influence the quantity and spatial distribution of individuals in the regenerative layer. The density of seedlings is lower than 5 plant/m, and individuals with DBH 2 - 10 cm are not common. In Q3, the density of seedlings is lower than 8 plant/m, and individuals with DBH 2 - 10 cm are absent, owing to the plentiful rock outcrops and human influence. In Q4, the density of seedlings is greater than 10 plant/m, individuals with DBH 2 - 10 cm are relatively abundant, about 4 plant/m, and form a more obvious undergrowth layer. It is apparent that in the Reserve fractal dimension values for the patterns of *B. gymnorrhiza* populations have a close relationship with the individual quantity of its sapling groups. The *B. gymnorrhiza* population has a clumped distribution in Q4, but has a random distribution in Q1, Q2 and Q3. The fractal dimensions for the clumped population are higher than those for the random population. All these imply that in *B. gymnorrhiza* community, if seedlings and saplings are abundant,

distribute unevenly and clumpily, the fractal dimension will be higher, and, on the contrary, if they are sparse and random, the fractal dimension will be lower. Therefore, the values of fractal dimension are closely related not only to the number of individuals, but also to the complex degree of their horizontal spatial arrangement.

The use of fractal dimension to evaluate the complexity of patterns has the advantages that may not be found in conventional complexity measures. The results of this paper suggest that patterns of *B. gymnorrhiza* populations have a fractal nature, and that the fractal dimension, as a quantitative measure of pattern complexity, can serve as a valid tool for the determination of their characteristics and distinction to different aggregation intensions. The box counting is a useful and efficient method to establish fractal dimension of patterns.

References

[1] Burrough P A. Fractal dimensions of landscapes and other environmental data. Nature, 1981, 294: 240-242.

[2] Loehle C. The fractal dimension and ecology. Specul. Sci. Tech., 1983, 6: 131-142.

[3] Frontier S. Applications of fractal theory to ecology. In: Legendre P. & Legendre L (eds.), Developments in numerical ecology. Berlin: Springer-Verlag. 1987, 335-378.

[4] Kenkel N C, Walker D J. Fractals and ecology. Abst. Bot., 1993, 17: 53-70.

[5] Zeide B. Fractal geometry in forestry applications. For. Ecol. Manag., 1991, 46: 179-188.

[6] Morse D R, Lawton J H, Dodson M M, Williamson M H. Fractal dimension of vegetation and the distribution of arthopod body lengths. Nature, 1985, 314:731-733.

[7] Vlcek J, Cheung E. Fractal analysis of leaf shapes. Can. J. For. Res., 1986, 16: 124-127.

[8] Tatsumi J, Yamauchi A, Kono Y. Fractal analysis of plant root systems. Ann. Bot., 1989, 64: 499 503.

[9] Zeide B, Pfeifer P A method for estimation of fractal dimension of tree crowns. For. Sci., 1991, 37: 1 253-1 265.

[10] Ma K M, Zu Y G. Fractal properties of vegetation pattern. Acta Phytoecol Sin., 2000, 24: 111-117.

[11] Liang S C, Wang B S. Fractal characteristics of the height structure of Bruguiera gymnorrhiza population. Acta. Phytoecol. Sin., 2002, 26: 408-412.

[12] Sugihara G, May R M. Applications of fractals in ecology. Trends. Ecol. Evol., 1990, 5: 79-86.

[13] Farnsworth E J. Issues of spatial, taxonomic and temporal scale in delineating links between mangrove diversity and ecosystem function. Global. Ecol. Biogeogr. Lett., 1998, 7: 14-25.

[14] Ogata Y, Katsura K. Maximum likelihood estimates of the fractal dimension for random spatial patterns. Biometrika, 1991, 78: 463-474.

[15] Kostylev V, Erlandsson J. A fractal approach for detecting spatial hierarchy and structure on mussel beds. Mar. Bio., 2001, 139: 497-506.

[16] Li B L. Fractal geometry applications in description and analysis of patch patterns and patch dynamics. Ecol. Model., 2000, 132: 33-50.

[17] Zhang W H, Zu Y G, Ma K M. Analysis on the fractal characteristics of distribution patterns of Adenophora lobophylla and A. potaninii. Acta. Phytoecol. Sin., 1999, 23: 31-39.

[18] Ni H W, Ma K M, Zhao F C. The fractal character of the distribution pattern of *Deyeuxia angustifolia* population I.boxcounting dimension. Bull. Bot. Res., 2000, 20: 229-234.

Marine Science Bulletin

Marine Science Bulletin publishes papers on marine science and technology including physical oceanography, chemical oceanography, marine biology, marine geology, environmental oceanography, estuarine & coastal sciences, marine technology, digital ocean, coastal zone management, ocean engineering, marine economics, etc., and aims to promote international academic exchange.

Editor-in-Chief: Lin Shaohua（林绍花）
Deputy Editor-in-Chief: He Guangshun（何广顺） Yang Ying （杨　鹰）
Executive Editor: Lin Baofa（林宝法） He Xuewu （何学武） Zhang Deshan（张德山）
Zhang Xiaoxian（张潇娴） Wang Zhankun（王占坤）
Computer typist: Cheng Xiuchun （程秀春）

Marine Science Bulletin **(Vol . 6 No. 2 Oct. 2004)**

Responsible Institution:
State Oceanic Administration of China
Edited and Published Semi-annually by:
National Marine Data and Information Service
Address: 93 Liuwei Road, Hedong District, Tianjin 300171, China
E-mail: msb@mail.nmdis.gov.cn

ISSN1000-9620
CN12-1271/N